INFORMATION TO USERS

This manuscript has been reproduced from the microfilm master. UMI films the text directly from the original or copy submitted. Thus, some thesis and dissertation copies are in typewriter face, while others may be from any type of computer printer.

The quality of this reproduction is dependent upon the quality of the copy submitted. Broken or indistinct print, colored or poor quality illustrations and photographs, print bleedthrough, substandard margins, and improper alignment can adversely affect reproduction.

In the unlikely event that the author did not send UMI a complete manuscript and there are missing pages, these will be noted. Also, if unauthorized copyright material had to be removed, a note will indicate the deletion.

Oversize materials (e.g., maps, drawings, charts) are reproduced by sectioning the original, beginning at the upper left-hand corner and continuing from left to right in equal sections with small overlaps.

Photographs included in the original manuscript have been reproduced xerographically in this copy. Higher quality 6" x 9" black and white photographic prints are available for any photographs or illustrations appearing in this copy for an additional charge. Contact UMI directly to order.

ProQuest Information and Learning 300 North Zeeb Road, Ann Arbor, MI 48106-1346 USA 800-521-0600



Detection of Particulate Impurities on Semiconductor Surfaces

Jason Patrick Wright

Department of Chemical Engineering McGill University, Montreal

July 1999

A thesis submitted to the Faculty of Graduate Studies and Research in partial fulfillment of the requirements of the degree of Master of Engineering



National Library of Canada

Acquisitions and Bibliographic Services

395 Wellington Street Ottawa ON K1A 0N4 Canada Bibliothèque nationale du Canada

Acquisitions et services bibliographiques

395, rue Wellington Ottawa ON K1A 0N4 Canada

Your file Votre rétérance

Our Sie Notre référence

The author has granted a nonexclusive licence allowing the National Library of Canada to reproduce, loan, distribute or sell copies of this thesis in microform, paper or electronic formats.

The author retains ownership of the copyright in this thesis. Neither the thesis nor substantial extracts from it may be printed or otherwise reproduced without the author's permission.

L'auteur a accordé une licence non exclusive permettant à la Bibliothèque nationale du Canada de reproduire, prêter, distribuer ou vendre des copies de cette thèse sous la forme de microfiche/film, de reproduction sur papier ou sur format électronique.

L'auteur conserve la propriété du droit d'auteur qui protège cette thèse. Ni la thèse ni des extraits substantiels de celle-ci ne doivent être imprimés ou autrement reproduits sans son autorisation.

0-612-64255-0



Thesis i

Abstract

Contamination in an microelectronics manufacturing environment can cause severe problems with the reliability and yield of semiconductor devices. Meeting the aggressive requirements for contamination control requires the development of advanced techniques in defect detection, prevention, and surface preparation. Thus in order to control the device manufacturing environment, it is necessary to detect the presence and if possible the origin of the contaminant, airborne or otherwise, actually found in the cleanroom.

In this project a technique using preferential nucleation of water vapor on particulate contaminants was developed to detect fine (10µm - 100µm) particles. The wettability of various semiconductor and related surfaces was determined by measuring the contact angle of different solutions and droplet growth rates. Nucleation experiments to determine if preferential nucleation occurred were successful for both water soluble and insoluble particles. The droplet growth rate was determined to be a function of the temperature difference between the gas phase and the substrate, contact angle, carrier gas flow rate, and solution concentration where applicable.

Thesis ii

<u>Résumé</u>

La contamination dans l'industrie de la microélectronique peut engendrer de sérieux problèmes au niveau de la fiabilité et du rendement des appareils semi-conducteurs. Compte tenu des exigences pour le contrôle de la contamination, il est nécessaire de développer des techniques avancées dans la détection d'avaries, la prévention et le mode de conditionnement des surfaces. Dans cette optique, il est nécessaire de détecter la présence, si possible l'origine des impuretés qu'elles proviennent de l'air ou autres, présentent dans la chambre propre.

Dans ce projet, une technique de détection utilisant la nucléation préférentielle de la vapeur d'eau sur les impuretés a été développée afin de détecter les particules fines (10 à 100µm). 'Wettability' des différents semi-conducteurs et des surfaces associées a été déterminé par la mesure de l'angle de contact des différentes solutions et le taux de croissance des gouttelettes.

Des expériences sur la nucléation préférentielle dans le cas d'impuretés solubles et insolubles dans l'eau ont été menées avec succès. Le taux de croissance des gouttelettes a été exprimé en fonction de la différence de température entre la phase gazeuse et le substrat, l'angle de contact, le débit du gaz porteur et la concentration de la solution si applicable.

Thesis iii

Acknowledgments

I would like to take this opportunity to expression my appreciation to all those who have helped, supported, and encouraged me throughout this project.

- My thesis supervisor Dr. D. Berk, for his guidance and support.
- Jim Fraser and John Powell of Nortel Networks in Ottawa for their assistance, guidance, and help supplying the needed materials for this project.
- The fellow students whose friendship helped make the past two years an enjoyable time full of wonderful memories. A special thanks to Daniel Duarte, Remy Dumortier, Isabelle Fortin, Terry Murphy, Sanjay Vadodaria, and Fujing Wang, for their support, encouragement, and friendship.
- To my family for their support, encouragement, and patience.

Thesis iv

Table of Contents

ADSU	ract
Résu	ı m é ii
Ackr	nowledgments iii
Tabl	e of Contentsiv
List	of Figuresvii
List	of Tables xiii
Nom	enclature xiv
Chaj	pter 1: Introduction
1.1	General Introduction 1
1.2	Problem Statement and Objectives
Chap	oter 2: Background and Literature Review
2.1	Wettability6
2.2	Nucleation and Droplet Growth 9
2.3	Heterogeneous Nucleation - Thermodynamics
2.4	Heterogeneous Nucleation - Kinetics
2.5	Nucleation on Insoluble Particles 14
2.6	Condensation on Soluble Nuclei
Char	oter 3: Materials and Methods
3.1	Introduction 18
3.2	Materials and Instrumentation
3.3	Experimental Set-Up
3.4	Experimental Conditions and Constraints
	3.4.1. Types of Surfaces

Thesis v

	3.4.2. Contaminant Particles and Seeding Techniques	22	
•	3.4.3. Humidity Measurements	23	
3.5	Surface Roughness Measurements	24	
3.6	Surface Tension Measurements	26	
3.7	Equilibrium Contact Angle Measurements	27	
3.8	Particle Detection Experiments	28	
3.9	Image Analysis	30	
3.10	Calculation of Droplet Growth Rates	31	
3.11	Spot Analysis (X-ray Analysis)	33	
Cha	pter 4: Contact Angle - Results and Discussion		
4.1	Introduction	34	
4.2	Surface Roughness and Surface Waviness Measurements	34	
4.3	Surface Tension Measurements	38	
4.4	Effect of Time on Contact Angle Measurements		
4.5	Sodium Chloride and Sodium Sulfate Solution Characterization	45	
4.6	Contact Angle Measurements	46	
	4.6.1 Contact Angle as a Function of Temperature	47	
	4.6.2 Left and Right Contact Angle Consistency	47	
	4.6.3 Equilibrium Contact Angle Measurements	48	
Cha	pter 5: Particle Detection - Results and Discussion		
5.1	General Observations	59	
5.2	Preliminary Experiments	60	
5.3	Droplet Height and Width Trends (For Soluble Particles)	63	
5.4	Droplet Volume	65	
5.5	Initial Droplet Growth Rate Reproducibility	67	
5.6	Effect of ΔT on Initial Rate (dV/dt)	68	
5.7	Contact Angle as a Function of Time	73	
	5.7.2 Effect of Concentration on the Growth Rate		

Thesis vi

	5.7.3	Droplet Height, Width, and Growth Rate Trends	79
5.8	Conta	mination Distribution and Composition	82
5.9	Nucle	ation on Particulate Impurities	84
	5.9.1	Nucleation on Soluble Particles (Various Surfaces)	84
	5.9.2	Nucleation on Insoluble Particles (Borosilicate Glass Surfaces)	94
	5.9.3	Nucleation on Insoluble Particles	94)
5.10	Recon	nmended Conditions for Preferential Nucleation	96
Chaj	pter 6:	Conclusions and Recommendations	
6.1		usions	
6.2	Recon	nmendations	99
Chap	pter 7:	References	
7.1	Litera	ture Cited	100
App	endix A	4	
Image	Analys	sis Techniques	103
	A.1 M	Ianual Contact Angle Measurements	104
	A.2 T	hreshold Function	105
	A.3 H	eights and Width Measurements	106
	endix I	B n of Droplet Volume for Batch Type Nucleation	107
App	endix (C	
Image	s of Pre	eferential Nucleation on Silicon Particles	113

Thesis vii

List of Figures

Cha	apter 1	
1.1	Phases of Preferential Nucleation and Condensation on a soluble parti	cle3
Cha	apter 2	
2.1	Contact Angle	7
2.2	Heterogeneous nucleation from the α phase on a flat substrate	10
2.3	Heterogeneous nucleation in a cylindrical cavity	13
Cha	apter 3	
3.1	Experimental Set-Up	20
3.2	Percent Relative Humidity Transient	23
3.3	Percent Relative Humidity	24
3.4	Surface Roughness and Waviness graph	25
3.5	Surface Roughness and Waviness measurement	25
3.6	An Ideal Image	30
3.7	A Problematic Image	31
3.8	Height and Width Measurements	32
3.9	Extrapolation of Initial Rate vs. Time Data	33
Cha	pter 4	
4.1	Roughness Measurements of the various glass surfaces	36
4.2	Waviness Measurements of the various glass surfaces	36
4.3	Roughness Measurements of the various semiconductor surfaces	37
4.4	Waviness Measurements of the various semiconductor surfaces	37
4.5	Surface Tension as a function of Sodium Chloride Concentration (Temperature = 23°C)	39

4.6	Surface Tension as a function of Sodium Sulfate Concentration	40
4.7	α as a function of concentration (borosilicate glass)	41
4.8	α as a function of concentration (silicon)	41
4.9	α as a function of concentration (silicon dioxide)	42
4.10	Initial Wetting Dynamics (Temperature = 23-25°C)	43
4.11	Height and Width as a function of time (evaporating droplet) (water on borosilicate glass)	44
4.12	Volume as a function of time (evaporating droplet)(water on borosilicate glass)	44
4.13	Receding Contact Angle of an evaporating droplet	45
4.14	Variation of left and right contact angle (Surface: silicon, Particle: sodium sulfate, T _{base} =20°C)	47
4.15	Variation of left and right contact angle	48
4.16	Contact Angle as a function of Sodium Chloride Concentration	49
4.17	Contact Angle as a function of Sodium Chloride Concentration	50
4.18	Contact Angle as a function of Sodium Sulfate Concentration	50
4.19	Contact Angle as a function of Sodium Sulfate Concentration	51
4.20	Contact Angle as a function of Sodium Chloride Concentration	54
4.21	Contact Angle as a function of Sodium Chloride Concentration	54
4.22	Contact Angle as a function of Sodium Sulfate Concentration	55
4.23	Contact Angle as a function of Sodium Sulfate Concentration	55
4.24	Contact Angle as a function of Sodium Chloride Concentration	56
4.25	Contact Angle as a function of Sodium Chloride Concentration	56

Thesis ix

4.26	Contact Angle as a function of Sodium Sulfate Concentration
4.27	Contact Angle as a function of Sodium Sulfate Concentration
4.28	Comparison of Contact Angles (Particle: sodium chloride, T _{base} = 20°C)
4.29	Comparison of Contact Angles (Particle: sodium sulfate, T _{base} = 20°C)
Chap	oter 5
5.1	Water droplet surrounded by a clear ring (Various Experimental Conditions) 60
5.2	Droplet height as a function of time
5.3	Droplet width as a function of time
5.4	Droplet volume as a function of time
5.5	Contact Angle as a function of time
5.6	Typical increase of the droplet height with time
5.7	Typical increase of the droplet width with time
5.8	Rate of change of the height and width
5.9	Volume as a function of time (2 nd Order Polynomial Trend)
5.10	Volume as a function of time (plateau is being reached)
5.11	Volume as a function of time (plateau is reached)
5.12	Initial droplet growth rate reproducibility
5.13	Initial droplet growth rate reproducibility
5.14	Effect of the temperature difference (ΔT) on the rate of nucleation
5.15	Effect of the temperature difference (ΔT) on the rate of nucleation
5.16	Formation of Boundary Layer having Reduced Humidity

5.17	Effect of the temperature difference (ΔT) on the rate of nucleation (Various Surfaces, Particle: sodium chloride, Q_{N2} =417 ml/min)	71
5.18	Effect of the temperature difference (ΔT) on the rate of nucleation	72
5.19	Effect of the temperature difference (ΔT) on the rate of nucleation	72
5.20	Effect of the temperature difference (ΔT) on the rate of nucleation	73
5.21	Contact Angle as a function of time (Surface: borosilicate glass, T _{base} =20°C)	74
5.22	Contact Angle as a function of time (Surface: silicon, Tbase=20°C)	74
5.23	Contact Angle as a function of time (Surface: silicon dioxide, T _{base} =20°C)	75
5.24	Rate as a function of Contact Angle	77
5.25	Rate as a function of Contact Angle(Surface: silicon dioxide, Particle: sodium sulfate, Q _{N2} =842 ml/min)	77
5.26	Diagram of a Droplet in a Saturated Environment	78
5.27	Variation of Pressure Difference with Sodium Chloride Concentration	78
5.28	Variation of Pressure Difference with Sodium Sulfate Concentration	79
5.29	Effect of Wettability on the Droplet Height	80
5.30	Effect of Wettability on the Droplet Width	80
5.31	Rate (height) versus time for various surfaces	81
5.32	Rate (width) versus time for various surfaces	82
5.33	Silicon Dioxide wafer with impurities	85
5.34	Enlargement of an impurity	85
5.35	Spot Analysis of Silicon Particle	85
5.36	Silicon wafer with a salt deposit	86
5.37	Spot Analysis of salt deposit	86
5.38	Silicon wafer with a silicon dioxide impurity	87
5.39	Spot Analysis of a silicon dioxide impurity	87
5.40	Marks produced by Laser Lithography	88
5.41	Enlargement of marks produced by Laser Lithography	88
5.42	Spot Analysis of Silicon Particle	88

Thesis xi

5.43	Salt deposit on Titanium Nitride Surface
5.44	Enlargement of Impurity89
5.45	Spot analysis of salt deposit
5.46	Edge of Titanium Nitride Surface 90
5.47	Spot Analysis of Titanium Nitride Surface
5.48	Salt deposit on a Photoresist Surface
5.49	Salt deposit on a Photoresist Surface
5.50	Spot Analysis of salt deposit
5.51	Edge of Photoresist Layer
5.52	Spot Analysis of Photoresist Layer
5.53	Edge of Wafer
5.54	Edge of Wafer
A .1 1	endix A Threshold of a Droplet 106 endix B
B.1	Droplet Volume as a Function of Gas Phase Temperature and Percent Relative Humidity
C .1	Image #1 (time index: 10:55:30 AM)
C.2	Image #2 (time index: 11:01:38 AM)
C .3	Image #3 (time index: 11:02:00 AM)
C.4	Image #4 (time index: 11:02:58 AM)
C .5	Image #5 (time index: 11:03:20 AM)
C .6	Image #6 (time index: 11:10:33 AM)
C.7	Image #7 (time index: 11:10:55 AM) 117

Thesis	xii

.

C .8	Image #8	(time index: 11:11:11 AM)	118
C.9	Image #9	(time index: 11:24:27 AM)	118

.

Thesis xiii

List of Tables

CHAPIEL 7	Cha	pter	4
-----------	-----	------	---

4.1	Overall Surface Roughness	35
4.2	Overall Surface Waviness	35
4.3	Contact Angle Measurements of Water on Wafer Surfaces	52
Cha	pter 5	
5.1	Experimental Conditions for Preferential Nucleation	97
App	oendix B	
B .1	Calculated Results	112

Thesis xiv

Nomenclature

A_{6}	area of αβ surface at the critical size
f(O)	defined function, Equation (7)
I,	nucleation rate per unit area of the condensed phase
k	boltzmann's constant
k _s	specific reaction rate constant
M	molecular weight of the vapor
m	mass of condensed phase
N _a	Avogadro's Number
Na _s	number of atoms per unit area of singly adsorbed vapor molecules
N_L	number of molecules per unit volume of liquid
N _s °	number of atoms per unit area in contact with the surface
P	pressure
P ′	pressure (with respect to the solution droplet)
Pc	vapor pressure in equilibrium with the bulk liquid
Po	vapor pressure over pure water
P _o '	vapor pressure over the solution
Q	nitrogen flowrate
г	radius
R _c	critical nuclei radius
R_g	gas constant
S	supersaturation ratio
Sc	critical supersaturation ratio
Γ	temperature
1'	chemical potential per gram of water
V	droplet volume
V _c	specific volume of the crystal
V_m^{β}	molar volume of the condensed β phase
,	vibrational frequency of adsorbed molecules

Thesis xv

- $v_{\rm M}$ number of moles of ions in the solute
- v_o molecular volume
- W_s work required to form a critical nucleus

Greek Symbols

- α (γ_{sv} - γ_{si}) represents the difference between the interfacial tension between the substrate and the vapor phase and the interfacial tension between the substrate and the liquid phase.
- ΔG_{ad} free energy of adsorption
- ΔG_{des} free energy of desorption
- $\Delta G_{\rm m}$ free energy of motion (for component β in the solid phase)
- ΔG_v difference between the α and β phases of the standard Gibbs free energy per unit volume
- ΔG_v^R free energy for the change of β to the α phase
- ΔG^* free energy of forming the nucleus in bulk α
- ΔG^{s^*} standard Gibbs free energy of formation (ignoring strain)
- ρ_L ' density of the solution in the droplet
- γ_{ij} surface tension / specific interfacial energy between any two phases i and j
- θ contact angle
- θ_e equilibrium contact angle
- φ correction factor for the volume of a cap-shaped nucleus
- φ molal osmotic coefficient
- $\iota = \text{electrolyte factor} = v\phi$

Chapter 1

Introduction

1.1 General Introduction

Since contamination can fatally flaw any process step in integrated circuit manufacturing, contamination control is critically important to the yield and reliability of semiconductor devices. With the ever decreasing size of the semiconductor devices, the industry now faces the problem where the size of a contaminant particle is roughly the same size as an individual integrated circuit pathway. To that end, determining the particle type, its source and eliminating it from the process is extremely important.

Significant progress has been made in the past several years towards reducing contaminants in gases, liquids, and cleanrooms so that currently the principal remaining source of particles on wafers is the process equipment. In addition, more than half of the chemical processing now occurs in the back-end of the line where Chemical Vapor Deposition (CVD) reactors and plasma tools are used. In CVD and plasma tools, gas phase nucleation can become a potential source of sub - 0.1 micron particles. Meeting the necessarily aggressive conditions for manufacturing advanced devices will require research and development advances in defect detection, prevention, reduction, and surface preparation technologies to minimize the pre- and post-processing impact from contamination. Efforts in understanding the fundamentals of wet cleaning and all other aspects of contamination control are also essential.

The technique that is described in this thesis would allow the contaminant particulate impurities to be visible either to the naked eye or using a low magnification microscope. The entire duration for the process should be limited, occurring within a short period of time, such as five to ten minutes. The principle of the technique is the preferential nucleation and growth of water droplets on a particulate impurity on the surface.

For the purpose of this proposed technique it is desired that the droplet start nucleating and growing preferentially on the particulate impurity instead of the uncontaminated surface. In general, nucleation of a condensing phase may take place either homogeneously, that being freely in the volume of the original phase or heterogeneously where nucleation will occur on the surface of a condensed phase. The adsorption-nucleation process takes place when a vapor is in contact with a cooler solid substrate surface. In the condensation of a vapor, nucleation occurs only at the location of the active sites.

Figure 1.1 shows the three distinct phases of preferential nucleation and condensation. In the first diagram an impurity is present on the surface of the substrate, this impurity may be water soluble or insoluble. In the first phase preferential nucleation occurs on the particle and not on the surface. The second diagram shows a growing droplet which has a solid core at its center. If the particle is soluble it will begin to dissolve in the condensed water resulting in a saturated solution. If the particle is insoluble it will remain as a solid core; however the crystalline lattice structure may change shape when coming into contact with the water. The third diagram shows a fully formed droplet where the water soluble particle has completely dissolved in the condensed water and will continue to decrease in concentration as more water is condensed. However, if the particle is insoluble it will continue to remain as a solid core.

This process and growth of the droplets depend on four variables: surface characteristics (for example; roughness, waviness, and surface energy), vapor pressure, temperature difference (of the gas phase and the substrate), and wettability of the particle and surface (whether the particle is hydrophobic or hydrophilic in nature).

In order to detect particles within a reasonable time period (an important factor for industrial implementation) the nucleation and growth rate of the droplet must be reasonably "fast". One of the major factors effecting the rate is the wettability of the surface with the condensing liquid which can be determined by measuring the contact angle.

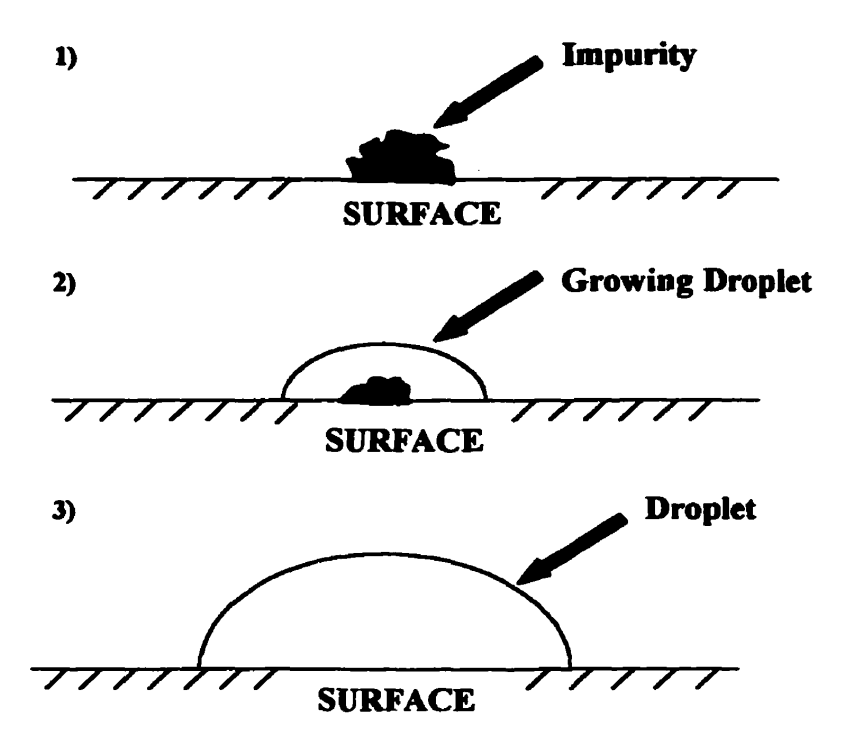


Figure 1.1 - Phases of Preferential Nucleation and Condensation on a soluble particle

1.2 Problem Statement and Objectives

Fine particles contaminating semiconductor wafer surfaces during the various manufacturing processes are generally not easy to detect or remove, even with specialized cleaning and rinsing techniques. One major factor is the varying wettability of the fine particles themselves, compounded also by their solubility and hygroscopic nature.

Generally, the two types of contaminant particles are either water soluble or water insoluble. The most common types of soluble contaminants and their sources are salts which are deposited from the rinsing process and human contact, insoluble contaminant particles are silica and silicon (the two most common types of substrate material), photoresist (masking material), silicon nitride, as well as the various metals used towards the end of the process. The sources of these particulate contaminants are numerous, they can come from an individual process stage, from human influences, such as wafer

handling and accidental contamination, and finally from the cleanroom atmospheric environment.

The main hypothesis of the work described in this thesis was that by passing saturated water vapor over a cooled surface, the water vapor would adsorb and nucleate preferentially on the foreign contaminating particles instead of the remaining surface. The supersaturated state of the water vapor in the vicinity of the surface is achieved by maintaining a temperature difference between the bulk gas and the solid surface and is metastable because the condensed phase is favored thermodynamically.

Once nucleation occurs, the droplet starts growing. Then it is possible to determine the contact angle of the condensate on the substrate, the height, width and subsequently the growth rate of the droplet by image analysis as a function of time. Factors that may affect the nucleation and growth of the droplet and therefore need to be optimized include substrate and vapor temperature difference and gas flow rate.

A vapor mixture consisting of water vapor and a nitrogen carrier gas was condensed onto several different industrially important surfaces chosen for the different hydrophilic / hydrophobic properties. The water soluble particles selected for the experiments were sodium chloride and sodium sulfate. The insoluble particles were silicon and silicon dioxide.

Specifically the main objectives of this thesis are as follows:

 To develop a technique which can reliably and reproducibly detect particles on semiconductor wafers. To this end one needs to determine the optimal experimental operating conditions, such as, the temperature of the substrate, temperature of the inlet and outlet gas, the volumetric flow rate of the carrier gas, and the lag time needed to produce the condensed particles.

2. To determine the relationship between the growth rate of a droplet to the wettability of the surface by measuring the contact angle of the droplets, as well as their height and width.

Chapter 2

Background and Literature Review

The basic principle of the process used for determining the presence of contaminants on surfaces is the nucleation and growth of water on a soluble or insoluble particle. The formation of a droplet of a condensing vapor is expected to occur preferentially on contaminated sites present on the surface since these are the nucleating or active sites. Adsorption is the tendency of molecules to adhere to the surface of a solid from an ambient fluid phase. Its origin is in the attractive forces between molecules, which creates a region of low potential energy near the solid surface, and as a result, the molecular density close to the surface is generally greater than that of the bulk gas. Thus this interaction and higher molecular density favors the nucleation and condensation of the vapor phase onto foreign particles. However, adsorption also depends on the selectivity, which is the difference in the affinity of the vapor for different components on the surface. A relatively straight forward indication of the affinity of the condensate to the surface is the wettability which can be measured by the contact angle. For example, the larger the contact angle between the condensate-substrate the weaker the affinity and the adsorption is more difficult. When the contact angle is smaller the opposite holds true.

In this chapter a brief overview of wettability and the classical theory of nucleation, entailing a description of the thermodynamics and kinetics of heterogeneous nucleation is given. Also presented is a description of nucleation on soluble and insoluble particles since both types of particles are encountered in industrial practice.

2.1 Wettability

The wettability of a particle or a solid surface can be determined by the contact angle. As shown in Figure 2.1, the contact angle is defined as the angle formed between the flat surface and the tangent to the droplet at the interface. The contact angle gives the relationship between the adhesion of the liquid to the solid surface, and its cohesion to itself. When the adhesion is less than the self-cohesion of the liquid the contact angle is

greater than zero as is shown in Figure 2.1; however when the adhesion is equal to or greater than the cohesion, the angle is zero. Also shown in the figure are the interfacial tensions where, γ_{lv} is the interfacial tension at the interface of the liquid and the vapor phases (surface tension), γ_{sl} at the interface of the solid and the liquid, and γ_{sv} present at the interface of the solid and the vapor phase.

Knowing γ_{lv} and the contact angle for a particular concentration, it is possible to calculate $(\gamma_{sv-}, \gamma_{sl})$ by using Young's Equation (equation 1), which is a balance of the interfacial forces at the three phase line and the contact angle formed by a liquid drop on a solid surface surrounded by the equilibrium vapor (Garnier et al., 1998). Basically the implication of this is that by calculating the difference of the interfacial energies it is possible to get a sense of the cohesion (γ_{sl}) of the liquid and the liquid's adhesion to the solid surface (γ_{sv}) .

$$\gamma_{sv} - \gamma_{sl} = \gamma_{bv} \cos \theta \tag{1}$$

The contact angle θ is an inverse measure of the wettability of the surface. By definition, the liquid spreads on the solid surface if $\theta = 0$ degrees, wets if $0 < \theta < 90$ degrees and is non-wetting for $\theta \ge 90$ degrees.

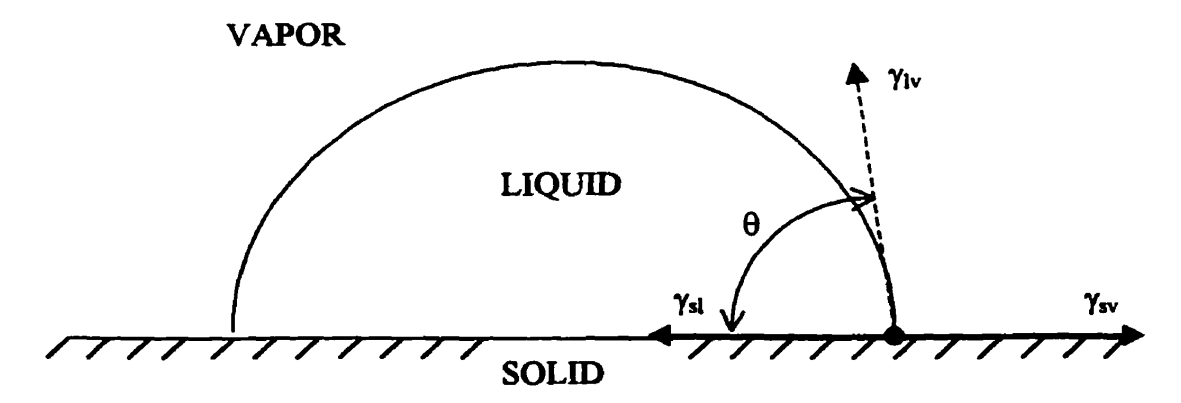


Figure 2.1 - Contact Angle

The contact angle is a function of the following properties of the surface and the fluid (Fowkes, 1964):

- fluid viscosity
- solution concentration
- surface roughness
- surface tension
- temperature of fluid & substrate (effect is generally neglected for small changes in substrate temperature)
- type of contaminant particle (water soluble or water insoluble)
- type of surface (low or high energy surface)

When considering the wetting properties of solid surfaces, it is convenient to identify the extremes of the specific surface free energies of the solids. The type of surface whether it is a low or high energy surface effects the contact angle and the wettability (of the surface). The specific surface free energies of most liquids are less than 100 ergs/cm². Soft organic solids have much lower melting points and the specific surface free energies are generally less than 100 ergs/cm², these surfaces are termed "low energy surfaces". Examples are waxes, and most solid organic compounds. High energy surfaces, such as those used in the majority of the present work, are classified as hard solid surfaces which have surface free energies ranging from about 500 to 5000 ergs/cm², the value being higher the greater the hardness and the higher melting point. Common types of surfaces include, metal oxides, nitrides, silica and glass (Fowkes, 1964).

The Coefficient of Spreading is defined as (Fowkes, 1964):

$$S = \gamma_{sv} - \gamma_{ls} - \gamma_{lv}$$

$$S = \gamma_{lv} \cos \theta - \gamma_{lv}$$

$$S = \gamma_{lv} (\cos \theta - 1)$$

$$(2-a)$$

$$(2-b)$$

$$(2-c)$$

Spreading of the liquid on the surface is thermodynamically favored for S > 0. If $S \le 0$, no spreading occurs, but the drop reaches an equilibrium contact angle (θ_e) where θ_e is a thermodynamic property of the chemical composition of the phases and the temperature for smooth surfaces.

2.2 Nucleation and Droplet Growth

Most of the literature on this subject is related to the seeding of storm clouds and heterogeneous catalysis. Thus the following sections are based on the work of Zettlemoyer published in 1969.

The phrase "nucleation and growth" is used to describe discontinuous changes of phase which are large in degree but at least initially small in their extent in space. When one phase transforms in this manner to another which is more thermodynamically stable, the atoms in some regions of the first phase must become arrayed in a configuration characteristic of the second. In this process, a surface is formed which separates atoms in the new configuration from those in the old. Such a surface can, however, be formed only at the cost of energy and constitutes a barrier to the change of phase. The size of this barrier is proportional to the number of atoms in surface sites and predominates at small cluster sizes, while the motivating free energy is proportional to the number of atoms in the more stable configuration and predominates at larger sizes. The balance of these two influences results in a critical size and a critical motivating potential for nucleation (Zettlemoyer, 1969).

Nucleation may take place either homogeneously (that is, freely in the volume of the original phase) or heterogeneously (on surfaces of a container, on foreign particles, on suspended particles, and on structural imperfections). Heterogeneous nucleation may occur at a smaller motivating potential than that required for homogeneous nucleation; thus most nucleation events take place heterogeneously. Formation of a condensate on a cold substrate by heterogeneous nucleation usually occurs via adsorption during the physical cooling of the substrate in contact with the vapor.

2.3 Heterogeneous Nucleation - Thermodynamics

As indicated above, the nucleation of most phase transformations take place heterogeneously on container walls, particulate impurities, or structural imperfections. In

treating such nucleation, consider a spherical cap of radius R of β (nucleus) on a flat nucleating substrate, s, immersed in matrix α . As shown in Figure 2.2, θ is the contact angle at equilibrium with respect to horizontal force components. Balance of the vertical force components implies that the substrate-nucleus contact should be lens-shaped rather than completely flat; but the correction for this effect is small, save for substrates of high compressibilities, such as rubber.

All substrates characterized in a particular system by $\theta \le 180^\circ$ will serve as a nucleation catalyst for that system. For the configuration in Figure 2.2, the standard Gibbs free energy of formation, ΔG^{s^*} , can be written as

$$\Delta G^{s^*} = \pi r^2 (1 - \cos^2 \theta) W_s + 2\pi r^2 (1 - \cos \theta) \gamma_{\alpha\beta} - \frac{\pi}{3} r^3 (2 + \cos \theta) (1 - \cos \theta)^2 \Delta G_v$$
 (3)

where r is the radius and ΔG_v represents the difference between the α and β phases of the standard Gibbs free energy per unit volume.

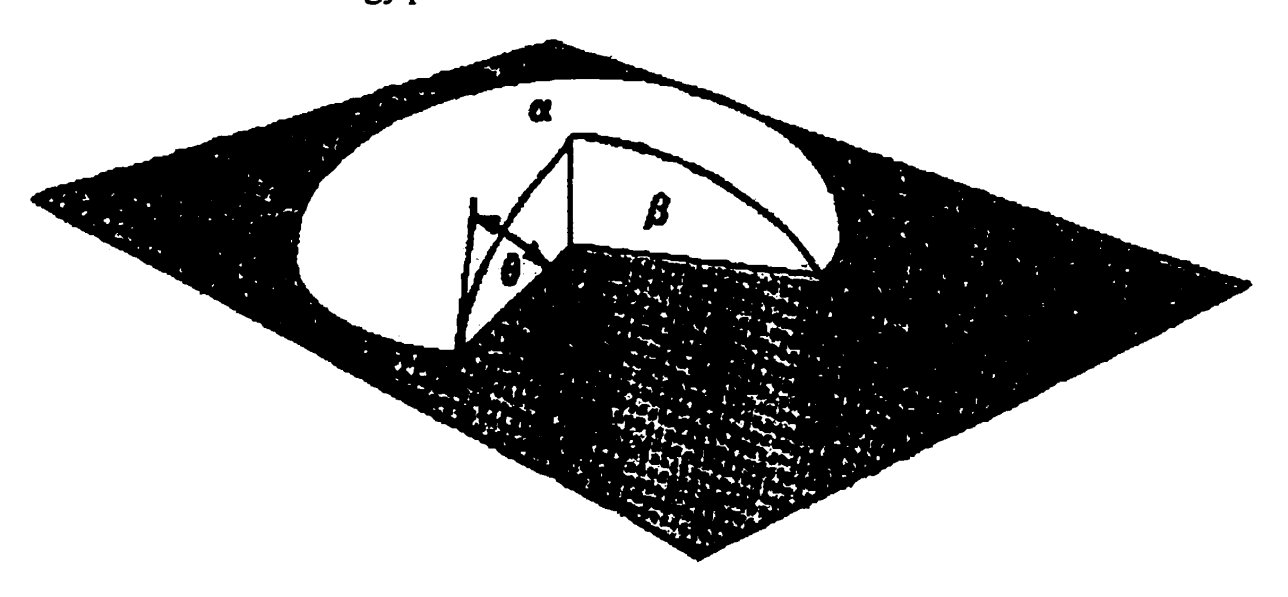


Figure 2.2 - Heterogeneous nucleation from the α phase on a flat substrate (Zettlemoyer, 1969)

Solving for the critical nucleus, R_c

$$R_c = \frac{2\gamma_{\alpha\beta}}{\Delta G_{..}} \tag{4}$$

where ΔG_v is the standard Gibbs free energy per unit volume.

$$\Delta G^{s^*} = \frac{4\pi \gamma_{\alpha\beta}^{3}}{3} \cdot \frac{(2 + \cos\theta)(1 - \cos\theta)^2}{\Delta G_{\alpha}^{2}}$$
 (5)

thus
$$\Delta G^{s^{\bullet}} = \Delta G^{\bullet} \cdot f(\theta)$$
 (6)

where ΔG^{s^*} stands for the standard Gibbs free energy of formation (ignoring strain) and ΔG^* is the free energy of forming the nucleus in bulk α , represented by

$$\Delta G^{\bullet} = \frac{16\pi}{3} \cdot \frac{\gamma^3_{\alpha\beta}}{\Delta G_{\nu}^2} \tag{7}$$

and

$$f(\theta) = \frac{(2 + \cos\theta)(1 - \cos\theta)^2}{4} \tag{8}$$

Equation (4) is identical to that for homogeneous nucleation. However, because heterogeneous nucleation generally takes place at different values of the standard Gibbs free energy per unit volume, ΔG_v , than does homogeneous nucleation, the curvatures of the critical nuclei are different for the two cases. The ΔG_v for condensation can be obtained from:

$$\Delta G_{\nu} = \frac{R_{g}T}{V_{m}^{\beta}} \cdot \ln \frac{P}{P_{e}} \tag{9}$$

where P is the actual pressure and P_e is the vapor pressure in equilibrium with the bulk liquid and V_m^{β} is the molar volume (assumed constant) of the β phase.

The ΔG^{s^e} at which heterogeneous nucleation takes place is approximately in the same range as the ΔG^* at which homogeneous nucleation occurs in the particular system. This might be anticipated from the comparable thermal energy for the two cases.

The general action of a heterogeneous substrate is to reduce the barrier to nucleation represented by the surface energy. When a nucleus forms on a substrate, in addition to the creation of the nucleus-matrix surface (as in homogeneous nucleation), the substrate surface is replaced by a lower substrate-nucleus surface, thereby resulting in a smaller over-all surface contribution. Equations (7) and (8) show that the thermodynamic barrier of nucleation on a substrate should decrease with decreasing θ , and approach zero as θ approaches zero. Potent nucleation catalysis is favored by similar configurations of atoms in the interface planes in nucleus and substrate.

A subject of considerable interest in the area of heterogeneous nucleation is the retention of embryos in cavities of foreign bodies or in the substrate. This problem was treated in detail by Turnbull (1950) for conical or cylindrical cavities. In the latter case, embryos will be retained in the cavities of radius less than R_c, where

$$R_c = \frac{2\gamma_{\alpha\beta}\cos\theta}{\Delta G_{\alpha}^{\ R}} \tag{10}$$

Here θ is the angle pictured in Figure 2.3 and ΔG_v^R is the motivating free energy for the change of β to the α phase. Embryos retained in cavities, will not serve as nuclei unless the radius at the cavity opening equals or exceeds the critical nuclei radius (R_c).

2.4 Heterogeneous Nucleation - Kinetics

By arguments similar to those for homogeneous nucleation, an expression for the nucleation rate per unit area in condensed phase, I_s, is as follows

$$I_{s} = k_{s} \exp \left[\frac{-\left(\Delta G^{s^{\bullet}} + \Delta G_{m}\right)}{kT} \right]$$
 (11)

For simplicity, ks can be taken as

$$k_s = v_o N_s^{\circ} \tag{12}$$

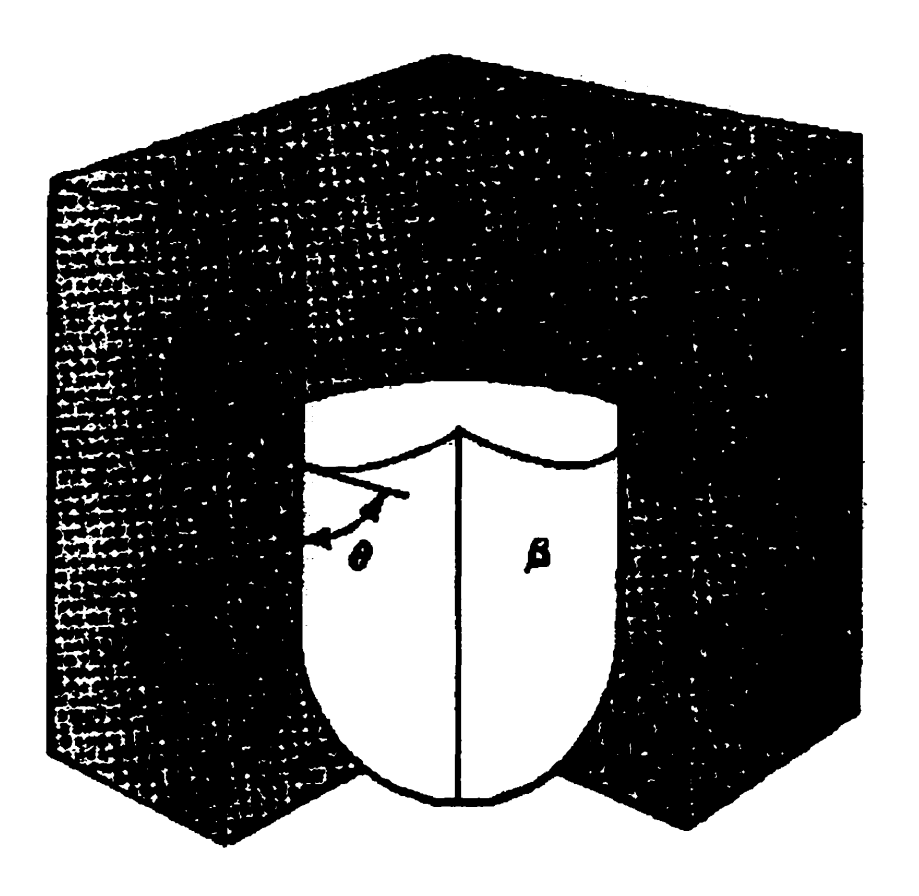


Figure 2.3 - Heterogeneous nucleation in a cylindrical cavity (Turnbull, 1950)

where v_o is the molecular volume, and N_s^o is the number of atoms per unit are in contact with the surface.

While equation (11) is similar to its counterpart for homogeneous nucleation there are a number of essential differences: in the exponential term, the standard Gibbs free energy of formation, ΔG^{s^*} , replaces the free energy of forming the nucleus in bulk α , ΔG^* , and the number of atoms per unit area in contact with the surface replaces the number of atoms per unit volume in the matrix. For condensation reactions, when growth of an embryo takes place by vapor molecules impinging directly on its surface is given by Dunning (1955).

$$I_{s} = \frac{2\pi R_{c}^{2} P^{2} (1 - \cos \theta)}{2\pi m k T v} \cdot \exp \left[\frac{-(\Delta G^{s^{\bullet}} + \Delta G_{ad})}{kT} \right]$$
(13)

k is the boltzmann's constant; m is the mass of condensed phase; ν is the vibrational frequency of adsorbed molecules normal to the surface; and ΔG_{ad} is the free energy of adsorption.

While the spherical cap model of heterogeneous nucleation is often a convenient one to use, in several cases of interest it may not always seem to represent the best morphological model for the heterogeneous nucleus.

In the preceding sections the concepts of thermodynamics have been applied to the problem of nucleation and expressions for the critical size of a cluster, its work of formation, and the rate of nucleation have been derived in terms of macroscopic quantities such as surface tension, radius of curvature, and the like.

At this time we will now consider two special cases of the nucleation phenomena, that of nucleation on insoluble particles and condensation on soluble nuclei.

2.5 Nucleation on Insoluble Particles

If an insoluble particle is wettable, it forms a base on which a small amount of water can present a large radius of curvature and thus satisfy the Kelvin equation (Ref. equation 16) at a much lower supersaturation than would be the case if the same number of molecules was aggregated without a particle core. The Kelvin equation basically determines whether a cluster of water molecules of a particular radius, r, will grow. Once the clusters exceed a critical size given by the Kelvin equation these supercritical clusters tend to grow rapidly by condensation of the vapor phase.

The Kelvin equation was derived by considering the formation of an embryo droplet, assumed spherical, with a surface free energy proportional to its surface area

which produces an equilibrium vapor pressure higher than that of bulk water. As the embryo is formed from the vapor, its surface free energy goes from 0 to $4\pi r^2 \gamma$, where γ is defined as the surface free energy per unit area, or surface tension. For pure bulk water a vapor saturation ratio of less than one would mean that a free energy barrier would have to be surmounted for molecules to form liquid from the vapor. This is seen by writing the free energy differential for g molecules (under isothermal conditions),

$$dG = gkT \cdot d(\ln P) \tag{14}$$

As the molecules go from the vapor at pressure P to the liquid at tension P_o, the elevation of the free energy above the equilibrium of P_o would be obtained by integrating equation (14) to give

$$\Delta G = 4\pi r^2 \gamma - gkT \cdot \ln \frac{P}{P_a} \tag{15}$$

The curves produced by plotting ΔG against r for different supersaturation values represents a free-energy barrier to the growth of embryos at the given supersaturation, the free energy level must be at least as high as the peak, characterized by the critical radius which is expressed by differentiating equation (14) and obtaining the maximum at

$$R_c = \frac{2\gamma}{N_L kT} \cdot \ln \frac{P}{P_o} \tag{16}$$

which is the expression derived by Lord Kelvin.

The wettability is expressed in terms of the contact angle, θ , between the embryo and the particle surface. The size of the basic particle is a critical factor. A direct physical treatment of the problem is not available; however Fletcher (1992) developed a factor involving $\cos \theta$ and the radius of the insoluble particle, assumed to be spherical, which produced a result that seems to be reasonably valid. When $\cos \theta$ is equal to one, the

particle can be completely wetted by a thin film so that a liquid spherical surface with radius essentially that of the particle is exposed to the vapor. The equilibrium then is that of a droplet of pure water having the radius expressed in the Kelvin equation.

2.6 Condensation on Soluble Nuclei

As water collects around a soluble nucleus a solution droplet results. The watervapor pressure over most aqueous solutions is found to be less than that over pure water. For an electrolyte solution,

$$\ln \frac{P_o'}{P_o} = -v \varphi m W_s \cdot 10^{-3} \tag{17}$$

where P_o' is the vapor pressure over the solution, P_o is the pressure over pure water, ν is the number of moles of ions in the solute, φ is the molal osmotic coefficient, m is the mass of condensed phase, and W_s represents the work required to form a critical nucleus.

The equilibrium vapor pressure over a solution droplet bears a relation to the vapor pressure over the bulk solution similar to that of a pure droplet to pure bulk water. The increase in potential per gram is given by

$$u' - u'_o = \frac{R_g T}{W_r} \cdot \ln \frac{P'}{P'_o} \tag{18}$$

where the subscript o refers to the bulk solution and P' to the solution droplet. Suppose that an infinitesimal mass dm = $d(\rho_L' (4/3)\pi r^3)$ is added to a spherical droplet, where ρ_L' is the density of the solution in the droplet. The change in free energy is balanced by the change in surface free energy, $d(4\pi\gamma' r^2)$, such that:

$$\left[\rho_L'r^2 + \frac{1}{3}r^3\frac{d\rho_L'}{dr}\right] \frac{R_gT}{W} \cdot \ln\frac{P'}{P_o'} = 2\gamma r + r^2\frac{d\gamma'}{dr}$$
 (19)

In the range of droplet sizes ($r = 10^{-6}$ to 10^{-3} cm) the second term on each side of the equation is at least four orders of magnitude smaller than the first term. Therefore neglecting them, we find

$$\ln \frac{P'}{P'_o} = \frac{2\gamma W_s}{R_g T \rho_L r}$$
 (20)

The above expression shows the ratio of the vapor pressure over a solution droplet to that over the bulk solution.

The vapor saturation ratio for a solution droplet with reference to pure water is found by combining equations (17) to (20) and substituting into the right hand side of equations (5) and (16) to obtain

$$\ln \frac{P'}{P_o} = \frac{2\gamma W}{R_o T \rho_L r} - imW_s \cdot 10^{-3}$$
 (21)

where i represents the electrolyte factor.

For solution droplets containing any given mass of solute, there are two equilibrium radii for a given supersaturation, one stable and the other one in an equilibrium which, with an infinitesimal increase in surrounding vapor pressure, will become unstable. On the stable side, the droplet can only adjust to a new equilibrium as the saturation ratio changes, growing to a slightly larger size as the humidity goes up or evaporating to a smaller one as the humidity goes down.

In conclusion, it seems appropriate to note how successful the classical nucleation theory has been used for interpreting wide classes of phenomena associated with phase transformation.

Chapter 3

Materials and Methods

3.1 Introduction

This chapter will present the experimental procedures used for determining the percent relative humidity, contact angle, surface roughness, surface waviness, and the height and width of the droplets in order to determine the wettability properties and the growth rates of these droplets. It will also give a brief discussion of the choice of experimental conditions and types of surfaces used in the study.

3.2 Materials and Instrumentation

The experimental set-up consists of an environmental chamber (Rame-Hart), temperature controllers and monitors (Omega Engineering Inc.), and an anti-vibration table built in house. The images of the growing droplets were captured with a Sony Hi resolution CCD monochrome video camera with a video zoom microscope magnifying camera lens (Edmund Scientific - VZM II) with a primary magnification of 0.75X to 3.0X. The images were recorded with the use of a Sony SVHS HI-FI videocassette recorder (Model SVT-S3100) and analyzed on an IBM compatible PC. The captured images were analyzed with Visilog Pro5. The camera was positioned using an adjustable camera stand which consists of a horizontal camera rail (Newport Model PRL-24), a vertical camera rail (Newport Model 410RC), the Newport 460A-XYZ adjustable camera support, and a heavy load capacity rotary positioning stage (Newport Model M-481-A).

All solvents used were of HPLC or reagent grade. Distilled water was used at all times. All chemicals were used as received from Fisher Scientific Co. Barium sulfate, silicon, and silicon dioxide were powders; silver chloride were solid spherical particles; sodium chloride and sodium sulfate were crystalline. Borosilicate glass slides were also purchased from Fisher Scientific Co. The silicon, silicon dioxide, titanium nitride, and

photoresist wafers were used as received from the semiconductor manufacturing division of Nortel Networks.

3.3 Experimental Set-Up

The main piece of equipment was the environmental chamber where the substrate containing the particulate contaminant was placed. Connected to the environmental chamber base was an inlet and outlet cooling water stream which allowed for the substrate to be cooled if necessary. For the higher base temperature ranges a temperature controller and 115 volt / 300 watt electric heater was used.

The water vapor was produced by heating distilled water in a round bottom distillation flask in an electrothermal heating mantle (115 volt / 300 watt), the water was sparged with a nitrogen stream (to act as a carrier gas) and the mixture temperature was monitored with a thermocouple as a means of defining the saturation temperature. The outlet vapor stream passed through a section of heat resistant polypropylene tubing wrapped with an electrical heater so that the vapor temperature could be changed to the required value and was monitored with three surface thermocouples in order to maintain a constant and controllable vapor temperature. The outlet stream then proceeded to enter the environmental chamber where the nucleation and condensation would take place. Finally, the outlet vapor stream from the environmental chamber passed into the fume hood in order to remove it from the laboratory environment.

The condensation and nucleation of the water droplets was monitored and captured with the use of both a monochrome and color CCD camera in order to obtain a side and top perspective of the experimental runs and were recorded with a super VHS video recorder. The video microscope lens allowed for a magnification of between 48X and 160X. Figure 3.1 provides a rough schematic of the experimental set-up.

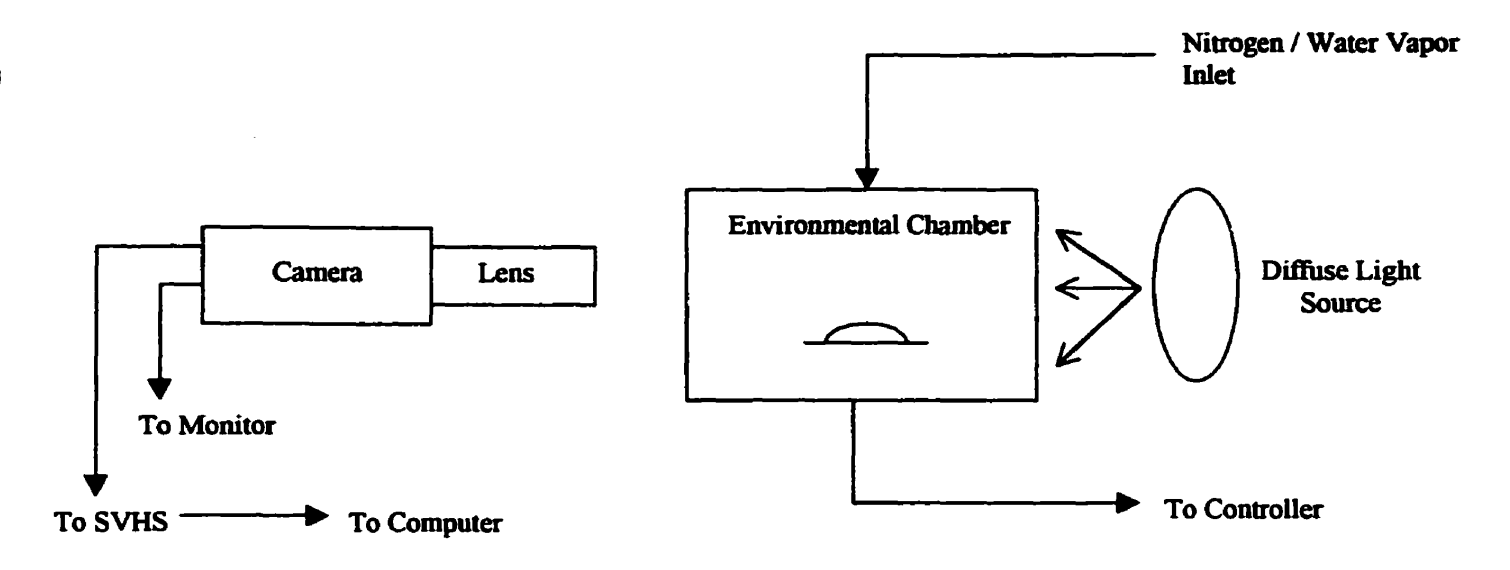


Figure 3.1 - Experimental Set-Up (Garnier et al., 1998)

3.4 Experimental Conditions and Constraints

The three variables that were controlled were: the nitrogen flow rate, the temperature of the water vapor, and the temperature of the base or substrate material. The variables that were measured were the droplet height, droplet width and the contact angle. From the height and width data the droplet volume was calculated.

In most experiments the nitrogen flow rate was fixed at either 417 ml/min or 842 ml/min ± 3%. The base temperature was between 20°C and 25°C while the vapor temperature was between 30°C to 90°C. The range of these settings was determined in preliminary experiments described in Chapter 5.

An important consideration for the selection of the range of the experimental parameters was that the process had to be suitable for a manufacturing environment. Thus nucleation and growth of the droplet should take place over a short period of time, should have low energy requirements (thus a low base and vapor temperature would be favorable), and should use a condensing medium that would be inert and not have any adverse affects on the process materials. To that end the above experimental conditions and materials were considered and examined.

Furthermore, to determine whether a batch or continuous flow of vapor was required, several calculations were performed to ascertain the produced droplet volume for a batch system. If the chamber were filled with saturated vapor and all vapor were condensed onto a particular point, the produced droplet would be large enough to detect visually. However, if there were multiple contaminants on the surface and taking into account possible condensation on the interior walls of the chamber itself, there would not be a sufficient amount of vapor to condense on these particles, thus a continuous flow of water vapor would be required. Appendix B shows the calculations which are based on the relative humidity (95% - 100%) and volume of the environmental chamber. The amount of water vapor present as a function of the gas phase temperature was ascertained.

3.4.1 Types of Surfaces

The various surfaces which were examined are:

- borosilicate glass (control surface)
- silicon
- silicon dioxide
- photoresist (baked)
- titanium nitride

Three classes of wafer surfaces (with the exception of borosilicate glass) were used and tested, these surfaces can be categorized as production wafers, monitor grade wafers, and reclaimed wafers.

A production wafer is a silicon wafer of the highest purity and quality and meets the strictest specifications with regards to scratches, haze, pits, surface roughness, surface waviness, chipped edges and any potential surface contamination. These types of wafers are used solely in the manufacturing process for the production of microelectronics.

The monitor grade wafers are of a lower quality and are used in the process to monitor the various process steps over a period of time. For example they can be used to see if any particulate contaminants are present within a specific process unit before running a series of production wafers.

Reclaim wafers are also of a lower quality and these are basically test wafers which have been used for a period of time and are then sent back to the wafer manufacturer to have its surface re-polished, removing any top layers, such as photoresist, nitride, or metal and any contaminants.

3.4.2 Contaminant Particles and Seeding Techniques

As mentioned before two general types of contaminant particles were considered for this project, water soluble and insoluble impurities. The soluble particles were sodium chloride and sodium sulfate, two compounds commonly found in process water. The insoluble particles were silicon and silicon dioxide, two materials which are common in the manufacturing of semiconductors and are deposited on the wafers during cutting and scribing.

The particulate impurities were affixed to the surface through a variety of methods. For the water soluble particles, a small drop (1.0 - 1.5μL) of a dilute aqueous solution (≈ 0.005 g/l) was applied to the surface and the water was allowed to evaporate leaving behind a salt deposit. For the insoluble particles another method was to use the small particles (less than 10μm) which were deposited on the solid surface when they were scribed to the required size. A third method was to seed physically the surface with either the water soluble or insoluble impurities. However, this technique had the disadvantage that it limited the particle size that could be used to no less than approximately 10μm. For this project all three were used to produce the required contaminant surfaces.

3.4.3 Humidity Measurements

Preliminary experiments on the variation of the humidity in the chamber with time have shown that initially a short transient does exist at all gas phase temperatures usually occurring within the first ten minutes. During this time the humidity rapidly increases from the initial value reaching a percent relative humidity of 95% - 100%. Figure 3.2 shows that for gas phase temperatures varying between 35°C and 55°C at the higher temperatures the humidity increases at a faster rate and thus reaches a relative humidity of 90% within a shorter period of time when compared to the lower temperatures.

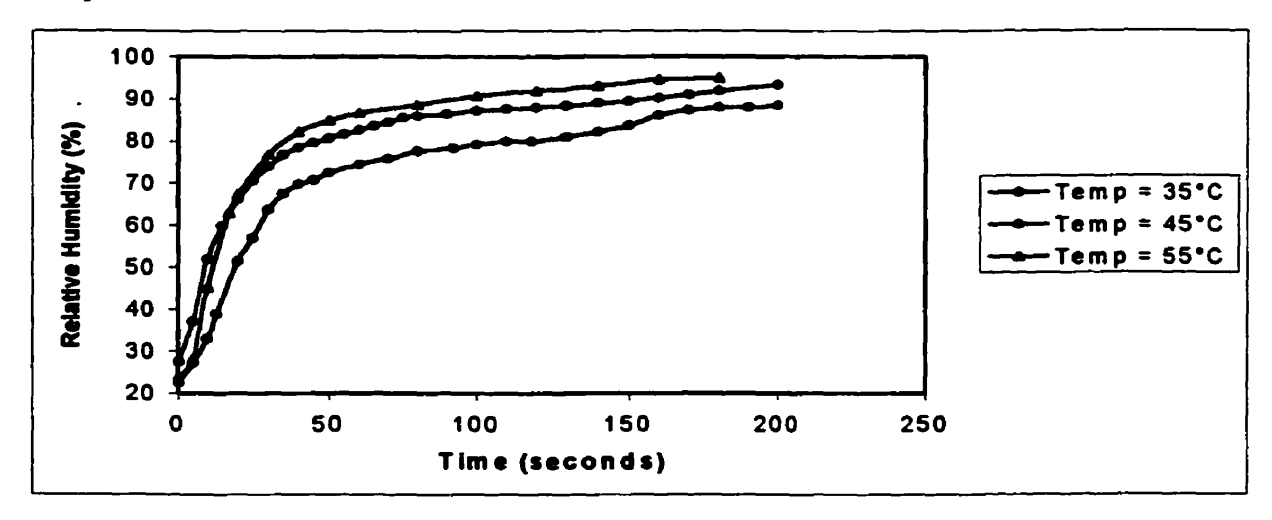


Figure 3.2 - Percent Relative Humidity Transient

Figure 3.3 shows how the initial humidity of the environmental chamber affects the transient. For instance when the chamber is initially set-up for the first run the chamber volume has had a significant amount of time to reach an equilibrium with the laboratory environment. This indicates that a sufficient amount of time for mixing between the volume of the chamber and that of the laboratory, resulting in an initially low relative humidity (approximately 23%). Due to this lower humidity the time necessary to reach 95-100% humidity is lengthened which subsequently results in a longer transient. However, for all following experiments the time between performing consecutive runs is short, varying between 15 and 20 minutes. Therefore, there is an insufficient amount of time for any significant mixing between the two environments which results in a higher

initial humidity and shorter transient. Thus for all gas phase temperatures it was seen that the transient required for the relative humidity to reach 95-100% is much smaller than the actual duration of the experimental run which may last up to 2 hours. For the experiments performed in this study only results from the second run onwards were considered

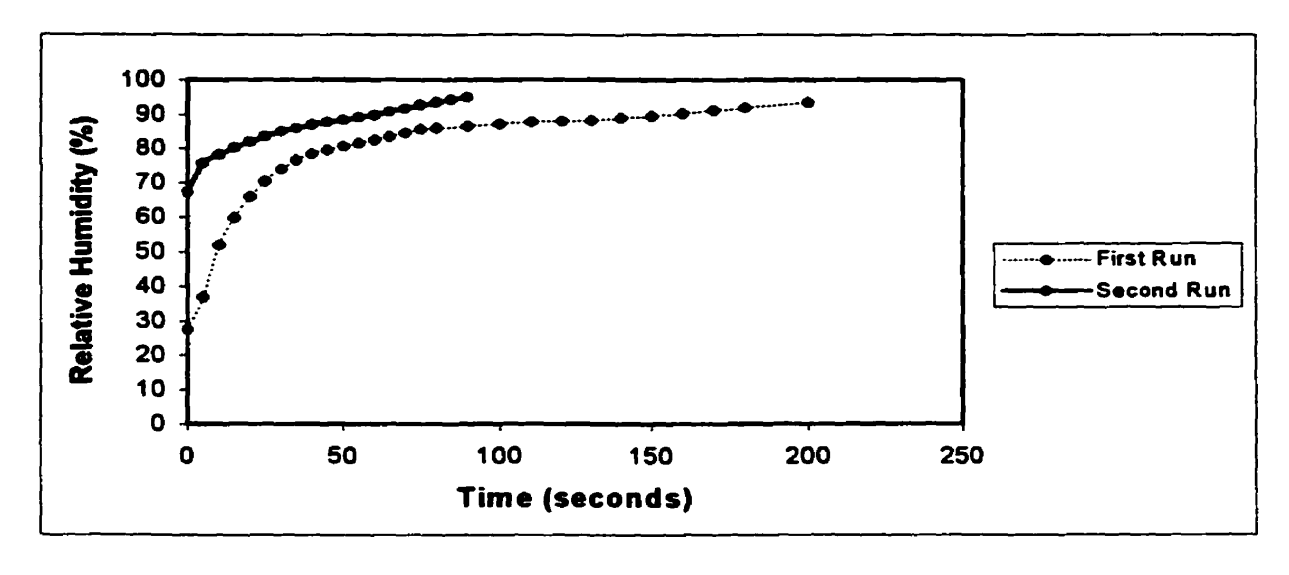


Figure 3.3 - Percent Relative Humidity

3.5 Surface Roughness Measurements

The surface roughness (Ra) and waviness (Wa) of several surfaces was measured using the Dektak³ Surface Profiler. The basic principle of operation is that measurements are made electromechanically by moving the sample beneath a diamond tipped stylus. The high precision stage moves the sample beneath the stylus according to a user-programmed scan length, speed, and stylus force. The stylus is mechanically coupled to a Linear Variable Differential Transformer (LVDT). As the stage moves the sample, the stylus rides over the sample surface. Surface variations cause the stylus to be translated vertically. Electrical signals corresponding to the stylus movement are produced as the core position of the LVDT changes respectively. An analog signal proportional to the position change is produced, which in turn is conditioned and converted to a digital format through a integrating analog to digital converter. The digitized signals are stored in the computers memory for display, manipulation, and printing. Figure 3.4 shows a typical surface roughness and waviness graph.

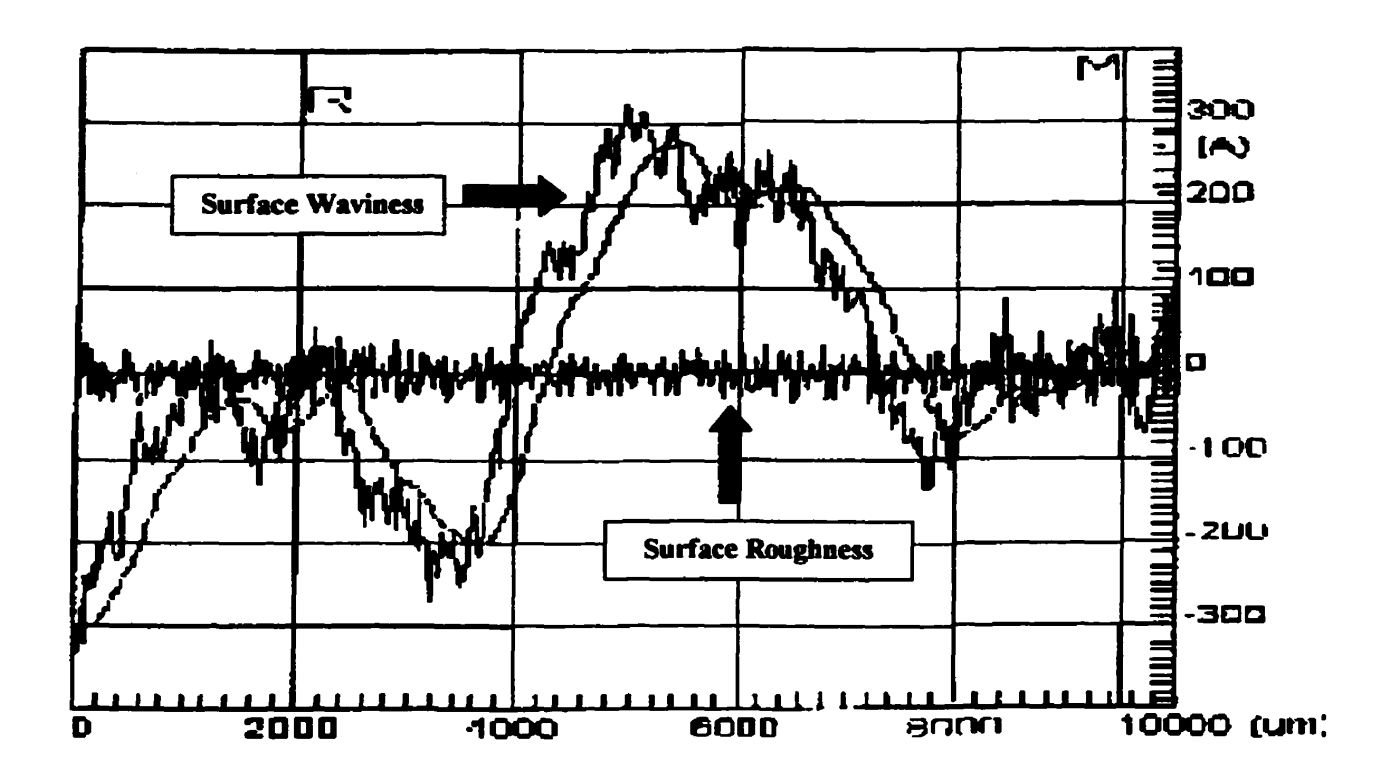


Figure 3.4 - Surface Roughness and Waviness graph

The arithmetic average roughness (Ra) is an international parameter and is the arithmetic average deviation from the mean line. The arithmetic average of waviness (Wa) is the average deviation of waviness from said mean line (corresponds to Ra). For each surface, six independent surface measurements were taken. Two separate areas of the substrate were chosen arbitrarily and subsequently three stylus line measurements were taken of each area in order to determine the reproducibility and accuracy, the resulting data was used to determine the average surface roughness and waviness. Figure 3.5, below, shows the procedure for the surface measurement.

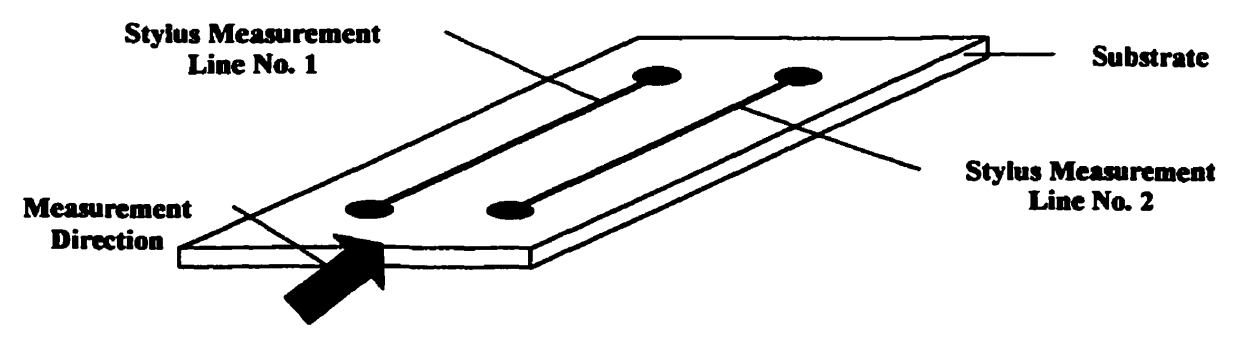


Figure 3.5 - Surface Roughness & Waviness measurement

3.6 Surface Tension Measurements

The surface tension measurements were carried out using the Fisher Autotensiomat[®] (model 215). The basic principal of operation is that measurements are made by the du Nouy ring method, where results are directly obtained in dynes/cm. Approximately 4 to 5 ml of the aqueous salt solution was placed in a 10 ml Pyrex beaker, positioned on the movable base platform and the chamber door securely closed. The platinum-iridium ring was flamed until it was white hot ensuring the effective removal of all contaminants. To guarantee that the ring was not inadvertently contaminated it was handled at all times with a pair of tweezers. The ring was attached to the instrument and the platform/sample was raised until the ring was totally submerged within the solution. The sample was then slowly lowered which allowed for a meniscus to form between the platinum-iridium ring and the salt solution. The resulting measurement of the surface tension was indicated with an analog display. The maximum observable surface tension was observed to occur just prior to the breaking of the meniscus and this was recorded as the surface tension for that particular solution concentration.

Three replicates were performed for each solution concentration where preceding each run the ring was flamed, the Pyrex beaker cleaned and thoroughly dried, and the solution replaced. The average surface tension of the three replicates are reported and discussed in detail in Chapter 4 section 4.3 - Surface Tension Measurements.

Preliminary measurements were performed on distilled water to see if there was good agreement between the measured values and those from literature. From the International Critical Tables (1977) the surface tension at 23°C is 72.28 ± 0.05 dynes/cm and the average measured value for distilled water at the above mentioned conditions was 71.8 ± 0.4 dynes/cm.

3.7 Equilibrium Contact Angle Measurements

The following section gives a brief description of the procedure used to measure the equilibrium contact angle that is formed between a solution and a surface. The surface to be tested was placed on the base of the environmental chamber, and the fluid whose contact angle was to be measured was placed in a 0.5-10 µL pipette. The solution temperature was taken prior to the experiment, generally it was at room temperature, approximately $22^{\circ}C \pm 2^{\circ}C$. The use of a pipette facilitated the formation of the droplets and insured an accurate and reproducible drop volume. For the contact angle experiments a drop volume of 1.5 µl was used. A droplet was formed and placed on the substrate and the static contact angle was measured after 30 seconds. Many researchers in measuring the contact angle record only a single angle; in other cases, both the advancing and the receding angles have been recorded. The advancing contact angle is defined as the angle observed in advancing the liquid boundary over a clean dry surface and the receding contact angle (when a droplet evaporates) is the angle observed in receding the liquid boundary over the previously wetted surface. When both angles are measured their mean can be taken as a fairly satisfactory approach to the equilibrium angle. This procedure receives some justification from the fact that the mean angle is more consistent than the advancing or the receding angle, and there is good agreement between the mean angle and the single angle.

For each measurement, 10 to 25 drops were created over 3-4 surfaces in order to ensure the accuracy and reproducibility of the results. The captured images were analyzed with the aid of Visilog 5.1, which is an image analysis program. Both the left and right apices were individually magnified by 4X and the threshold (Appendix A, section A.2 - Threshold Function) was taken in order to clearly show the profile of the apices. The contact angle was measured from the tangent of the apices and was done by tracing the profile of the magnified apex as closely as possible. The average contact angle and the 95% confidence interval of these 10 to 25 values are reported in Chapter 4.

3.8 Particle Detection Experiments

The particle detection experiments were performed to see if nucleation and condensation would occur on contaminant particles and to determine the variables directly affecting it.

Before each series of experiments the environmental chamber was completely disassembled and wiped down with generous amounts of acetone in order to remove any organic contaminants. The borosilicate glass slides were cleaned with nitric acid (69-70%), rinsed with distilled water and dried at 90°C for a 24 hour period. The wafers which were received from Nortel Networks were considered to be relatively clean (free of particles) since they were produced and scribed in a clean room environment as well as being shipped under controlled conditions; therefore they were used as received.

The substrate under consideration was placed on the base plate of the environmental chamber which allowed the control of its temperature by adjusting the base plate temperature. The temperature of the vapor was subsequently controlled and monitored with the use of three copper-constantan thermocouples which had a calibration precision within ± 0.5 °C and were used to ensure the vapor temperature entering the chamber was at the desired value. Distilled water was then placed in a one liter round bottom distillation flask and inserted into a spherical heating mantle which maintained the liquid temperature to within ± 2°C of the desired set point. The water vapor and nitrogen mixture subsequently passed from the flask into polypropylene tubing covered with an electrical heater which allowed the control over the vapor temperature entering into the environmental chamber. The temperature of the substrate on the base plate of the environmental chamber was controlled with the use of a cooled recirculating fluid and an electric heater. The cooling procedure used to produce a cold substrate, was the Constant, Low Substrate Temperature procedure whereby the substrate is set at a predetermined temperature and allowed to reach steady state. With this method the nucleation phenomena can be assumed to be at their steady state.

The temperature of the vapor mixture was allowed to stabilize for 15 to 30 minutes, it then circulated through the environmental chamber and came into contact with the cooler substrate surface on which the droplets were formed. Between 2 to 8 minutes were necessary in order for the chamber to reach 95 - 100% humidity.

The droplets were lit from behind with a strong focused light source with a diffuser. This light was shone directly into the camera lens. The camera was positioned so that the growing droplet was placed directly into the path of the light thus allowing the observation of the silhouetted drop profile. The camera was also tilted at a 2 to 3 degree angle above the horizontal. This allowed for a portion of the light to be reflected off the substrate as well as resulting in a background that has no sharp distinction between the substrate and the vapor as well as allowing for the drop reflection to be silhouetted. The importance of the reflection will be discussed in section 3.9.

The captured images were analyzed using Visilog 5.1 image analysis software. For measuring the contact angle the Measurement section of Visilog was used. With this method it was possible to manually trace the profile of the droplet along the apices as closely as possible and obtain the contact angle measurement. Only the static contact angle was examined, measured and analyzed. The static angle is defined as the angle taken when the droplet has reached an equilibrium with the substrate and from previous experiments was found to have values between those of the advancing and the receding contact angles. The height and width of the droplet was evaluated at several time indexes in order to observe the changes in the droplet's growth rate at the specified substrate and vapor temperatures. Microsoft Excel was used to treat the data contained within the image data files.

3.9 Image Analysis

In order to use the full set of functions in Visilog and achieve a useful set of results the following considerations must be made when recording the images. Figure 3.6 is an example of an ideal image that could be easily analyzed. There are a number of key features which should be pointed out, the first is the contrast between the background and the drop. Furthermore, the background should be as homogeneous as possible and there should be a sharp contrast between the edge of the drop and the background in order for the drop detection to work. Another important feature is the reflection of the droplet, a partial reflection is necessary in order to identify the apices of the drop.

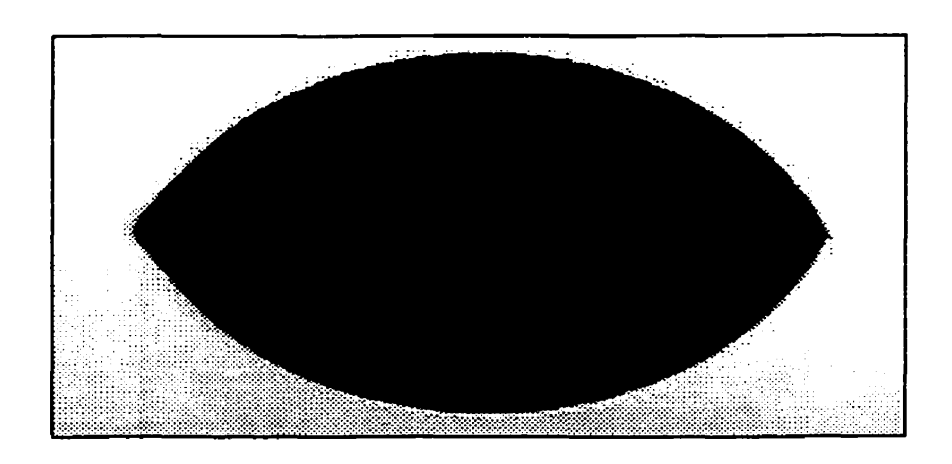


Figure 3.6 - An Ideal Image

An example of a droplet that shows several problems is seen in Figure 3.7. The first problem is the roughness of the substrate's surface which will cause some difficulty in determining the profile of the drop. The second problem is the reflection (bright spot) on the top of the droplet. The part of the drop with the reflection will not be registered as part of the droplet and this will cause problems in accurately determining the profile of the droplet. The third fault which may not be problematic at all is the difference in the brightness between the substrate and the surrounding ambient. The fourth flaw is the reflection on the drop away from the edges of the droplet because sometime depending on the intensity of the reflection it may cause problems in either detecting the profile of the actual drop or its reflection. In conclusion the final and probably the most severe flaw

is in the poorly defined apex which will prevent the accurate determination of the contact angle. A more detailed description of the contact angle measurement procedure is given in Appendix A.

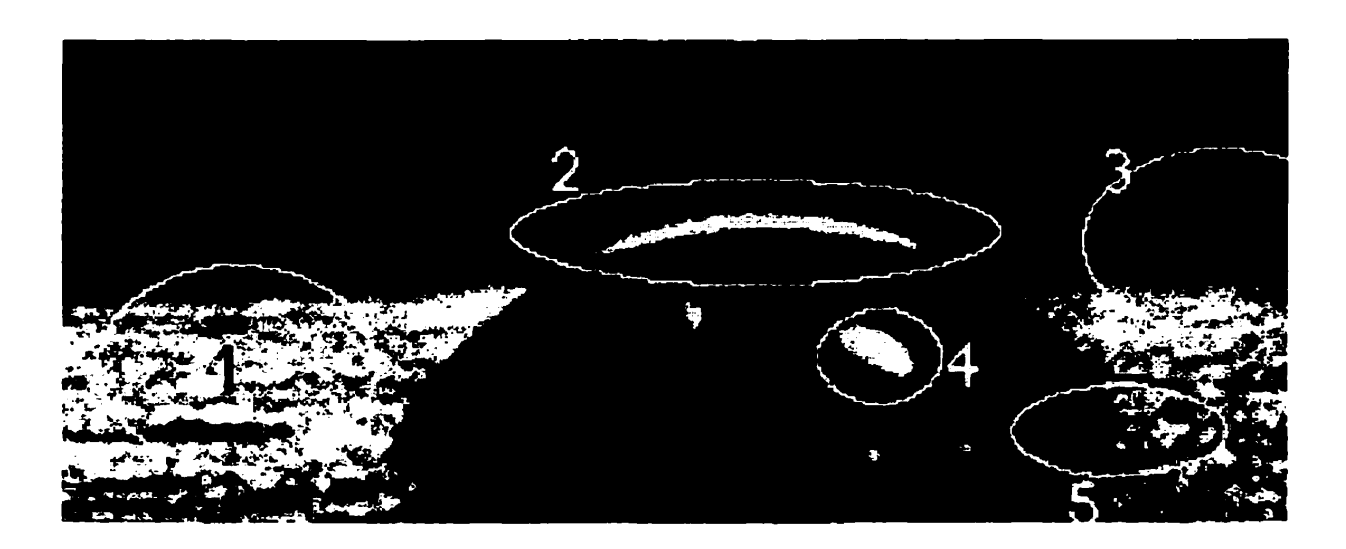


Figure 3.7 - A Problematic Image

3.10 Calculation of Droplet Growth Rates

The height and width of the growing droplet was determined experimentally as described in Appendix A.3. Once the height and width of the droplet (Figure 3.8) had been measured, it was possible to determine their rate, dh/dt or dw/dt; this was done by taking the derivative of the regression curve which was established for the variation of both the height and width with time. In addition, once these rates were known it was possible to determine the rate of volume change as a function of time or the growth rate (dV/dt), by using the chain rule as shown below:

$$\frac{dV}{dt} = \frac{\partial V}{\partial h} \cdot \frac{dh}{dt} + \frac{\partial V}{\partial w} \cdot \frac{dw}{dt}$$
 (22)

The two derivatives dh/dt and dw/dt can both be obtained from the experimental measurements, while $\partial V/\partial h$ and $\partial V/\partial w$ can be found from the equation which describes the volume of a spherical segment of one base:

$$V = \frac{1}{6}\pi h \cdot (3r^2 + h^2)$$
 (23)

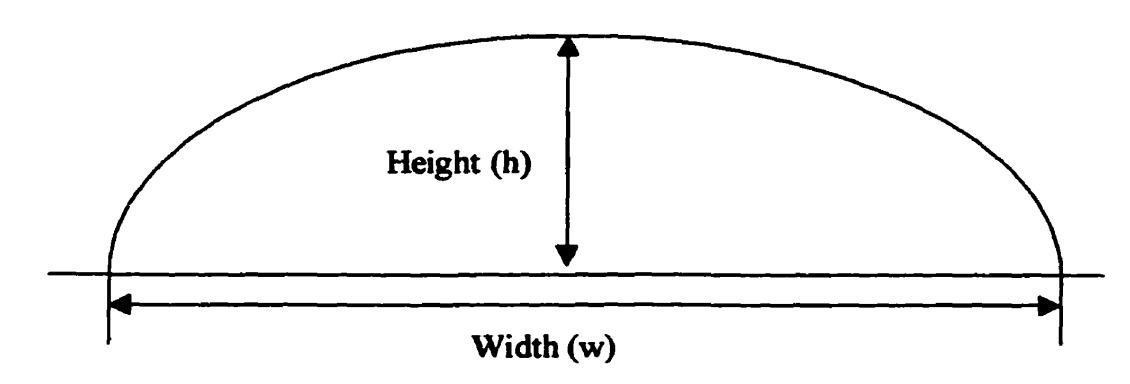


Figure 3.8 - Height and Width Measurements

The subsequent terms, $\partial V/\partial h$ and $\partial V/\partial w$, were derived as follows:

$$V = \frac{1}{2}\pi h r^2 + \frac{1}{6}\pi h^3 \tag{24}$$

since w = 2r or $w^2 = 4r^2$, substituting into equation (24)

$$V = \frac{1}{8}\pi h w^2 + \frac{1}{6}\pi h^3 \tag{25}$$

and

$$\frac{\partial V}{\partial h} = \frac{1}{8}\pi w^2 + \frac{1}{2}\pi h^2 \tag{26}$$

$$\frac{\partial V}{\partial w} = \frac{1}{4}\pi hw \tag{27}$$

therefore,

$$\frac{dV}{dt} = \left[\frac{1}{8}\pi w^2 + \frac{1}{2}\pi h^2\right] \frac{dh}{dt} + \left[\frac{1}{4}\pi h w\right] \frac{dw}{dt}$$
 (28)

Once the growth rate (dV/dt) versus time was calculated and plotted, a fifth order polynomial was fitted to the data using the least squares method and the initial rate was

obtained by extrapolating to t=0. A typical variation of the measured rate can be seen below in Figure 3.9.

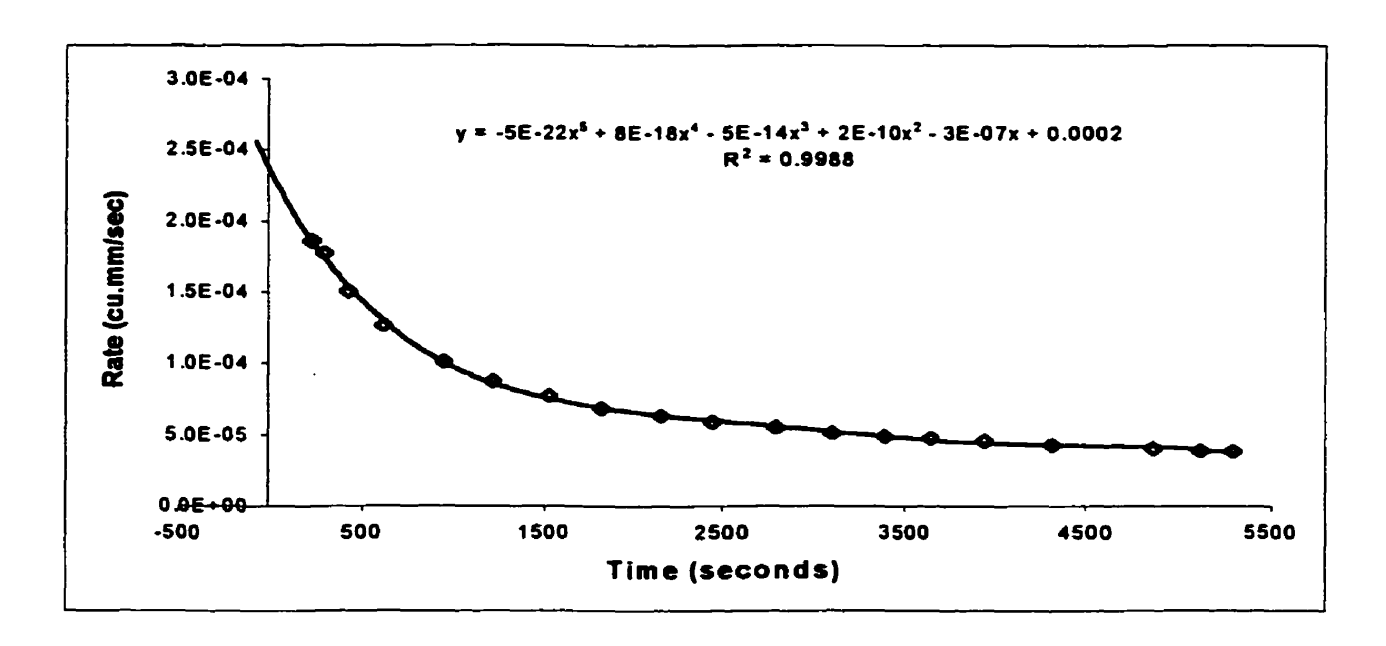


Figure 3.9 - Extrapolation of Initial Rate vs. Time Data (sodium chloride on silicon)

3.11 Spot Analysis (X- ray Analysis)

The various surfaces were all examined with a scanning electron microscope (SEM) in order to determine the distribution of any contaminants and a spot analysis which determines the elemental composition of the particulate impurities was performed on the surface and on any visible impurities in order to ascertain the composition and origin of the contaminant.

The x-ray analysis of an impurity uses the particles emitted energy signature when it is bombarded by x-rays to determine its elemental make up.

Chapter 4

Contact Angle - Results and Discussion

4.1 Introduction

The following sections are a discussion of the results which have been compiled from this study. This chapter will be divided into four general sub-sections; surface roughness and waviness, surface tension, preliminary experiments, and contact angle measurements.

4.2 Surface Roughness and Surface Waviness Measurements

The roughness of a solid surface can have a significant effect on the contact angle. On a rough surface, much higher apparent angles can be obtained. This is because the surface in contact with water consists partly of solid and partly of air, the solution being unable to penetrate into the air filled cavities unless at high pressure (Fowkes, 1964). The relation between the contact angle measured on a smooth surface and on that of a rough surface is given by

$$\cos\theta_{rough} = r\cos\theta_{smooth} \tag{32}$$

where r is the roughness factor.

The surface roughness and waviness were measured on five borosilicate glass slides cleaned with nitric acid, silicon production wafers, silicon monitor grade wafers, silicon reclaim wafers, oxide wafers (with & without the oxide layer etched off), titanium nitride, and photoresist. The average measured value and standard deviation for each of the two runs can be seen in Figures 4.1 to 4.4. Figure 4.1 and 4.2 indicate the roughness and waviness of the borosilicate glass surfaces and Figures 4.3 and 4.4 are for the silicon, silicon dioxide, titanium nitride, and photoresist surfaces. Tables 4.1 and 4.2 give the overall averages for the surface roughness and waviness, respectively. The legend shown

on page 38 gives a detailed description of the types of wafers and the processes they were subjected to.

From the SEMI standards it was seen that a surface roughness between one to three monolayers thickness, which can be roughly approximated to be 100 angstroms, is acceptable in a processing environment. Therefore, the measured values seen below are well within the acceptable limits and therefore the surfaces can be considered "smooth", and the contact angle is not expected tom be effected by the roughness.

Table 4.1 - Overall Surface Roughness

TYPES OF SURFACE	OVERALL ROUGHNESS (A)
Glass Slides	28
Silicon Production Wafers	18
Monitor Grade Wafers	13
Reclaim Wafers	16
Oxide Wafers	15
Monitor Grade Wafer (with oxide layer)	17
Monitor Grade Wafer (with oxide layer etched off)	21
Photoresist	15
Titanium Nitride	16

Table 4.2 - Overall Surface Waviness

TYPES OF SURFACE	OVERALL WAVINESS (A)
Glass Slides	269
Silicon Production Wafers	138
Monitor Grade Wafers	241
Reclaim Wafers	41
Oxide Wafers	162
Monitor Grade Wafer (with oxide layer)	56
Monitor Grade Wafer (with oxide layer etched off)	287
Photoresist	104
Titanium Nitride	176

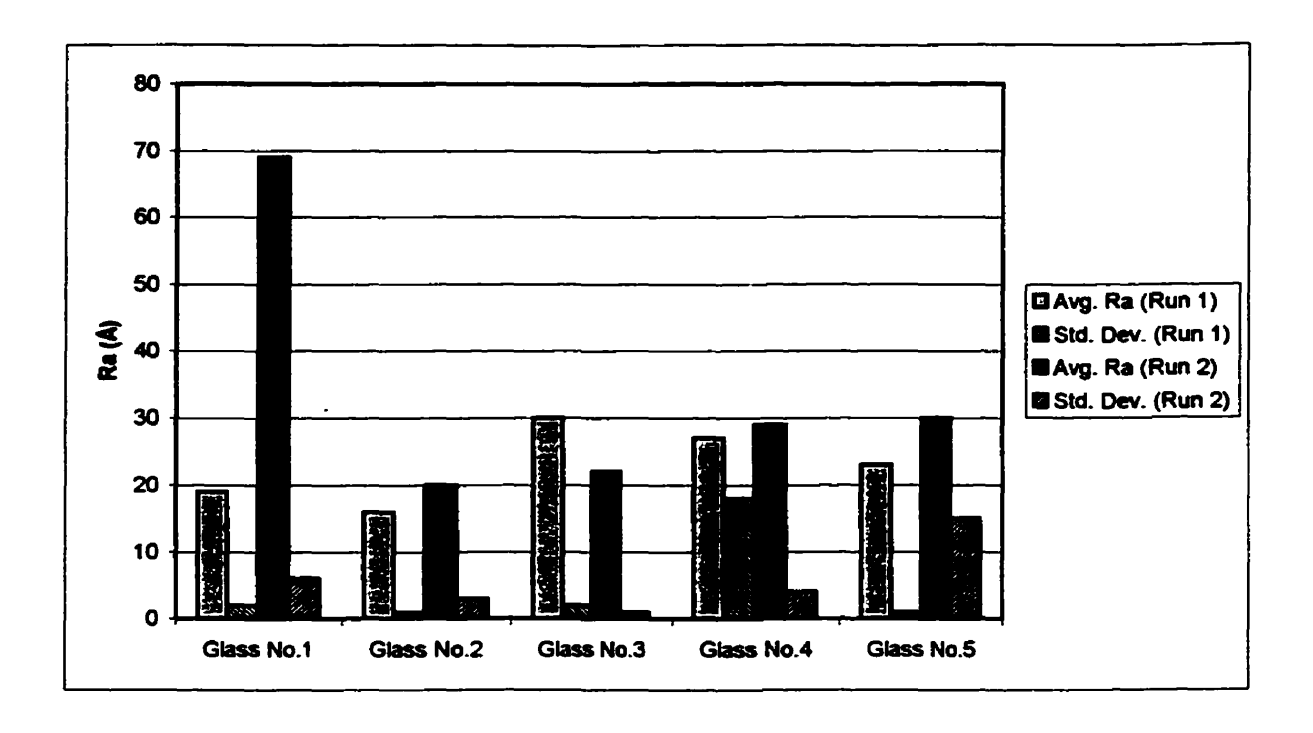


Figure 4.1 - Roughness Measurements of the various glass surfaces (legend on p.38)

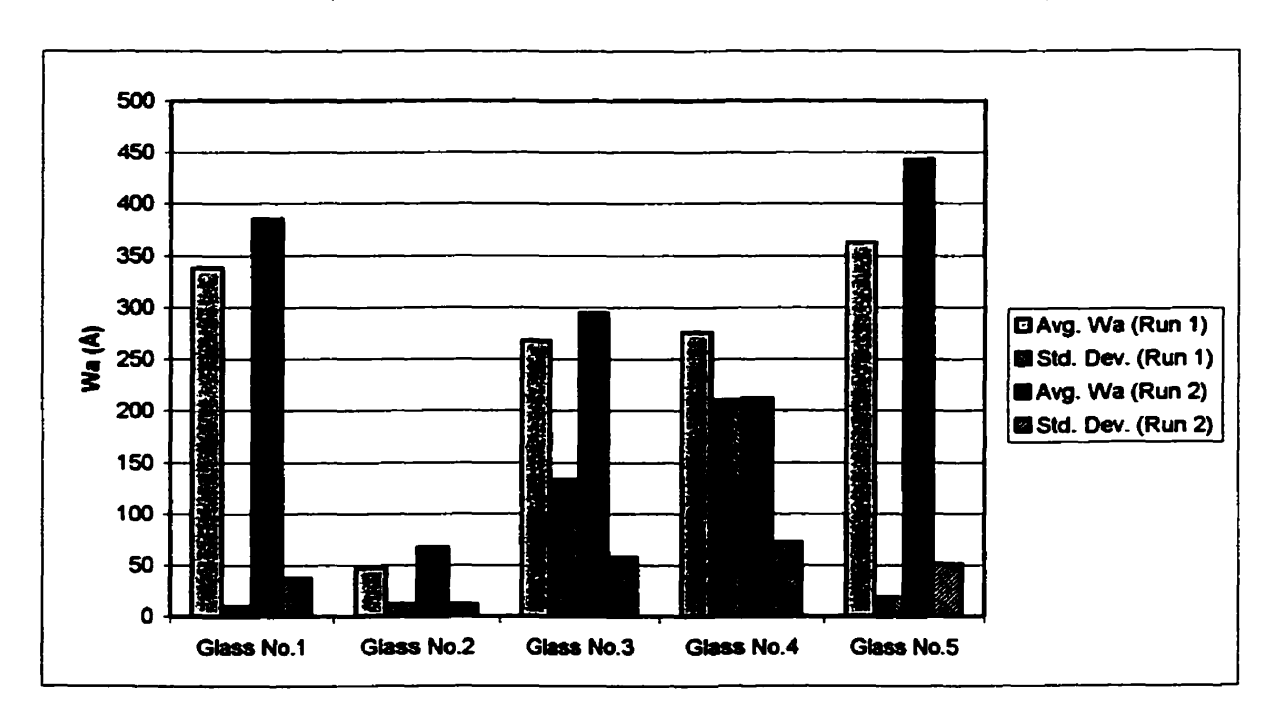


Figure 4.2 - Waviness Measurements of the various glass surfaces (legend on p.38)

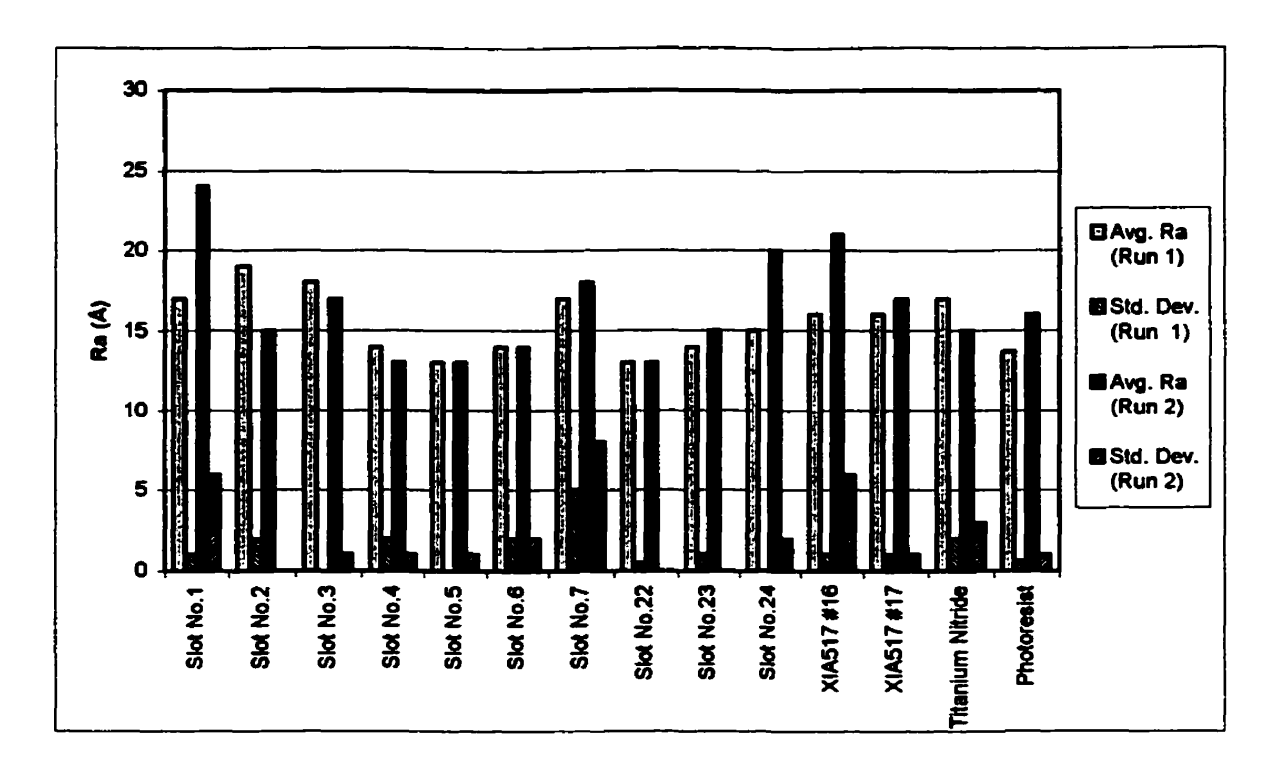


Figure 4.3 - Roughness Measurements of the various semiconductor surfaces (legend on p.38)

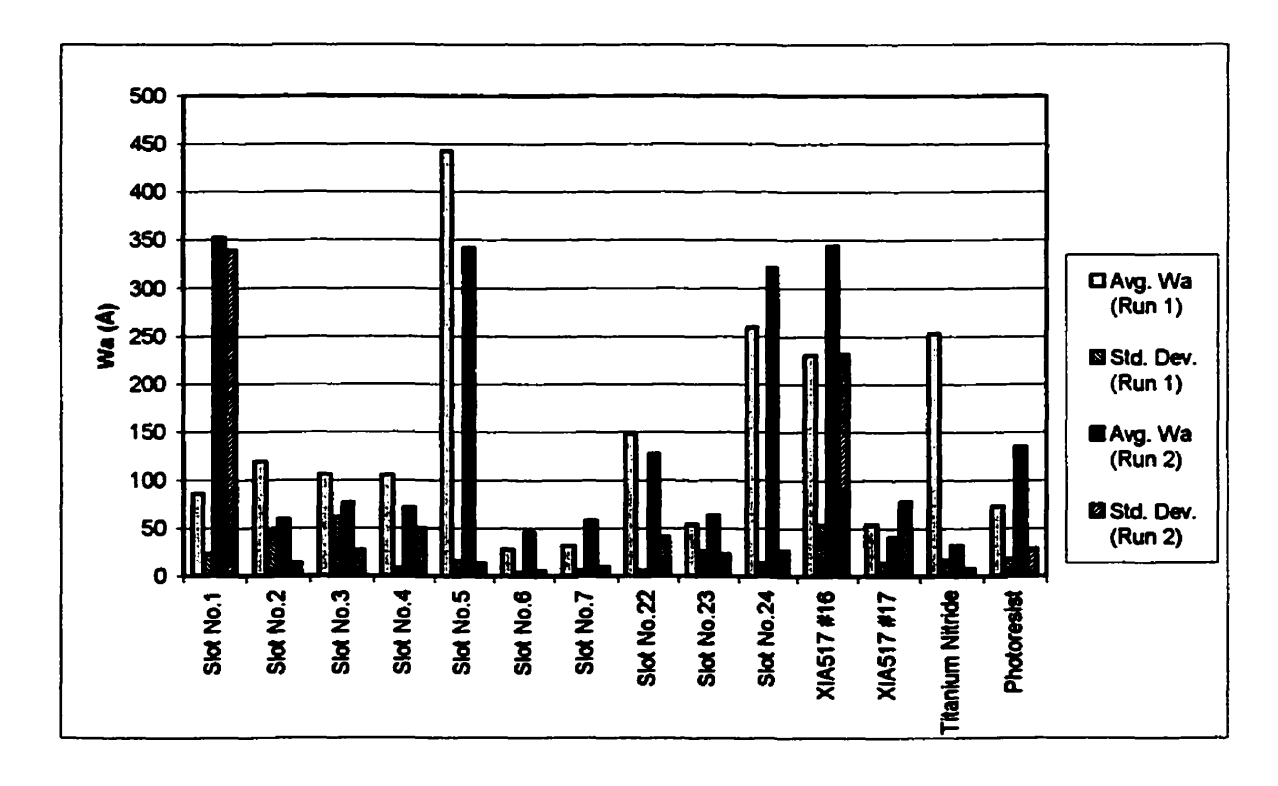


Figure 4.4 - Waviness Measurements of the various semiconductor surfaces (legend on p.38)

Legend

Slot Number	Description of Surface
Slot No.1	Production Grade Wafer
Slot No.2	Production Grade Wafer
Slot No.3	Production Grade Wafer + RCA Clean
Slot No.4	Monitor Grade Wafer
Slot No.5	Monitor Grade Wafer + RCA Clean
Slot No.6	Reclaim Wafer
Slot No.7	Reclaim Wafer + RCA Clean
Slot No.22	Oxide Wafer
Slot No.23	Oxide Wafer
Slot No.24	Oxide Wafer
XIA517 #16	Oxide Wafer (with oxide layer etched off) + RCA Clean
XIA517 #17	Oxide Wafer (no etch) + RCA Clean
Titanium Nitride	Titanium Nitride on Silicon Dioxide Substrate
Photoresist	IX 715 Photoresist Baked

4.3 Surface Tension Measurements

The surface tension (γ_{lv}) was measured for both the sodium chloride and sodium sulfate solutions over their entire concentration range, from 0 g/l to close to saturation. The obtained curves can be seen in Figures 4.5 and 4.6, respectively. The two main reasons for performing these surface tension measurements were to test the reliability of the salt solutions, making sure they were consistent with the values obtained from literature and more importantly to aid in the determination of the coefficient of spreading as documented in Chapter 2.

The experimental measurements show that the surface tension (γ_{lv}) increases with concentration for both the sodium chloride and sodium sulfate solutions. With the sodium chloride solution the surface tension increases by approximately 10 dynes/cm over a 330 g/l concentration range, while for the sodium sulfate solution it increases by approximately 3 to 4 dynes/cm over a 200 g/l concentration range.

Combining the measured surface tension with recorded contact angles (Chapter 4, section 4.6.3, Figures 4.16 to 4.27) the difference of the surface tensions, $(\gamma_{sv-}\gamma_{sl})$, can be calculated by using Young's Equation (Chapter 2, equation 1). In the subsequent discussion the difference of the surface tensions, $(\gamma_{sv-}\gamma_{sl})$, will be denoted by α (alpha). For both salt solutions α can be considered constant over much of the concentration range. For the sodium chloride solution, the concentration range of 0 to 20 g/l corresponds to α decreasing from 62 to 42 dynes/cm. Although α shows a slight increase from 41 to 45 dynes/cm, it can be basically assumed to be constant as shown by Figure 4.7. For the sodium sulfate solution the same general trend was observed where from 0 to 5 g/l, α decreases rapidly from 62 to 52 dynes/cm and then stabilizes at an average value of 55 dynes/cm and remains fairly constant for the rest of the concentration range.

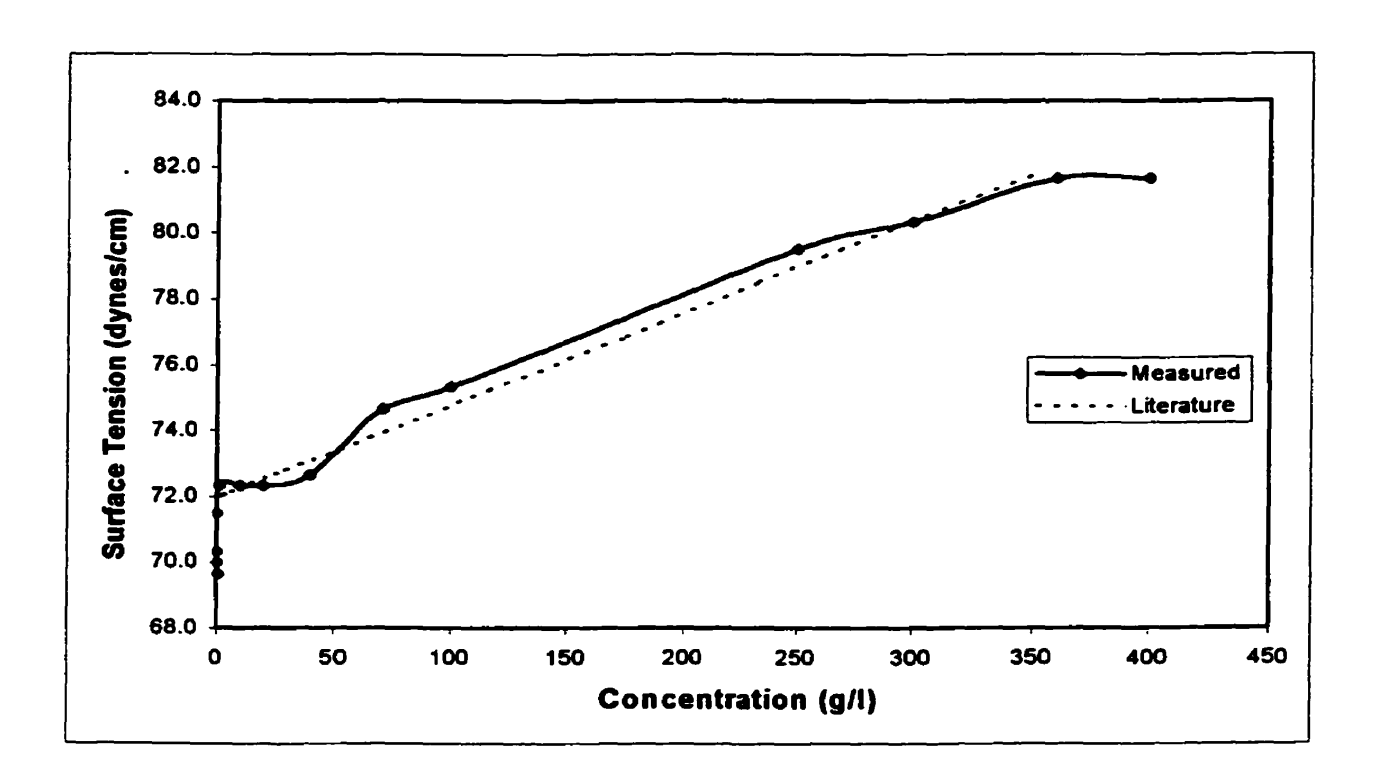


Figure 4.5 - Surface Tension as a function of Sodium Chloride Concentration (Temperature = 23°C)

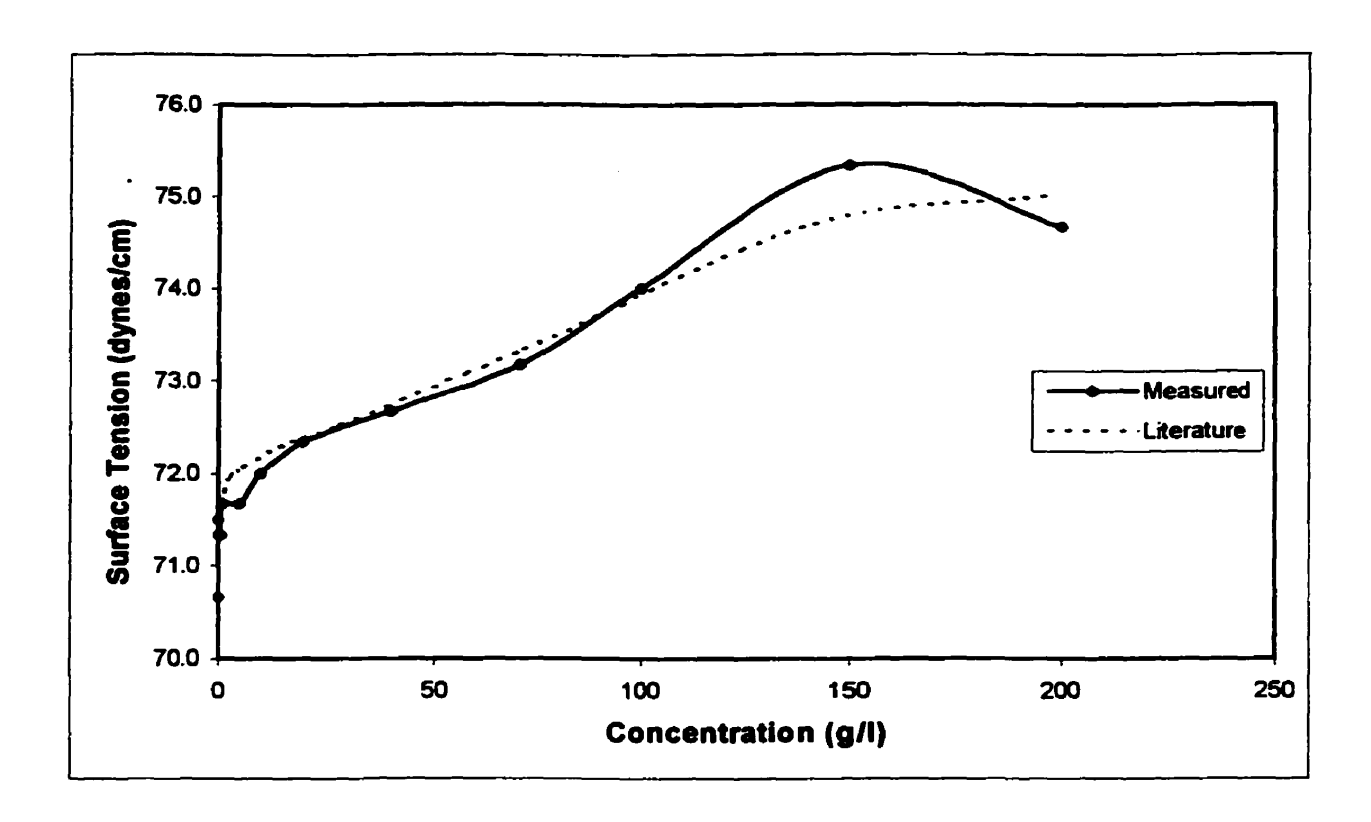


Figure 4.6 - Surface Tension as a function of Sodium Sulfate Concentration (Temperature = 23°C)

The implication of this is that by calculating the difference of the interfacial tensions (specific interfacial energies) it is possible to get a sense of the cohesion (γ_{sl}) of the liquid and the adhesion of the liquid to the solid surface (γ_{sv}). From inspecting Figure 4.7 one can see that when α increases in value the corresponding contact angle of the solution decreases as would be expected since the force of adhesion becomes larger than that of cohesion and a greater degree of spreading occurs. When α decreases in value whereby the contact angle of the solution increases due to the cohesion being greater than adhesion and less spreading of the droplet occurs.

The same reasoning regarding the changing adhesion and cohesion with respect to α can be applied to the data seen in Figures 4.8 and 4.9, which were produced for the salt solutions on both silicon and silicon dioxide surfaces.

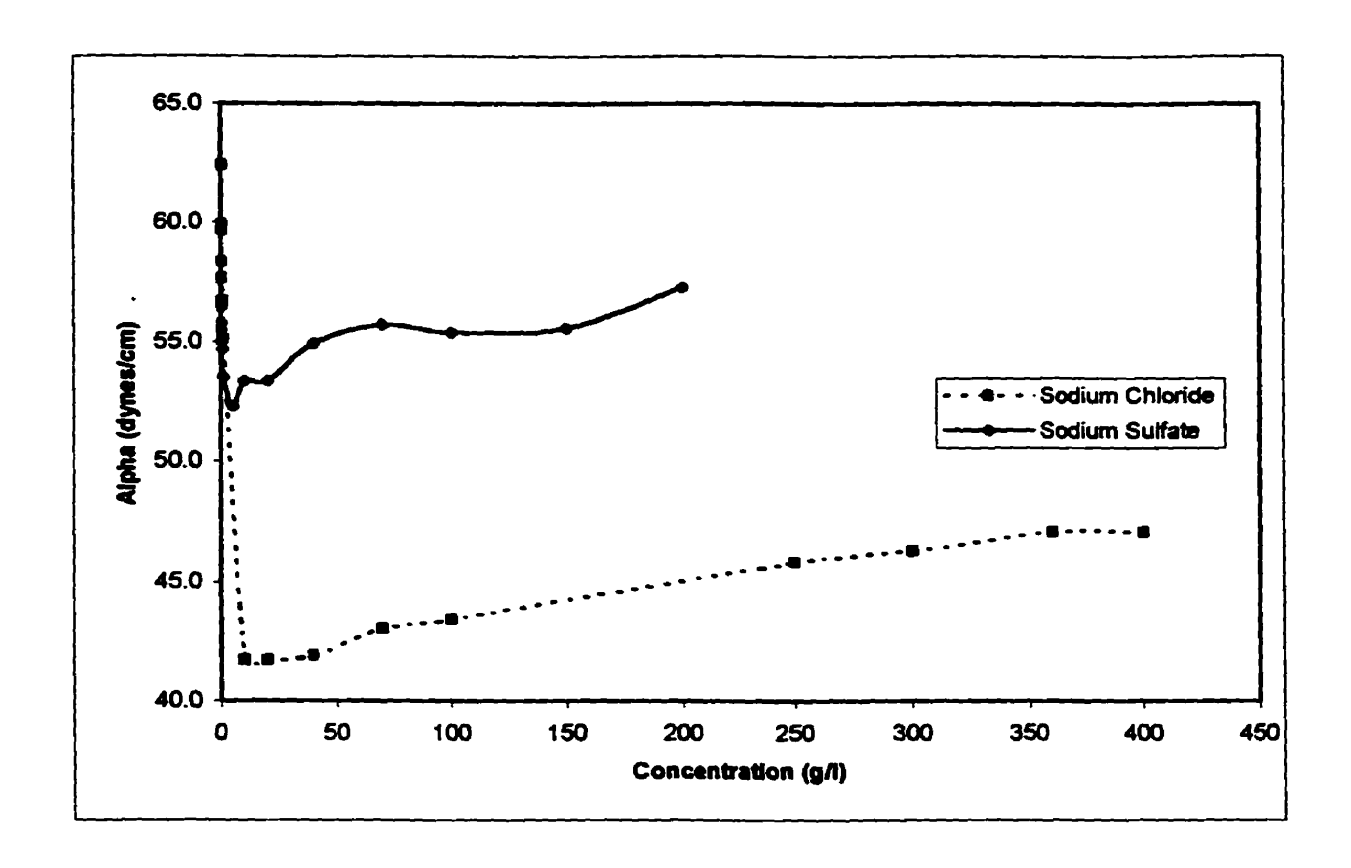


Figure $4.7 - \alpha$ as a function of concentration (borosilicate glass)

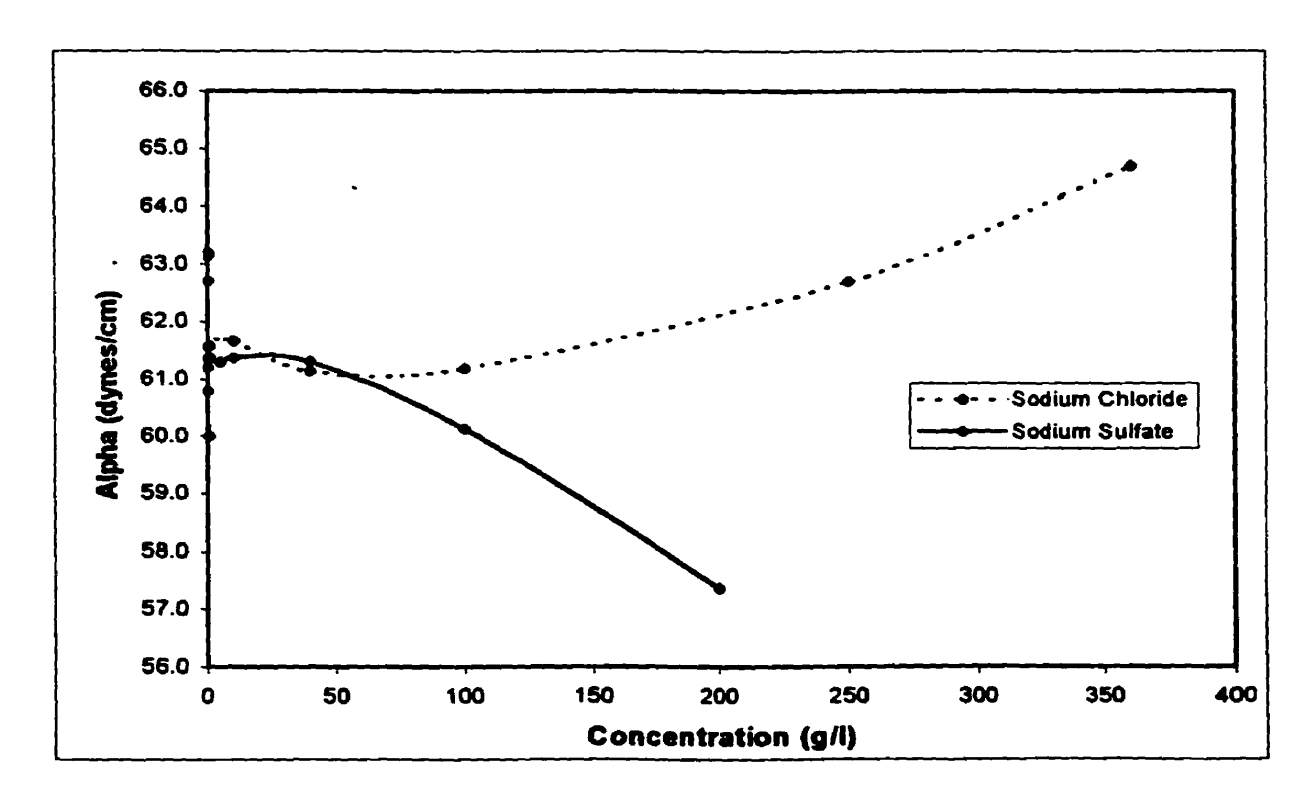


Figure 4.8 - α as a function of concentration (silicon)

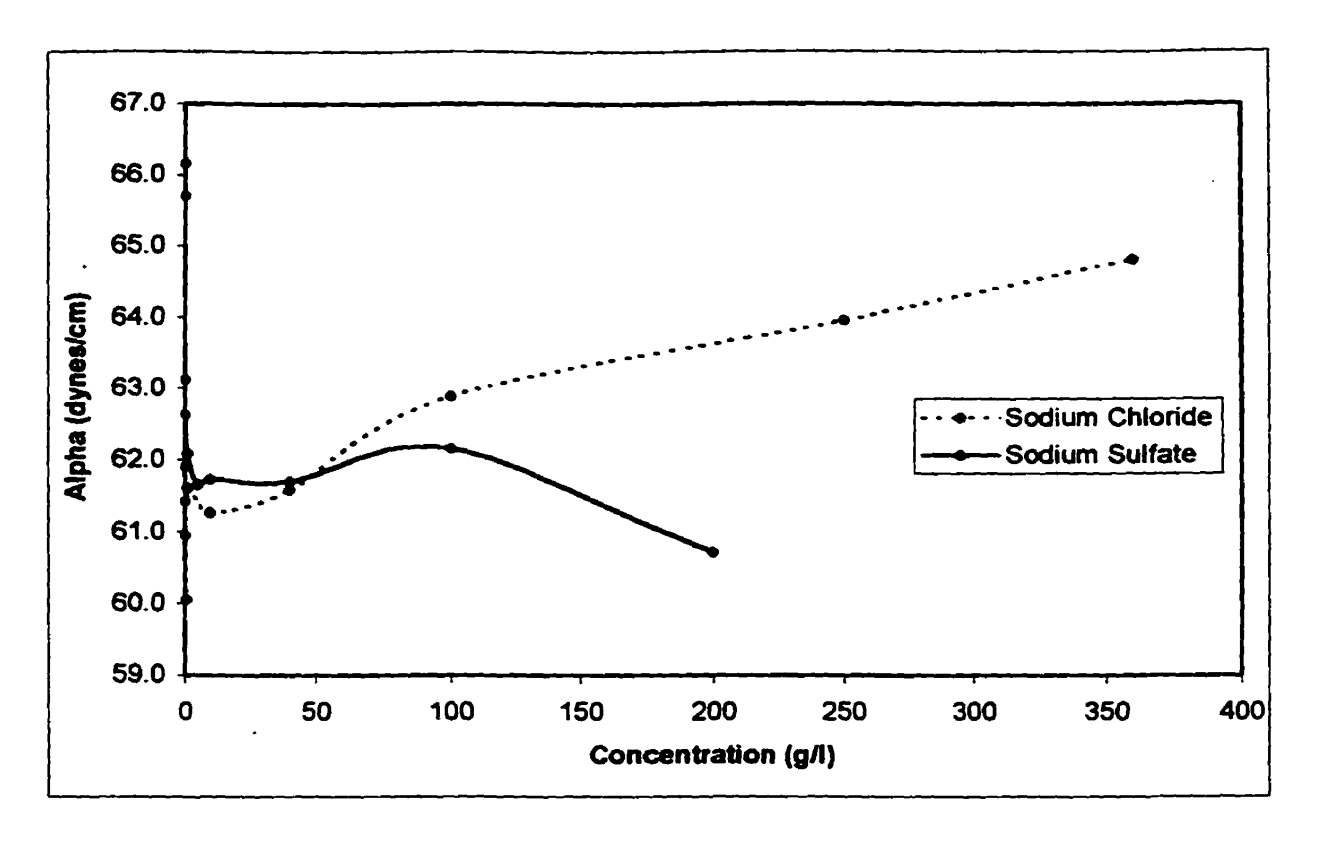


Figure 4.9 - α as a function of concentration (silicon dioxide)

The calculated values for the coefficient of spreading for both salt solutions on all surfaces were found to be negative in value, thus indicating that the solutions will not spread along the surface but will form an equilibrium angle.

4.4 Effect of Time on Contact Angle Measurements

A waiting period of 30 seconds was used to ensure that the liquid and solid surface have indeed reached an equilibrium before the contact angle was measured. Preliminary experiments, as shown by Figure 4.10, have indicated that roughly five to ten seconds was actually required for an equilibrium angle, θ_e , to be reached on all the various surfaces. The additional time was to allow for a margin of safety and to ensure that the angle was accurately θ_e . Also taken into account was the time required for the evaporation of the water droplets. As seen in Figure 4.11 and 4.12 the droplet height, width, and volume decrease in an almost linear fashion. The entire duration necessary for the complete evaporation of the droplet varied between 22 to 24 minutes. From Figure

43

4.13 it was observed that the contact angle for water on glass (during the evaporation of a droplet) was seen to continuously decrease from a high of 41 degrees to a low of 12 degrees, by definition the angles measured for the evaporating droplet are classified as the receding contact angle.

This indicates that when the equilibrium contact angle measurements were performed waiting 30 seconds before measuring the contact angle was sufficient to ensure that the system was in equilibrium, however it was short enough to neglect the effect of evaporation.

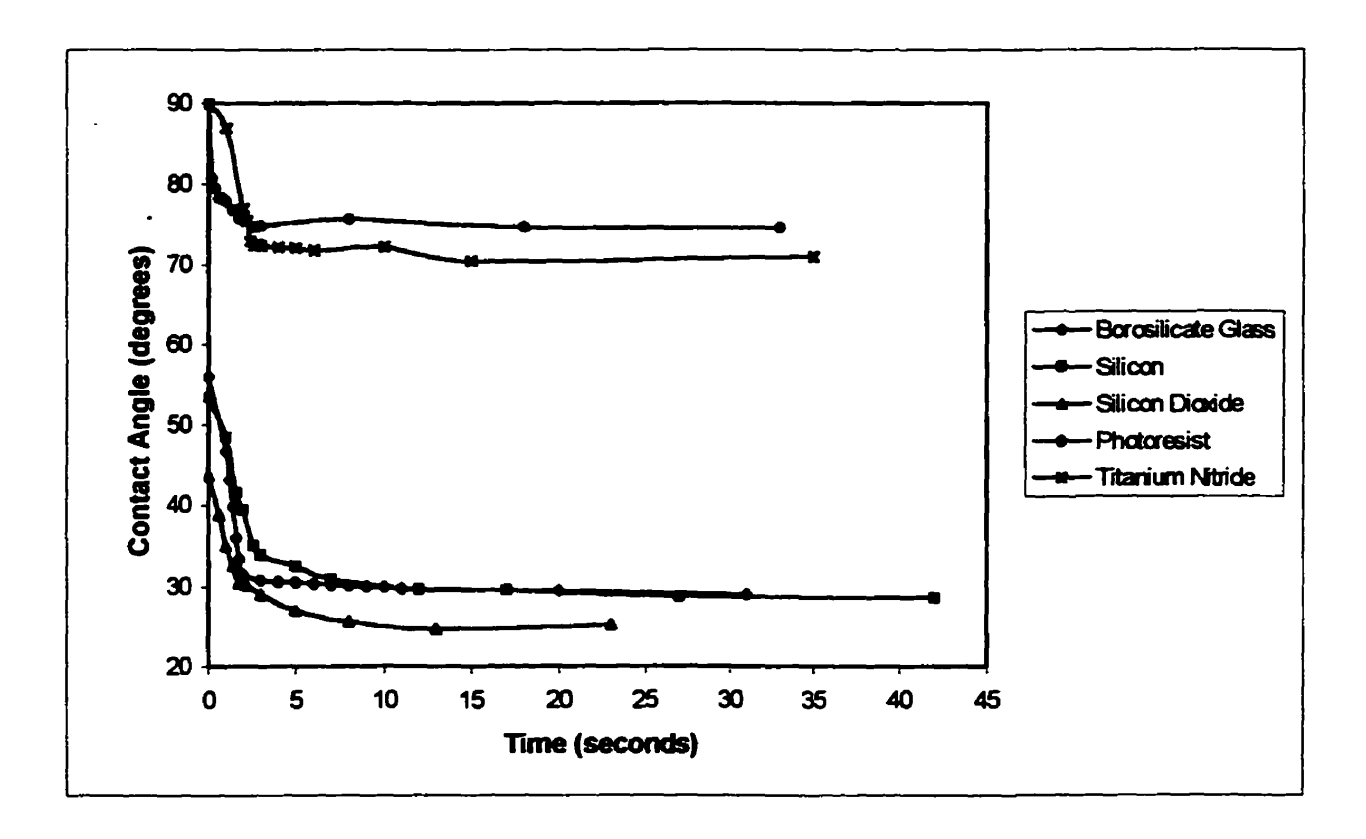


Figure 4.10 - Initial Wetting Dynamics (Temperature = 23-25°C)

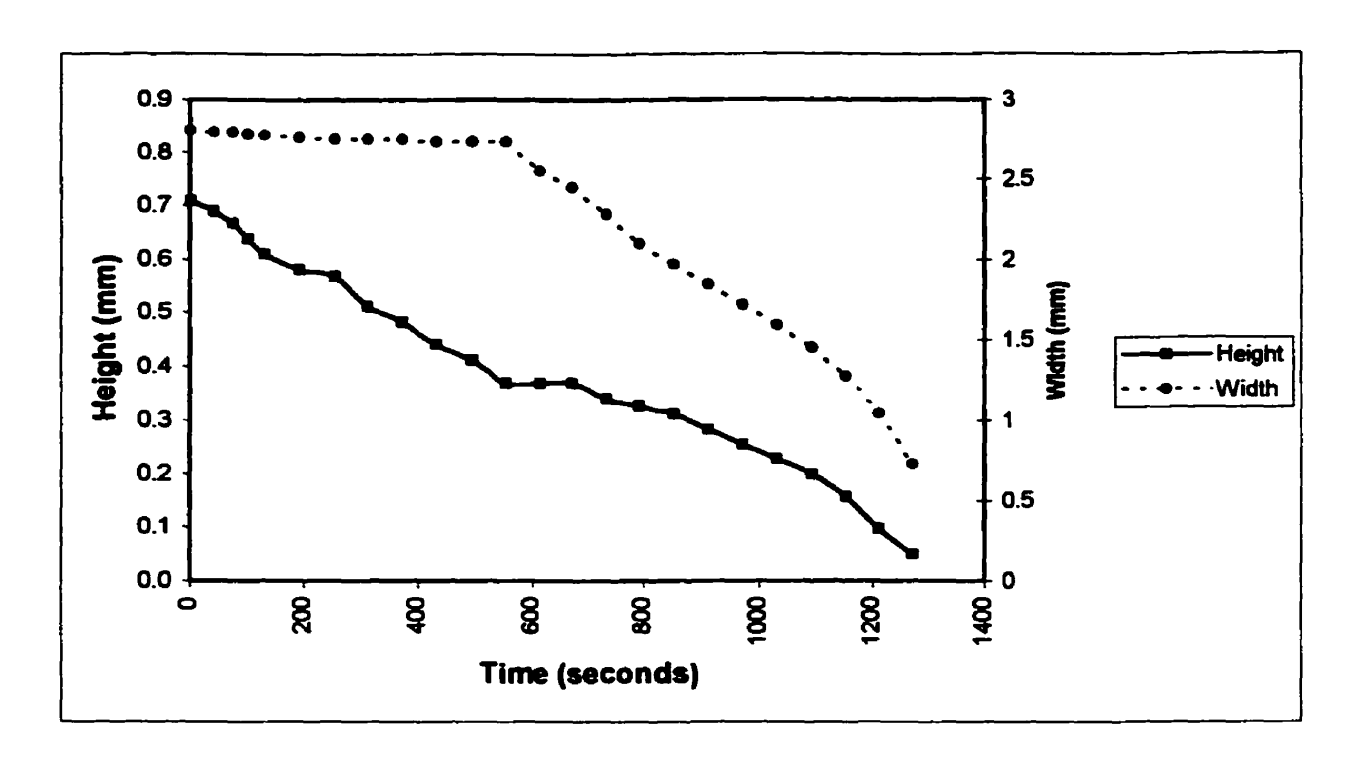


Figure 4.11 - Height and Width as a function of time (evaporating droplet) (water on borosilicate glass)

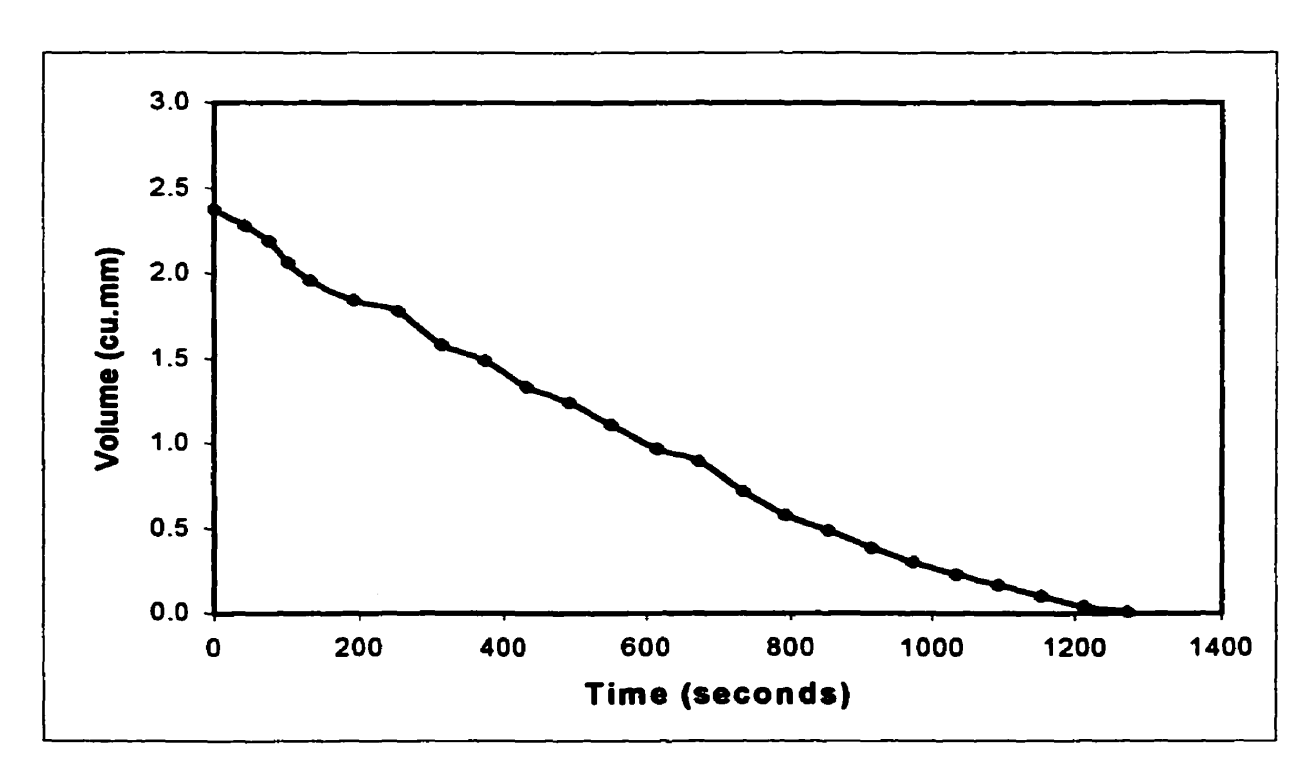


Figure 4.12 - Volume as a function of time (evaporating droplet) (water on borosilicate glass)

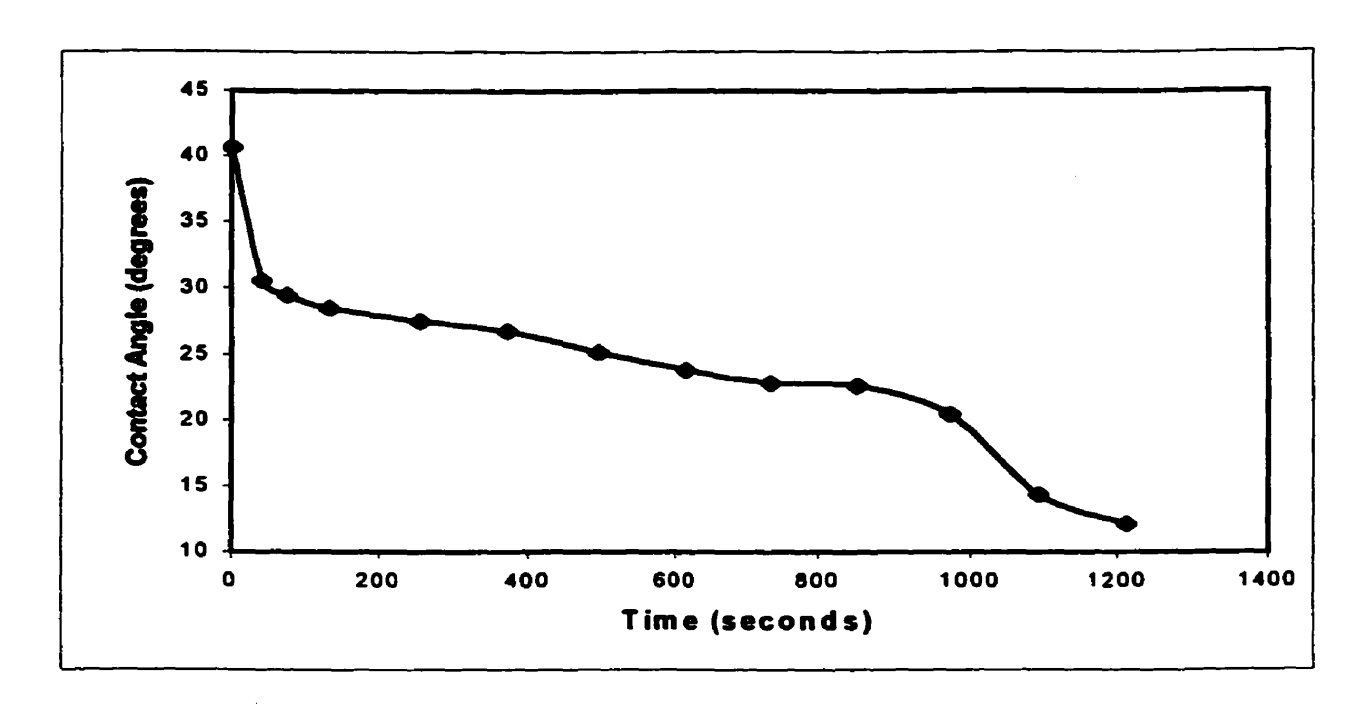


Figure 4.13 - Receding Contact Angle of an evaporating droplet (water on borosilicate glass)

4.5 Sodium Chloride and Sodium Sulfate Solution Characterization

The wetting and spreading kinetics are governed by the balance of three types of forces: gravity, viscous, and interfacial forces (liquid-solid and liquid-vapor). The importance of these forces is determined with three dimensionless numbers: the Bond number (Bo), Capillary number (Ca), and Weber number (We). From the volume of a droplet and the physical properties of the electrolyte solutions, the dimensionless numbers can be defined as (Fowkes, 1964);

Bond Number = gravity force / interfacial force

$$Bo = \frac{\rho g L^2}{\gamma} \tag{29}$$

Capillary Number = viscous force / interfacial force

$$Ca = \frac{\eta U}{\gamma} \tag{30}$$

Weber Number = inertial force / interfacial force

$$We = \frac{\rho U^2 L}{\gamma} \tag{31}$$

 ρ , η , γ , U, and L represent the density, viscosity, surface tension, droplet front line velocity, the characteristic length of the droplet, and g is the acceleration due to gravity, respectively.

For all aqueous solutions used in this study, the Bond, Capillary, and Weber numbers are less than one. When Bo is less than 1, the effect of gravity on the shape of the droplet is negligible, thus spherical sections can be assumed which provides credence to the volume equation which was being used to describe the droplet. When the capillary number is less than 1 (sm⁻¹). Since the velocity of the front line is likely to be much smaller than 1 ms⁻¹, Ca will remain less than 1 and the viscous forces can be neglected compared with the interfacial forces. Moreover, with We less than 1 the inertia force can be neglected as well.

4.6 Contact Angle Measurements

4.6.1 Contact Angle as a Function of Temperature

A majority of the experiments were performed with a base temperature of roughly that of room temperature (i.e. 20°C to 25°C) and it was assumed that there would be an insignificant temperature change between the base plate and the test surface, therefore, the two were considered to be at the same temperature.

As shown by the literature, the contact angle seems to vary very little with temperature. Studies on the temperature variation of contact angles are confined to ascertaining that close temperature control is unnecessary in measuring the angles. Adam and Elliot (1962) found no detectable variation for several aqueous solutions and various hydrocarbons between 20°C and 35°C. This is because it appears that temperature affects the surface tension and the adhesion to the solid to very nearly the same proportionate

extent. An increase in the thermal motions of the liquid is the cause of the decrease in its surface tension, and therefore in its work of cohesion, and the adhesion to the solid appears to be decreased in the same proportion.

4.6.2 Left and Right Contact Angle Consistency

The easiest way to show the consistency of the measured left and right contact angles is to examine the values obtained (for reference to the left and right angles see Chapter 3, section 3.7). In Figures 4.14 and 4.15 the left and right angles are similar to each other falling within a range of less than \pm 1 degree, which was common for all surfaces and salt solutions. The consistency of the left and right angles can be partially attributed to the environmental chamber being level.

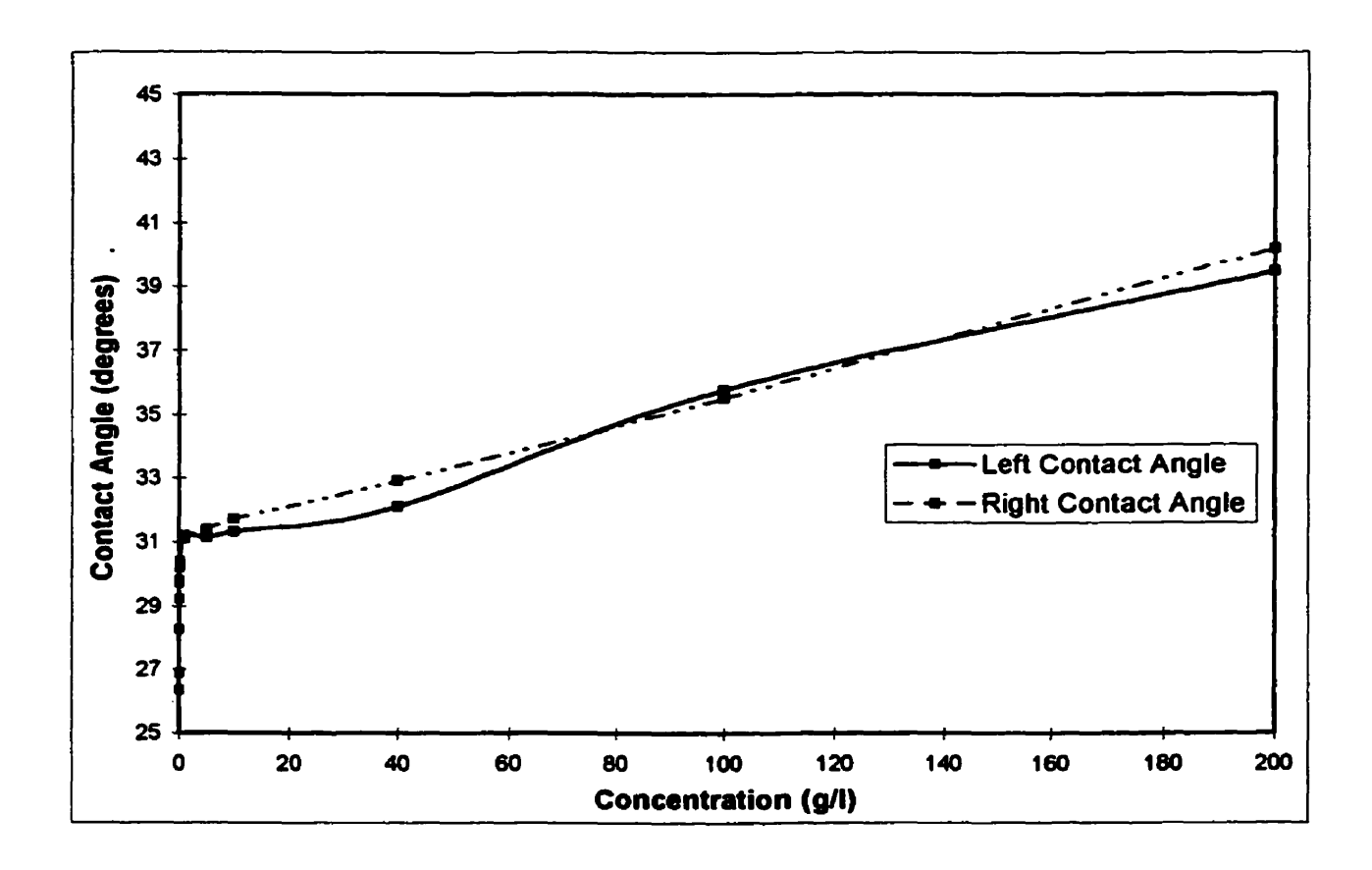


Figure 4.14 - Variation of left and right contact angle (Surface: silicon, Particle: sodium sulfate, T_{base} =20°C)

48

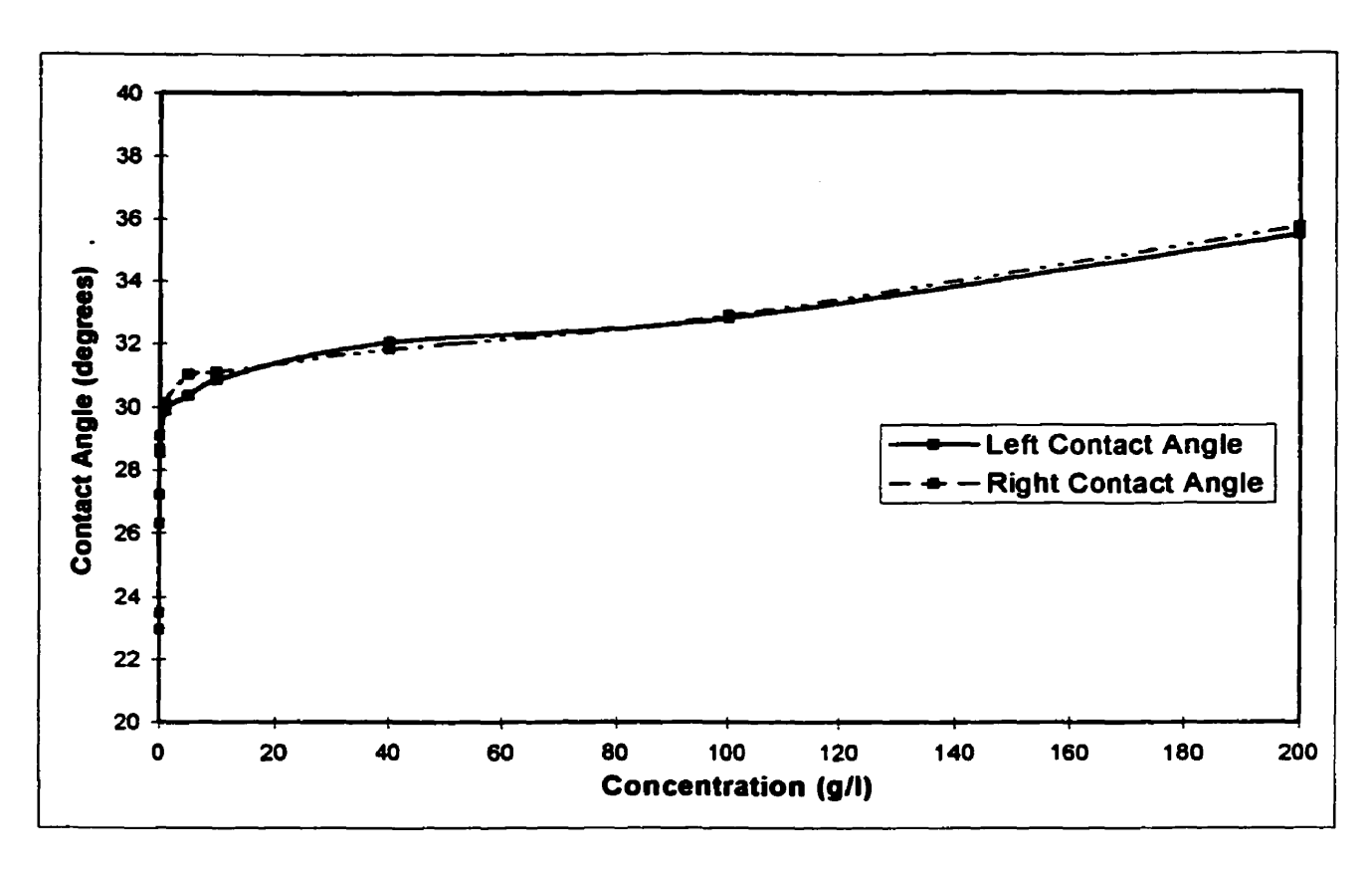


Figure 4.15 - Variation of left and right contact angle (Surface: silicon dioxide, Particle: sodium sulfate, T_{base}=20°C)

4.6.3 Equilibrium Contact Angle

The contact angle for distilled water was measured and compared to the values obtained from a personal communication (Garnier, 1998). Since glass is a high surface energy material it has the ability to adsorb low energy polar and non-polar vapors from the atmosphere or the environment. Furthermore because the contact angle may change depending on the cleaning technique, surface treatment, and chemical composition, consistent and accurate measurements are quite difficult and are subject to variation. The values which were measured produced an average angle of 29 degrees (at the above stated conditions) falling within the expected range.

The contact angle for a sodium chloride solutions on borosilicate glass were measured for a concentration range of 0 to 400 g/l (saturation limit at 360 g/l). The

measured angles were varied from 29 degrees (that of distilled water) and sharply increased until reaching a stable average value of 55 degrees (Figure 4.16).

For sodium sulfate the contact angle was measured over a concentration range of 0 to 200 g/l. The equilibrium contact angles varied from 29 degrees (that of distilled water) and increased until it reached an average value of 42 degrees (Figure 4.18).

In the figures below the reported values are the calculated average measured contact angles and the error bars represent the interval in which the 95% confidence interval falls.

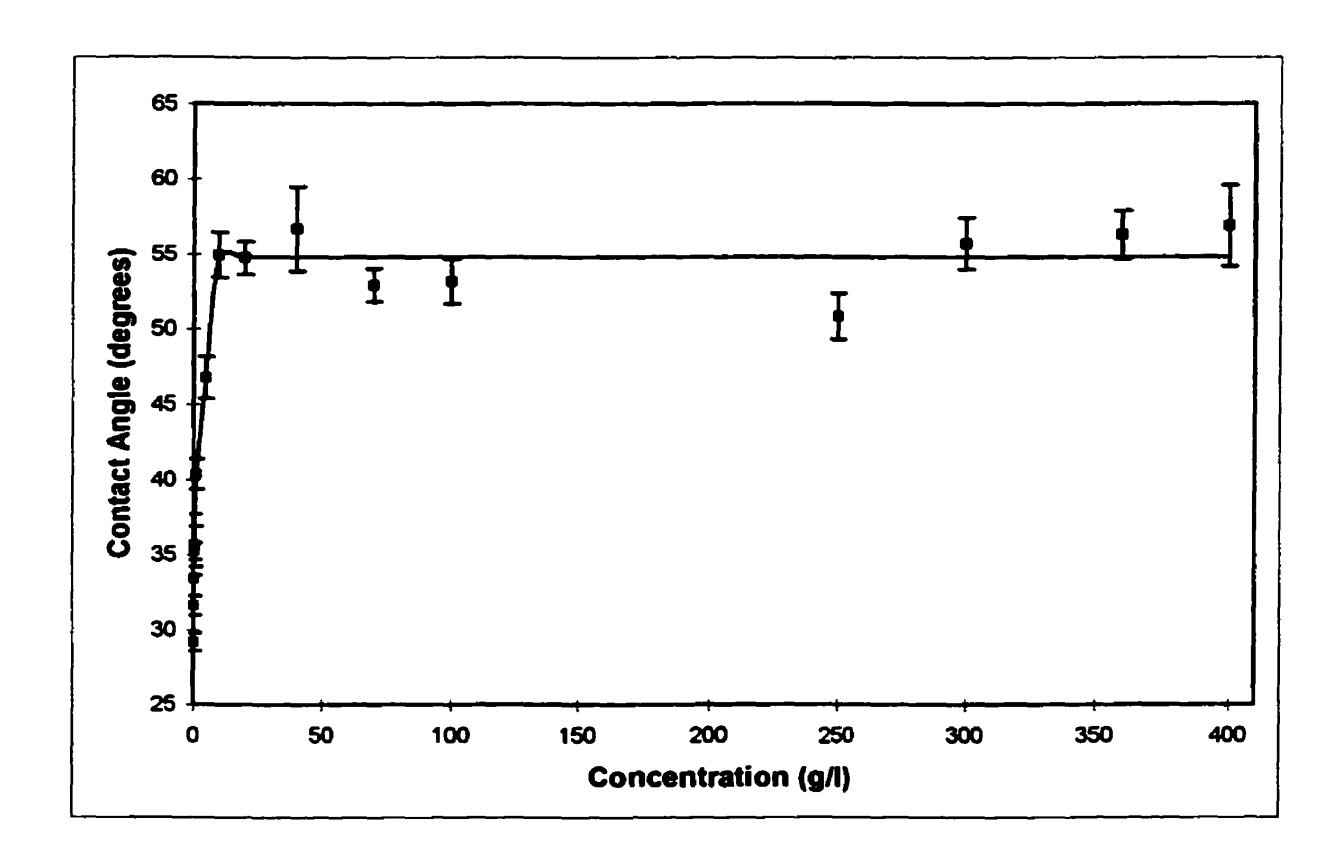


Figure 4.16 - Contact Angle as a function of Sodium Chloride Concentration (Surface: borosilicate glass, $T_{base} = 20^{\circ}$ C)

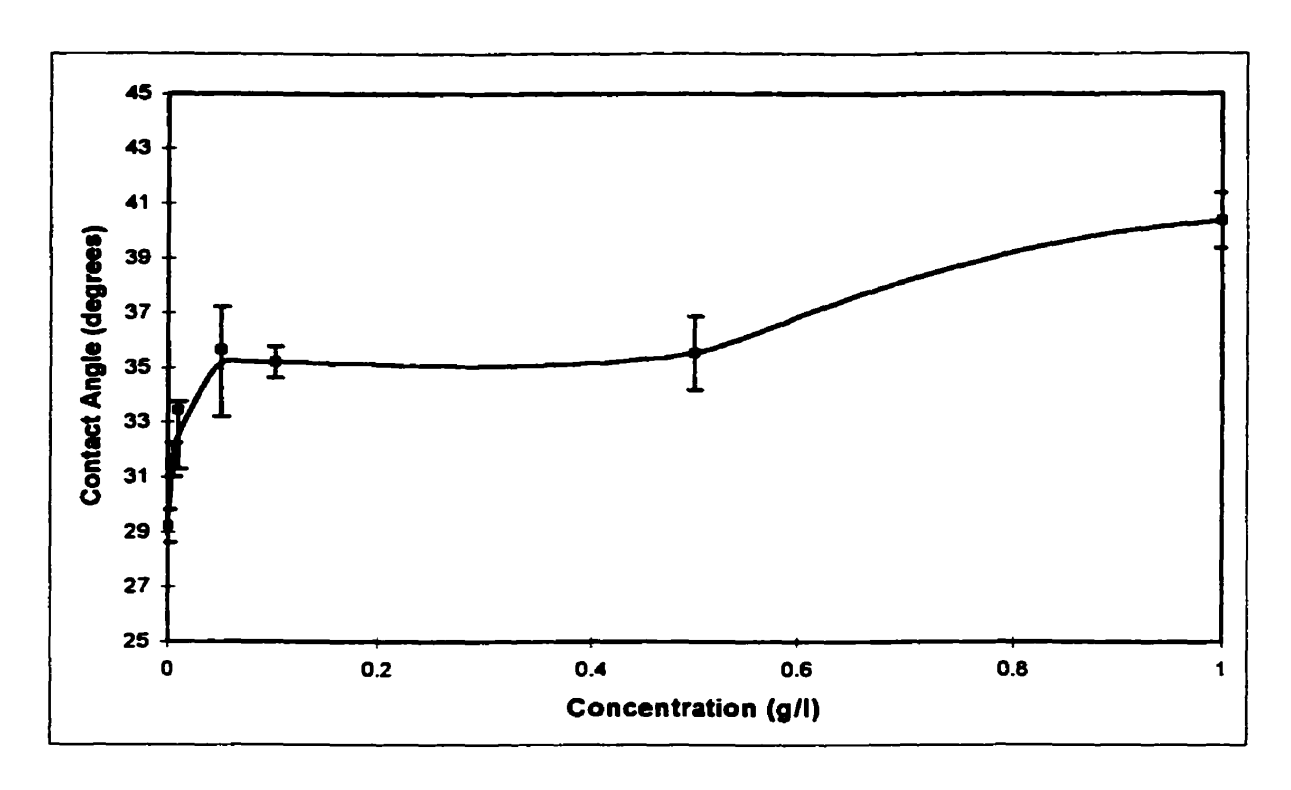


Figure 4.17 - Contact Angle as a function of Sodium Chloride Concentration (enlargement) (Surface: borosilicate glass, $T_{base} = 20^{\circ}$ C)

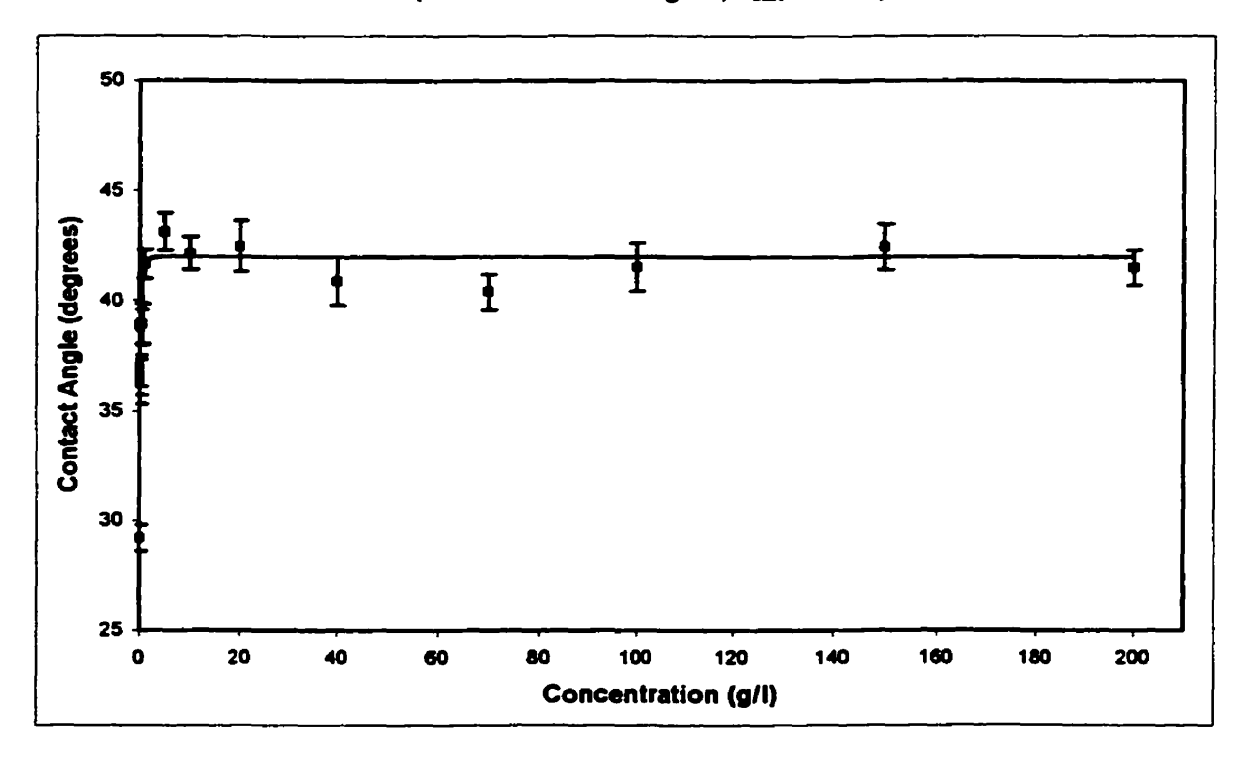


Figure 4.18 - Contact Angle as a function of Sodium Sulfate Concentration (Surface: borosilicate glass, $T_{base} = 20^{\circ}C$)

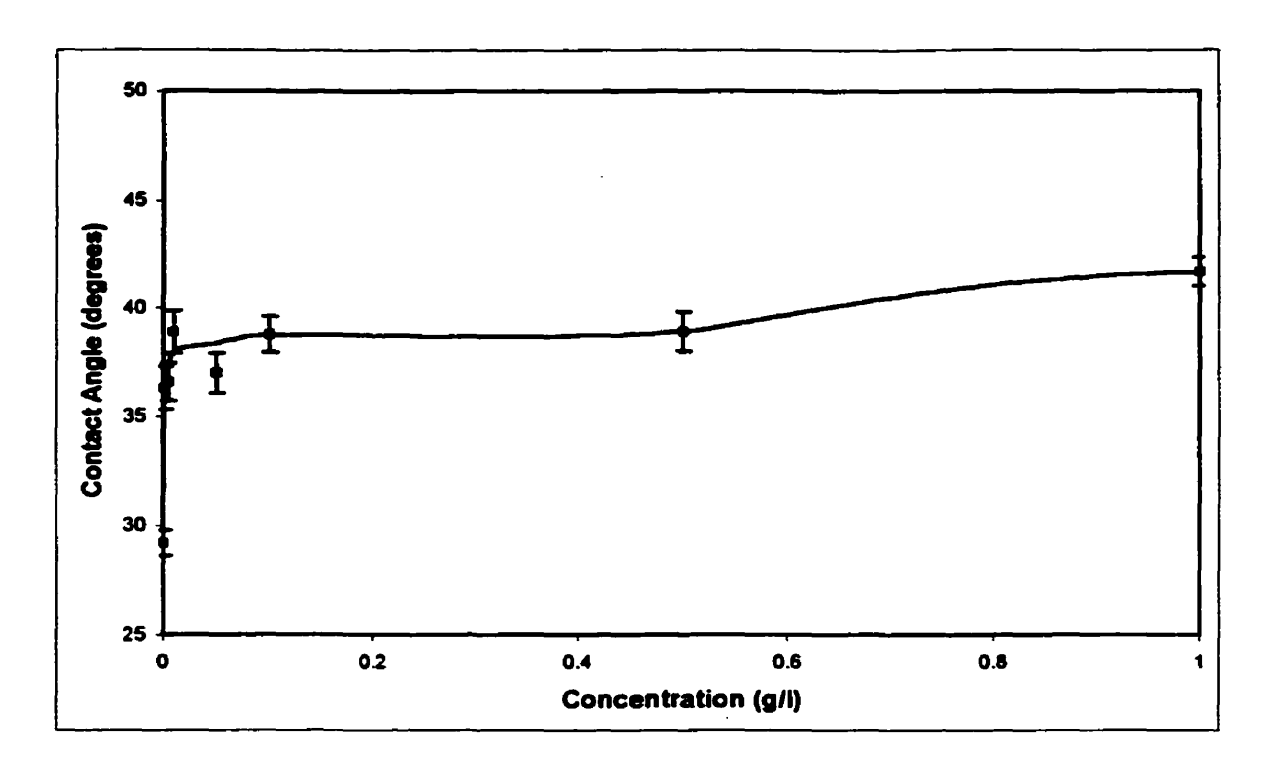


Figure 4.19 - Contact Angle as a function of Sodium Sulfate Concentration (enlargement) (Surface: borosilicate glass, T_{base} = 20°C)

With both sodium chloride and sodium sulfate when a dilute salt solution is present the contact angle varies substantially over a very small concentration range, increasing by almost 20 degrees, this increase in contact angle leads to a decrease in the wettability (spreading coefficient - Chapter 2, equations 2a to 2c) of the surface until a value of the salt concentration is reached beyond which any subsequent increase in the concentration has no effect. For the sodium sulfate solution this value was about 1 g/l, for sodium chloride beyond a concentration of 5 g/l there was no change in the contact angle or the wettability of the surface.

The contact angle for distilled water at 20°C on the semiconductor (wafer) surfaces was determined and the results were tabulated and shown in Table 4.3. When comparing the contact angles obtained on silicon and silicon dioxide to that of the glass one expects that the results should be similar to borosilicate glass since the latter is composed of 81% silicon dioxide. Compared to the monitor grade oxide wafer and the silicon production grade wafer it is indeed seen that the angles were similar.

Table 4.3 - Contact Angle Measurements of Water on Wafer Surfaces

TYPES OF SURFACES	CONTACT ANGLE (DEGREES)
Silicon Production Wafer	24 - 29
Silicon Production Wafer + RCA Clean	19
Monitor Grade Wafer	26
Monitor Grade Wafer + RCA Clean	23
Reclaimed Wafer	39
Reclaimed Wafer + RCA Clean	27
Oxide Wafer	23
Monitor Grade Wafer (with oxide layer)	30
Monitor Grade Wafer (with oxide layer etched off)	24
Photoresist	77
Titanium Nitride	76

The contact angles for both the sodium chloride and sodium sulfate solutions were measured on silicon and silicon dioxide as seen in Figures 4.20 to 4.27. Both salt solutions follow the same general type of behavior on both the silicon and silicon dioxide substrates. This behavior entails a low contact angle for distilled water (23-28°) and then a substantial increase of about 4 to 10 degrees over a 0 g/l to 1 g/l range (for both the sodium chloride and sodium sulfate solutions). After a concentration of roughly 1 g/l the contact angle increases over the remainder of the concentration range. At the end of the concentration range when saturation is achieved the contact angles were 35-37 degrees for the sodium chloride solution at 360 g/l on both silicon and silicon dioxide, whereas for the sodium sulfate solution (200 g/l) the contact angles vary from 35 degrees on the silicon dioxide substrate and 39-40 degrees on the silicon surface.

These results indicate that an increase in the salt concentration results in a decrease wettability of the surface, for all considered surfaces. Figures 4.28 and 4.29 show a comparison of the contact angles obtained for the three surfaces with the sodium chloride solution between 0-400g/l and sodium sulfate between 0-200g/l. These figures show that for the borosilicate glass, silicon, and silicon dioxide surfaces the contact angles change substantially at relatively low concentrations (less than 5 g/l) while at the

higher concentrations (greater than 10 g/l) they seemed to remain roughly constant varying less than five to ten degrees. The higher contact angle on borosilicate glass indicates that the surface is more hydrophobic than either the silicon or silicon dioxide and results in a decreased spreading.

The contact angle measurements on titanium nitride and photoresist for the salt solutions were not carried out over the entire concentration range as had been done with the other surfaces. This was in part due to the fact that it was observed that both surfaces were highly hydrophobic producing angles above 78 degrees for distilled water; thus the difference between contact angles for the low and high concentrations was very small.

In the figures below the values which are reported are the average measured contact angles and the error bars represent the interval in which the 95% confidence interval falls.

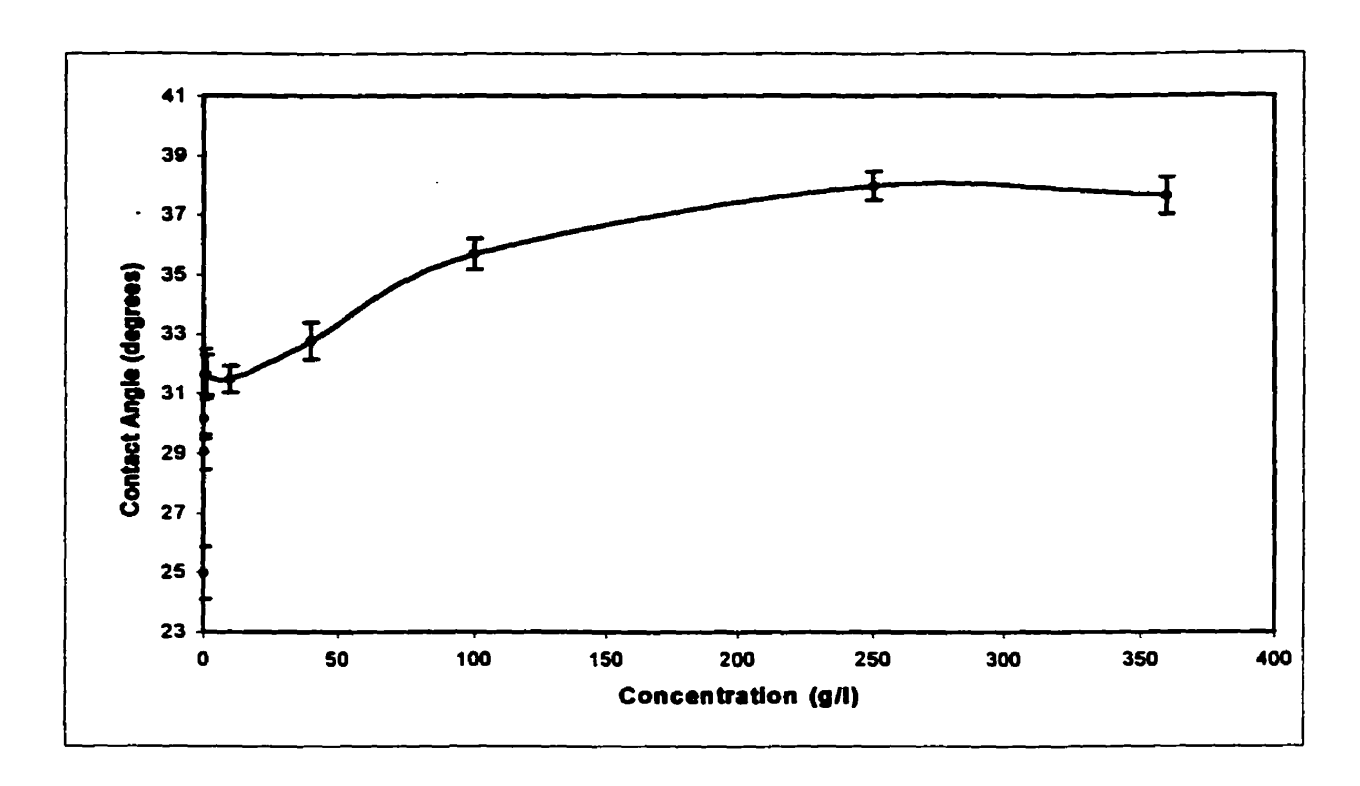


Figure 4.20 - Contact Angle as a function of Sodium Chloride Concentration (Surface: silicon, Particle: sodium chloride, $T_{base} = 20$ °C)

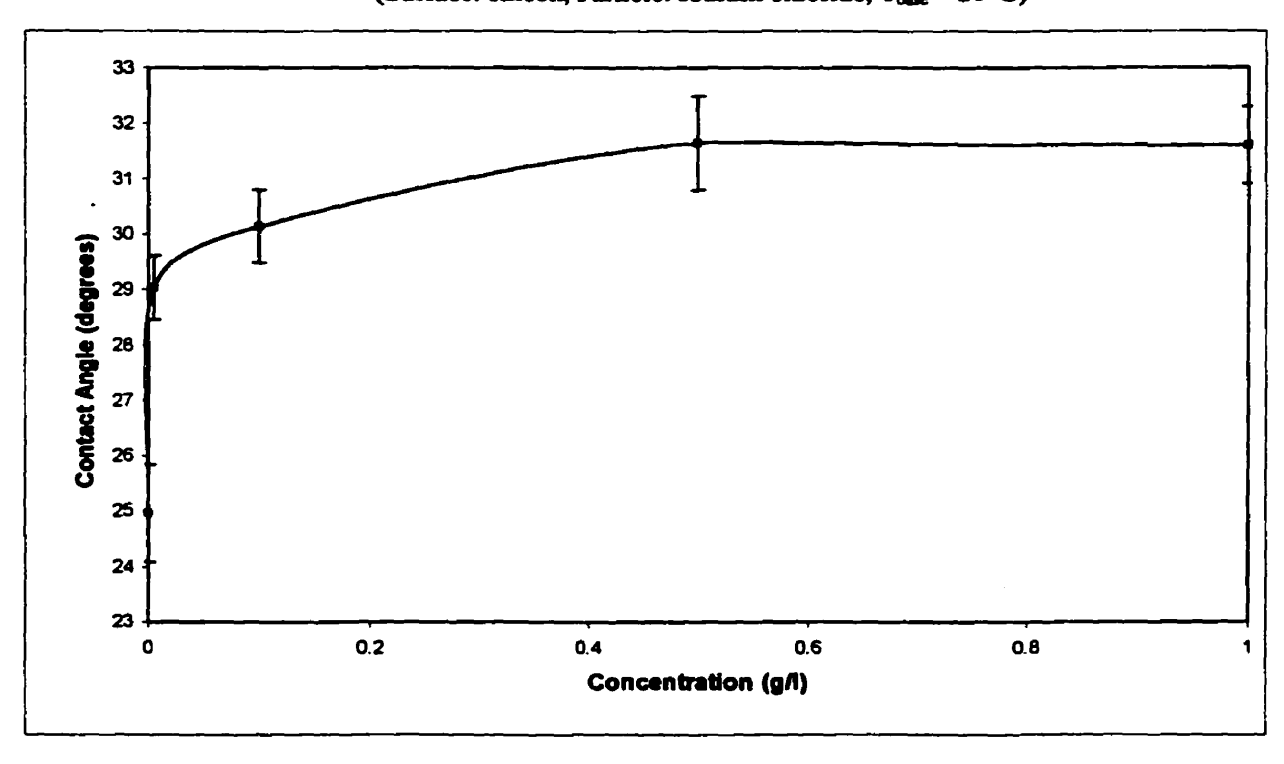


Figure 4.21 - Contact Angle as a function of Sodium Chloride Concentration (enlargement) (Surface: silicon, Particle: sodium chloride, $T_{beae} = 20$ °C)

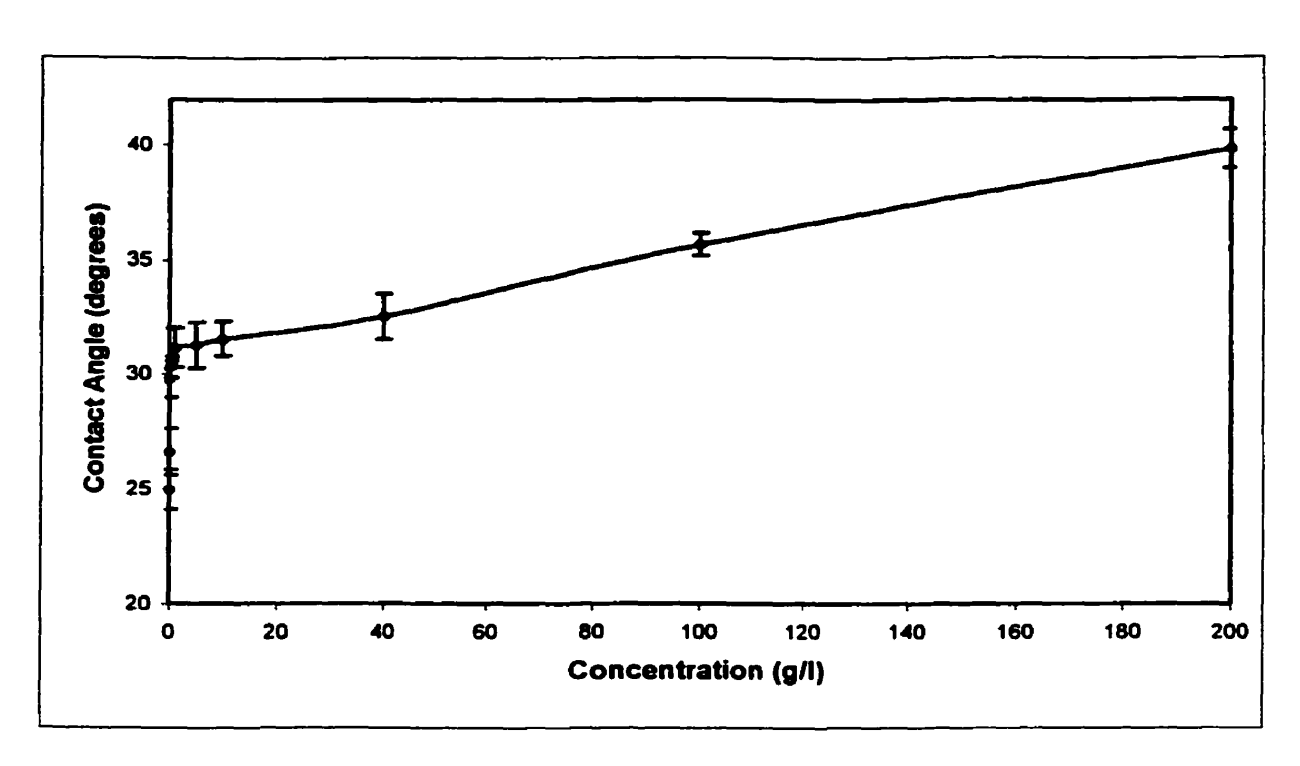


Figure 4.22 - Contact Angle as a function of Sodium Sulfate Concentration (Surface: silicon, Particle: sodium sulfate, $T_{base} = 20^{\circ}\text{C}$)

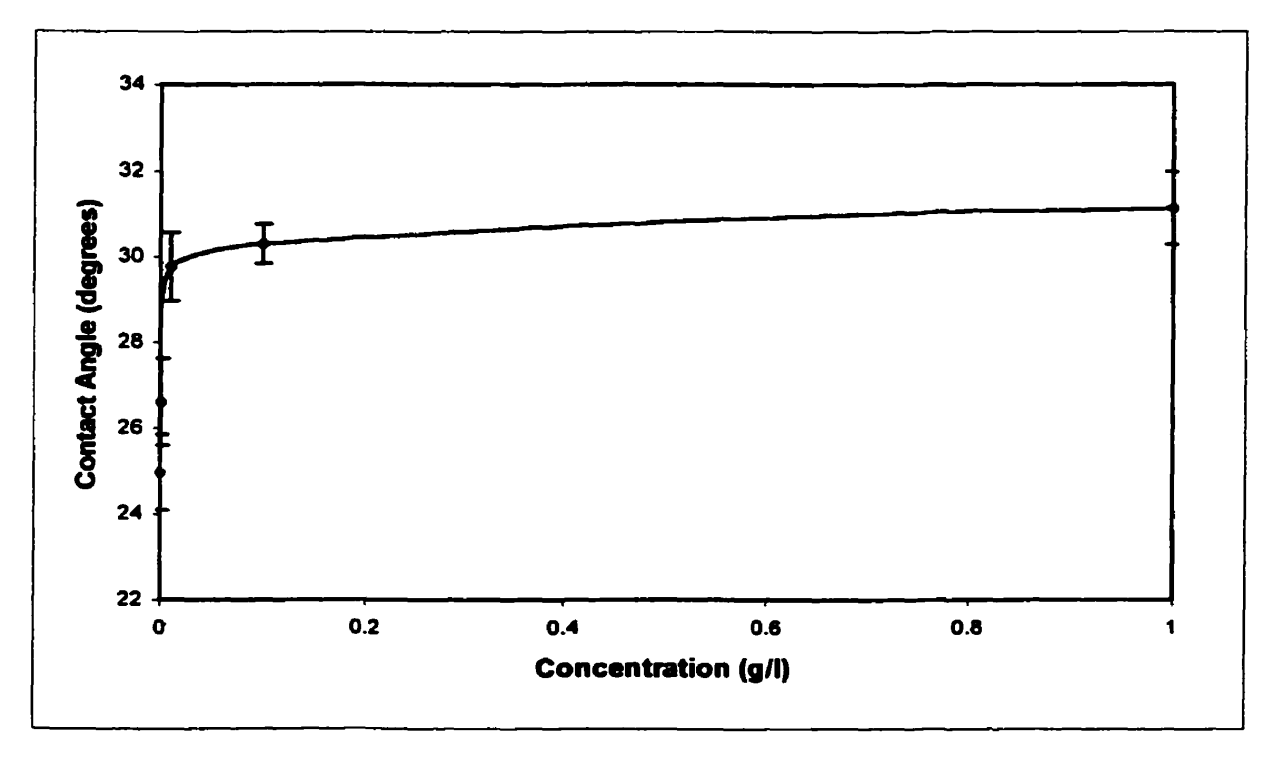


Figure 4.23 - Contact Angle as a function of Sodium Sulfate Concentration (enlargement) (Surface: silicon, Particle: sodium sulfate, $T_{base} = 20^{\circ}$ C)

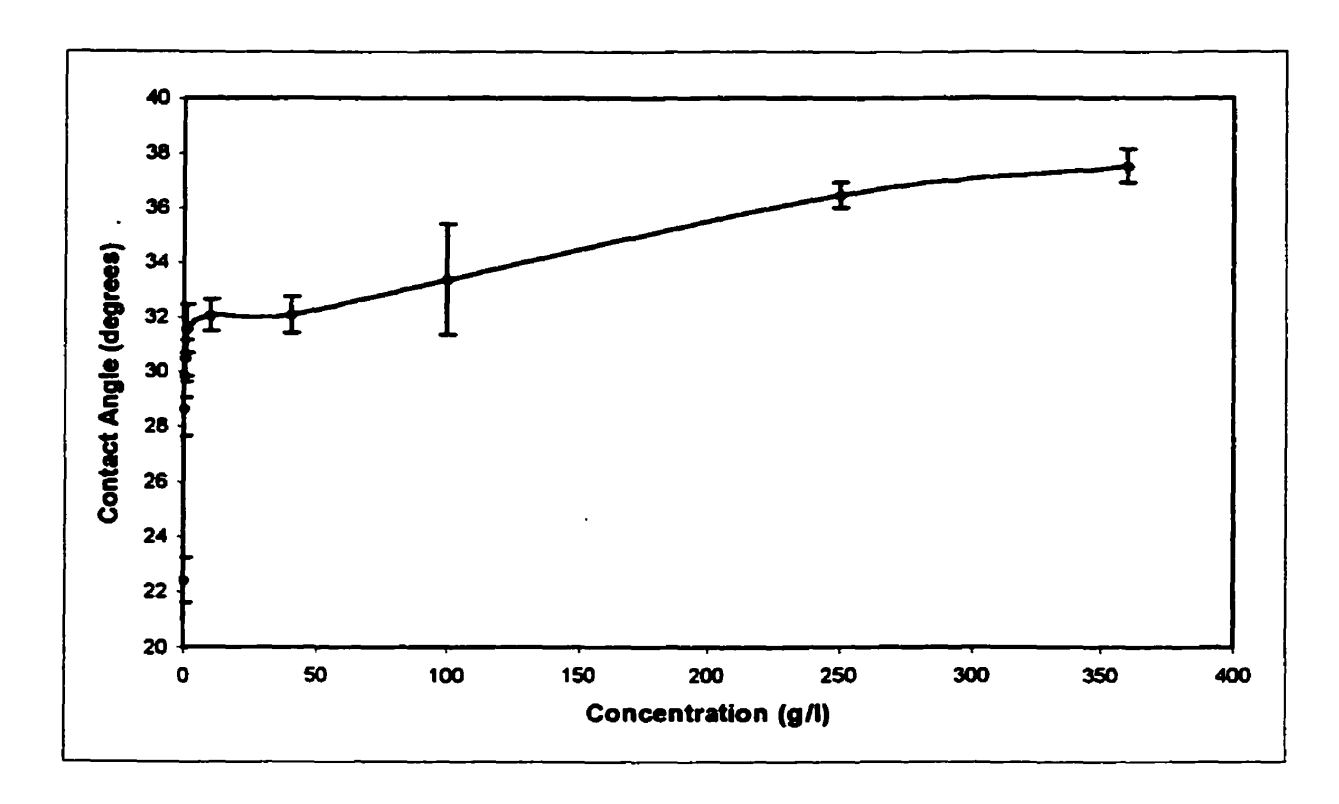


Figure 4.24 - Contact Angle as a function of Sodium Chloride Concentration at 20°C (Surface: silicon dioxide, Particle: sodium chloride, T_{base} = 20°C)

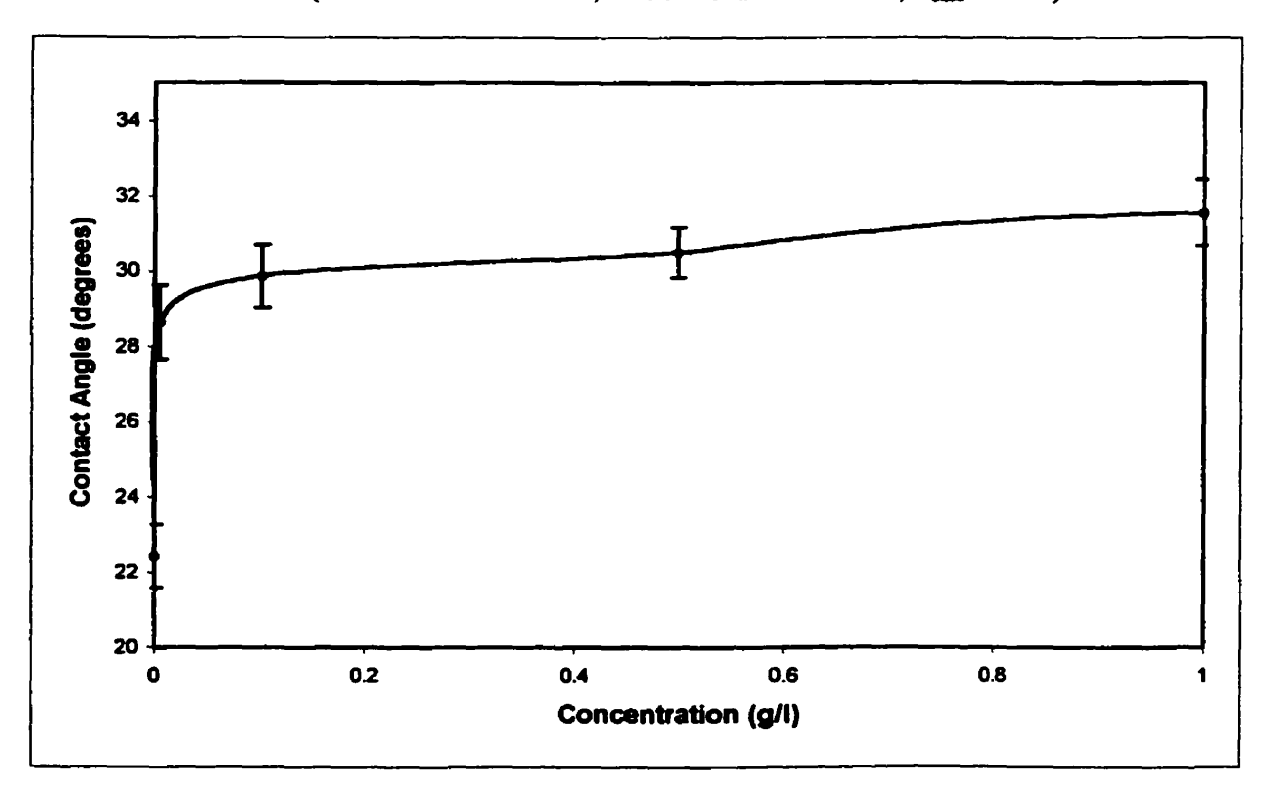


Figure 4.25 - Contact Angle as a function of Sodium Chloride Concentration (enlargement) (Surface: silicon dioxide, Particle: sodium chloride, $T_{base} = 20$ °C)

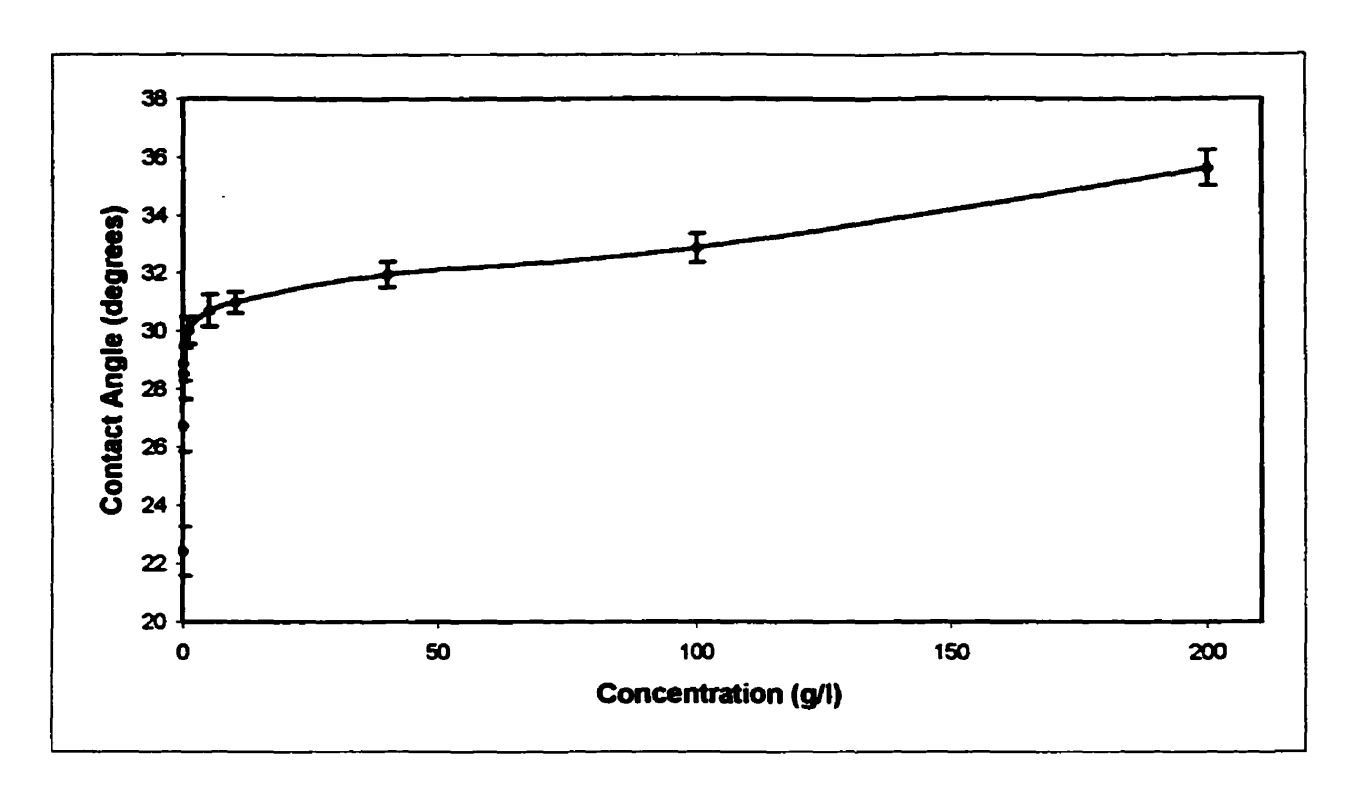


Figure 4.26 - Contact Angle as a function of Sodium Sulfate Concentration at 20°C (Surface: silicon dioxide, Particle: sodium sulfate, T_{base} = 20°C)

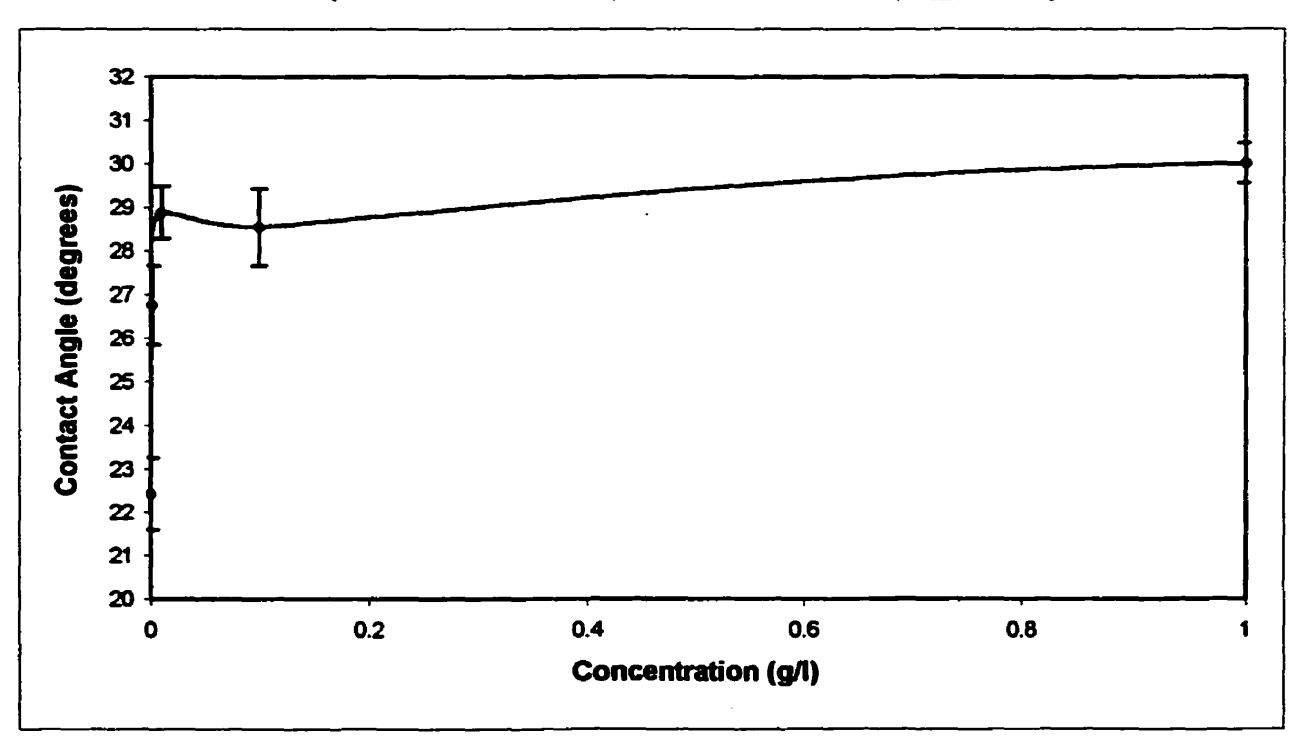


Figure 4.27 - Contact Angle as a function of Sodium Sulfate Concentration (enlargement) (Surface: silicon dioxide, Particle: sodium sulfate, $T_{best} = 20^{\circ}C$)

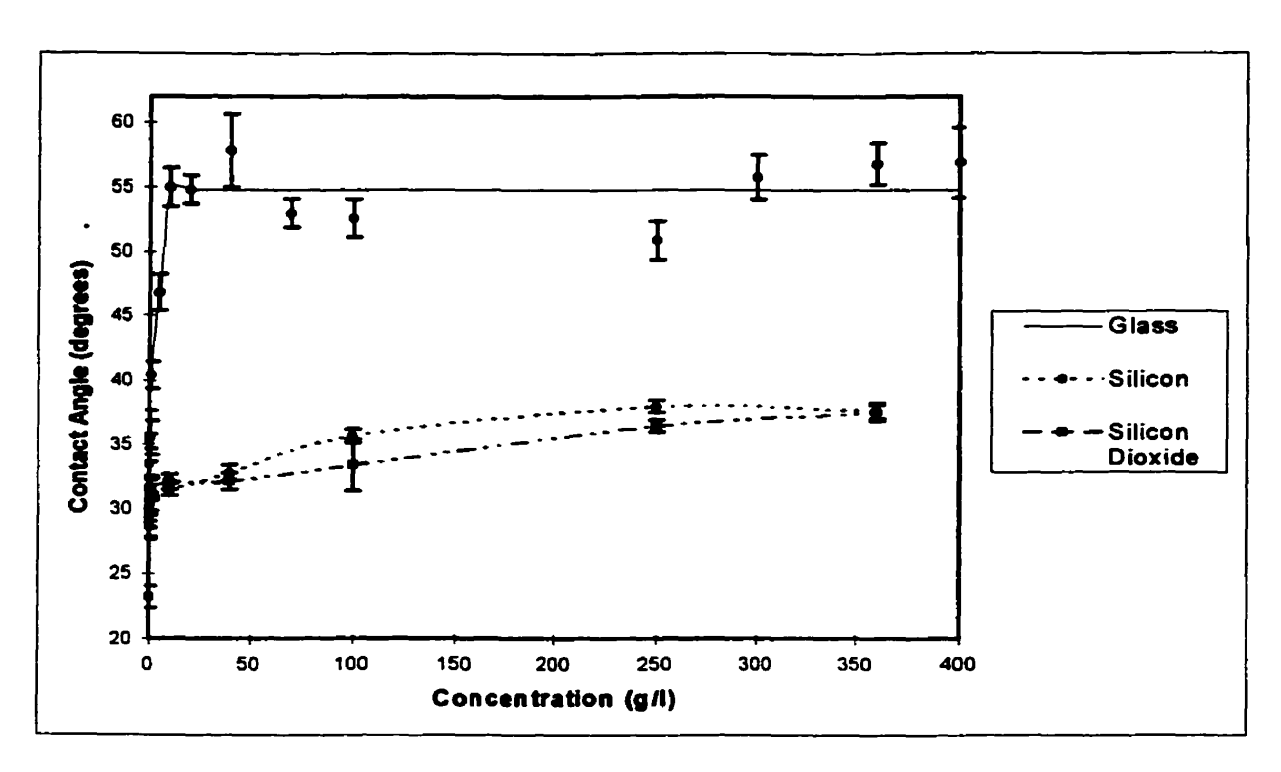


Figure 4.28 - Comparison of Contact Angles (Particle: sodium chloride, T_{base} = 20°C)

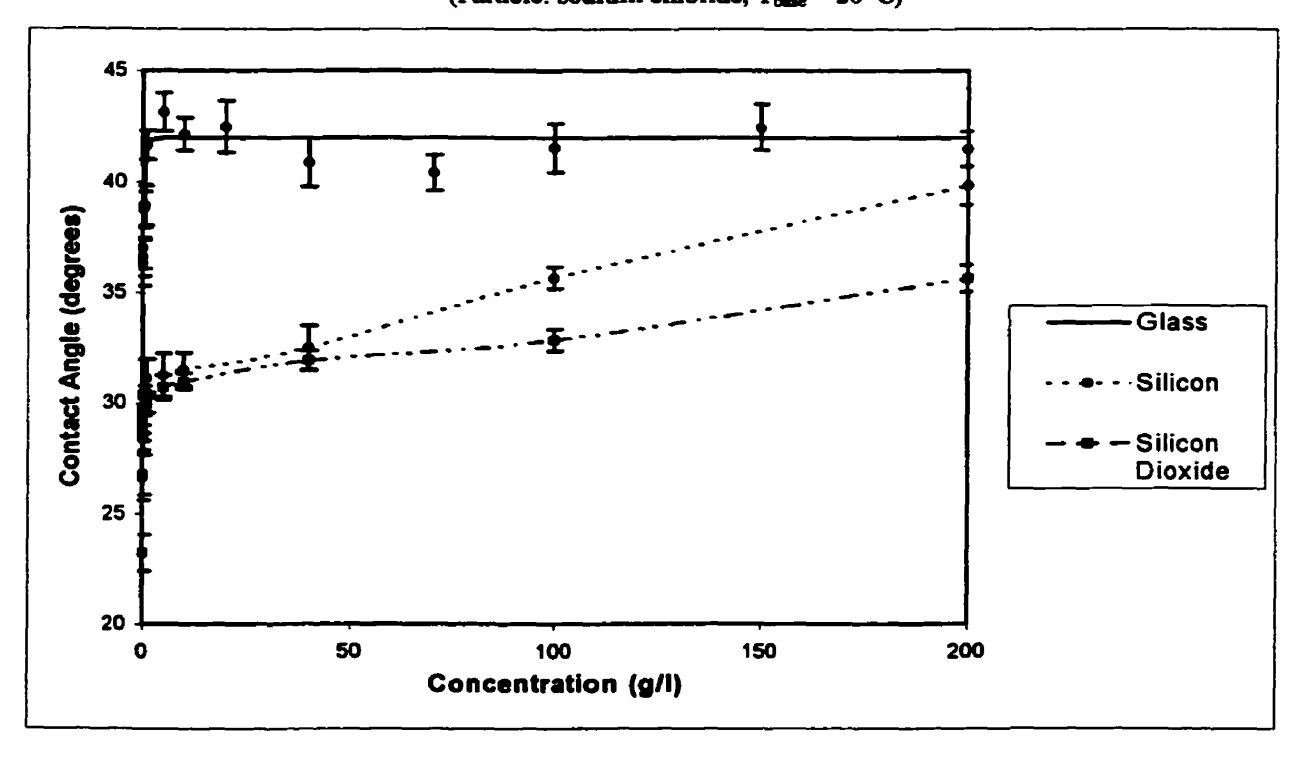


Figure 4.29 - Comparison of Contact Angles (Particle: sodium sulfate, $T_{base} = 20$ °C)

Chapter 5

Particle Detection - Results and Discussion

5.1 General Observations

The following chapter is divided into two general sub-sections; nucleation experiments on soluble particles and on insoluble particulate impurities. For the soluble particles a discussion of the observed droplet growth rates and the factors affecting them will be presented. This will be followed by a short discussion of the insoluble particulate impurities and the observed results.

There are three distinct stages of nucleation and condensation as seen in these experiments. Depending on the experimental conditions the following types of time dependent stages on the substrate were observed, (1) preferential nucleation on the particle, (2) thin layer of condensed water vapor on the substrate surface, and (3) overall surface condensation. In the first stage there was only preferential nucleation on the particle and no condensation on the rest of the surface. In the second, condensation began to occur on the surface, however only to a small extent. Several of the experimental conditions allowed for a thin layer of water to form on the surface. Even though this was undesirable, it was a condition that could be tolerated since it did not directly interfere with determining the location of the impurities because it was seen that a clear ring surrounded the particles in question. This phenomenon can be seen in Figure 5.1, where the condensed water droplet is 0.3mm in width and 0.08mm in height, while the edge of the clear ring is an addition 0.3mm from the edge of the droplet. This occurrence was seen to occur with soluble impurities and to some extent the insoluble contaminants. The clear rings surrounding the particles were anticipated especially for the soluble impurities where the concentration gradient would be partially responsible for the adsorption of the condensed surface water. To a lesser extent this was also observed to occur with insoluble particles where now the clear rings were formed solely by the adsorbed vapor molecules present on the solid surface joining the droplet probably by surface diffusion. In the third stage, a large amount of condensed water was present on the surface

obscuring all the contaminant particles making it impossible to determine if impurities were present. For the technique proposed in the thesis to be viable the first stage must occur, but the second would also be acceptable to a lesser extent.

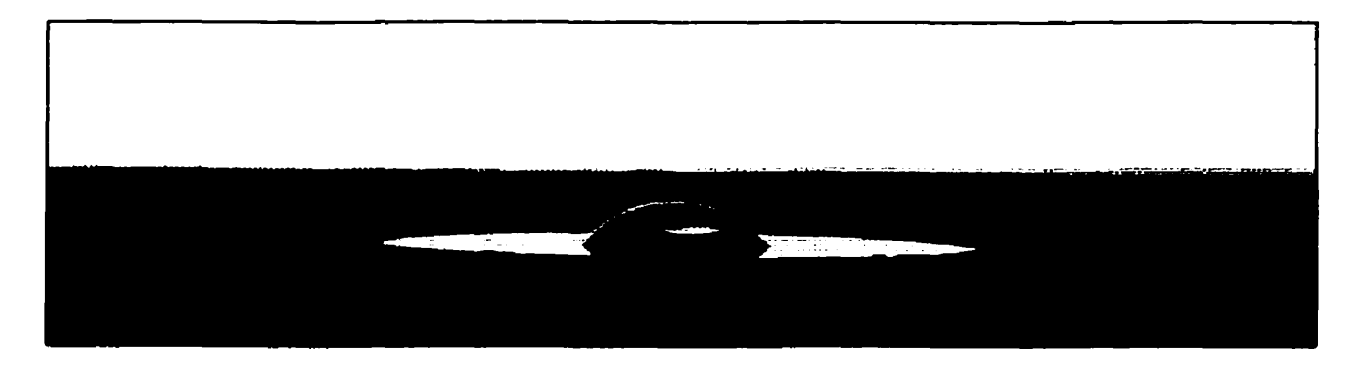


Figure 5.1 - Water droplet surrounded by a clear ring (Various Experimental Conditions)

5.2 Preliminary Experiments

The nitrogen gas flow rate had a specific value of 417 ml/min or 842 ml/min \pm 3% and will be referred to as either the low or high flow rate, respectively. The low flow rate was chosen as a limit, because during the initial optimization of the system it was found that for flow rates less than 417 ml/min the time for the nucleation and growth of the droplets on the particle was significantly longer. The upper limit of the flow rate was chosen since this was the maximum achievable flow rate with the current system.

The environmental chamber's base temperature had values between 20° C and 25° C, this range was determined during the preliminary phase of the experiments where initially the base temperature was varied between 15° C and 45° C. Both extremes of this range were found to produced conditions which were inhibitive to the nucleation experiments. At the lower temperature, condensation was found to occur over the entire surface regardless of the vapor temperature and type of surface material, as well as on the walls of the environmental chamber which caused the chamber to fill rapidly with water. At the higher temperature (45° C) condensation on the surface and the particles was hindered by the elevated base temperature. Furthermore, it was discovered that when there was condensation at a base temperature of 45° C the condensed water vapor went

through phases of adsorption and desorption, which resulted in a periodic variation of the droplet size and measured contact angle as shown in Figures 5.2 through 5.5.

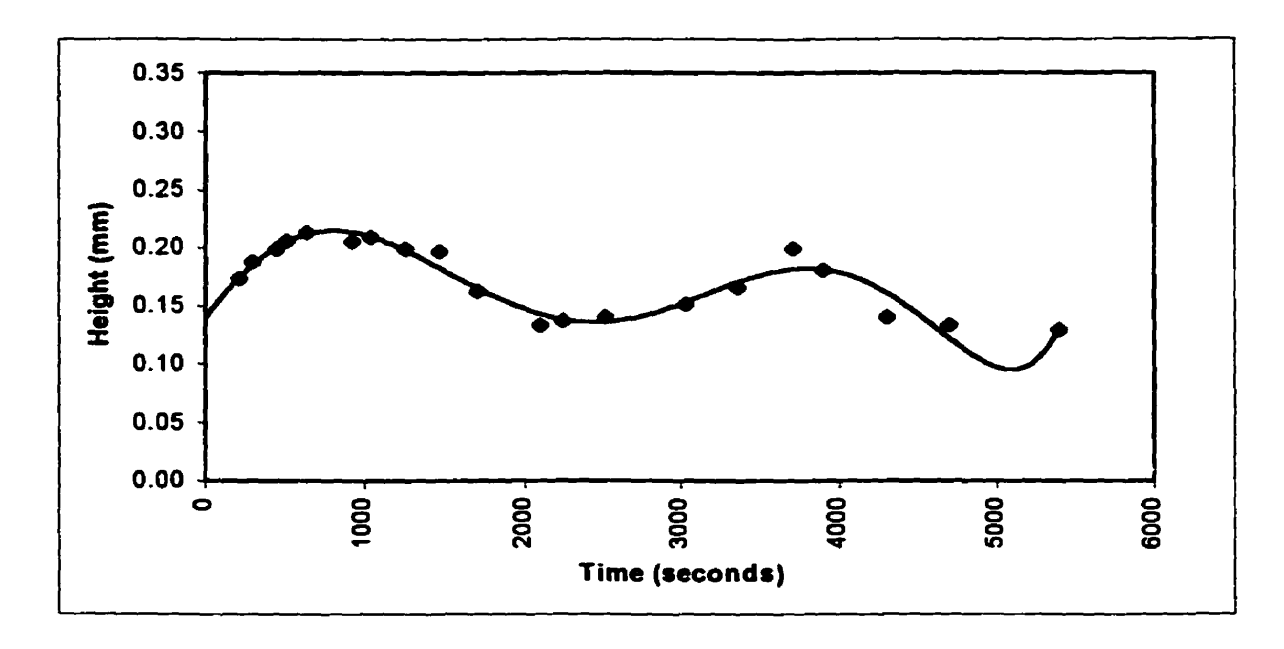


Figure 5.2 - Droplet height as a function of time (Surface: silicon, Particle: sodium chloride, $T_{base} = 45^{\circ}\text{C}$, $T_{vapor} = 56^{\circ}\text{C}$, $Q_{N2} = 417 \text{ ml/min}$)

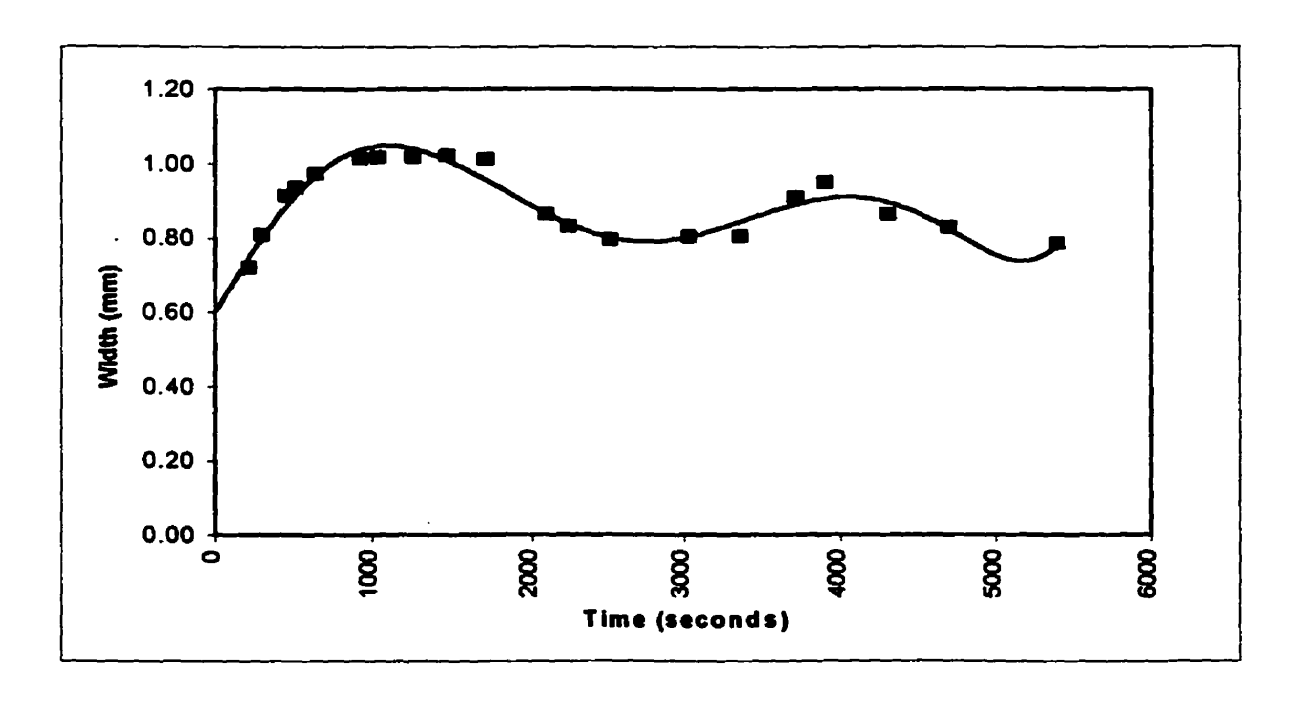


Figure 5.3 - Droplet width as a function of time (Surface: silicon, Particle: sodium chloride, $T_{base} = 45^{\circ}\text{C}$, $T_{vapor} = 56^{\circ}\text{C}$, $Q_{N2} = 417 \text{ ml/min}$)

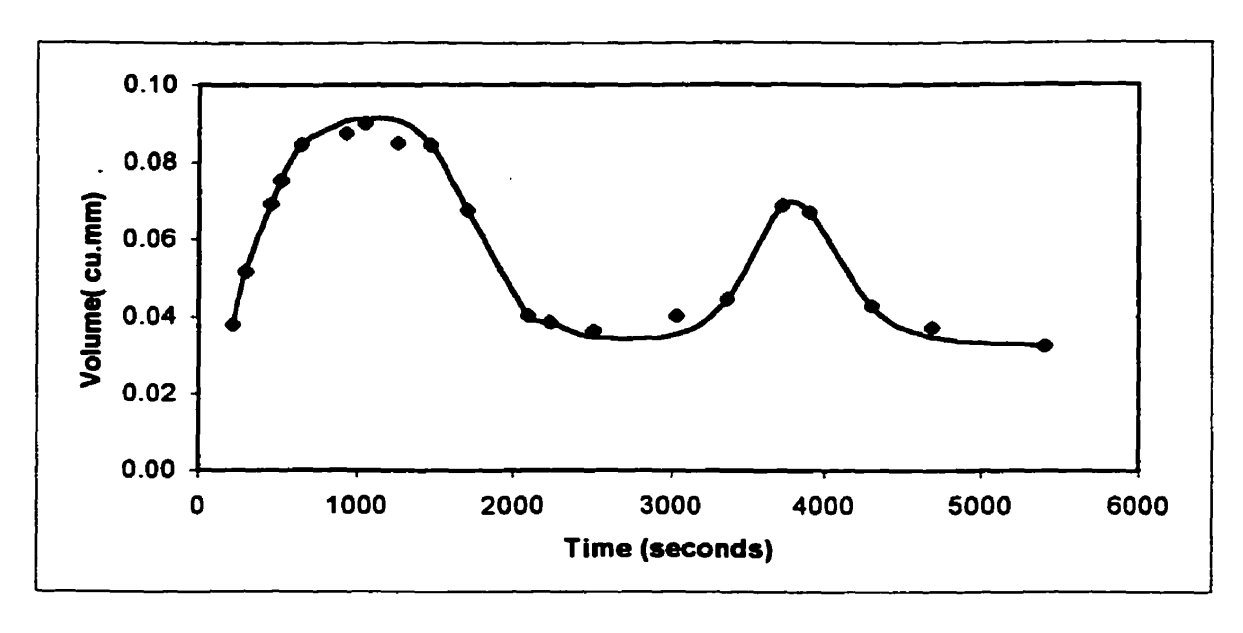


Figure 5.4 - Droplet volume as a function of time (Surface: silicon, Particle: sodium chloride, $T_{base} = 45$ °C, $T_{vapox} = 56$ °C, $Q_{N2} = 417$ ml/min)

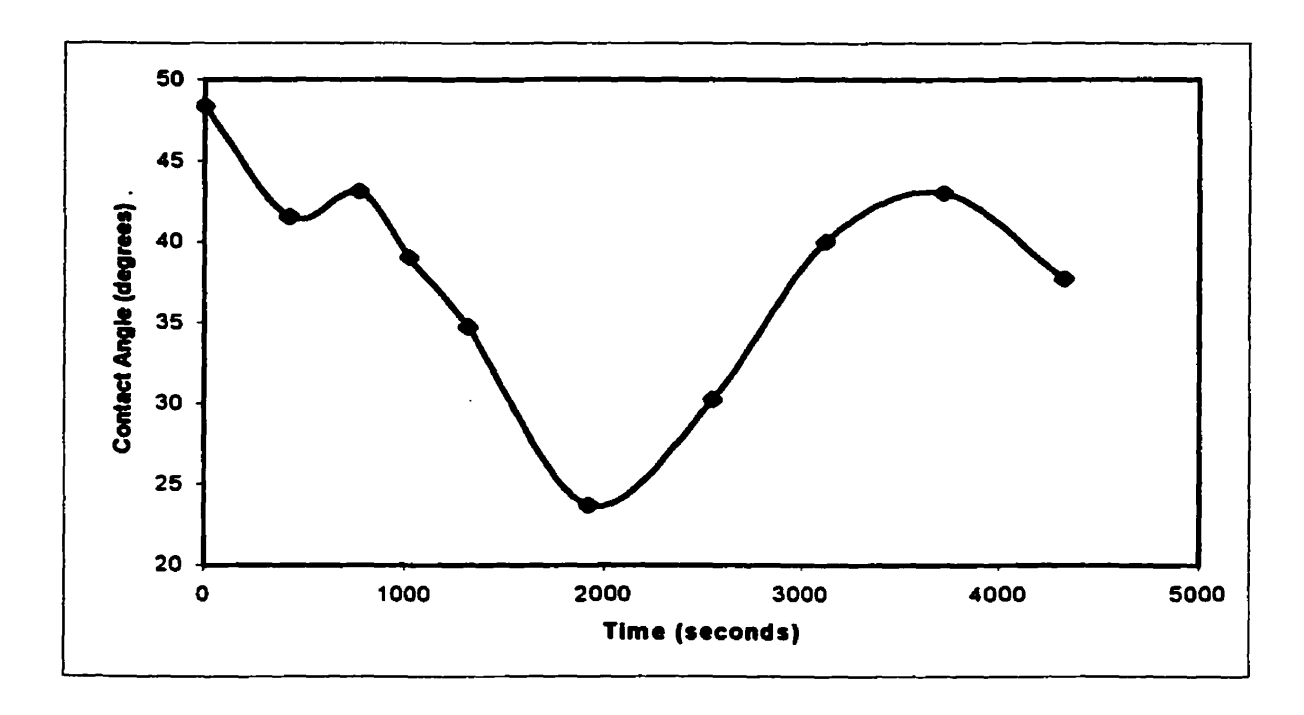


Figure 5.5 - Contact Angle as a function of time (Surface: silicon, Particle: sodium chloride, $T_{base} = 45$ °C, $T_{vapor} = 56$ °C, $Q_{N2} = 417$ ml/min)

For the vapor temperature, a range from between 30°C to 90°C (in increments of 10°C) was used in order to produce varying ΔT values in order to cover the largest range of values.

5.3 Droplet Height & Width Trends (For Soluble Particles)

From the nucleation experiments on water soluble particles, when the height and width of the droplet are plotted against time, an increasing trend is observed as seen by Figures 5.6 and 5.7. The rates of change of the height (dh/dt) and width (dw/dt) as shown by Figure 5.8 were determined by taking the derivative of the regression equations. From these two rates, the growth rate of the droplet volume (dV/dt) was calculated (Chapter 3, equation 28).

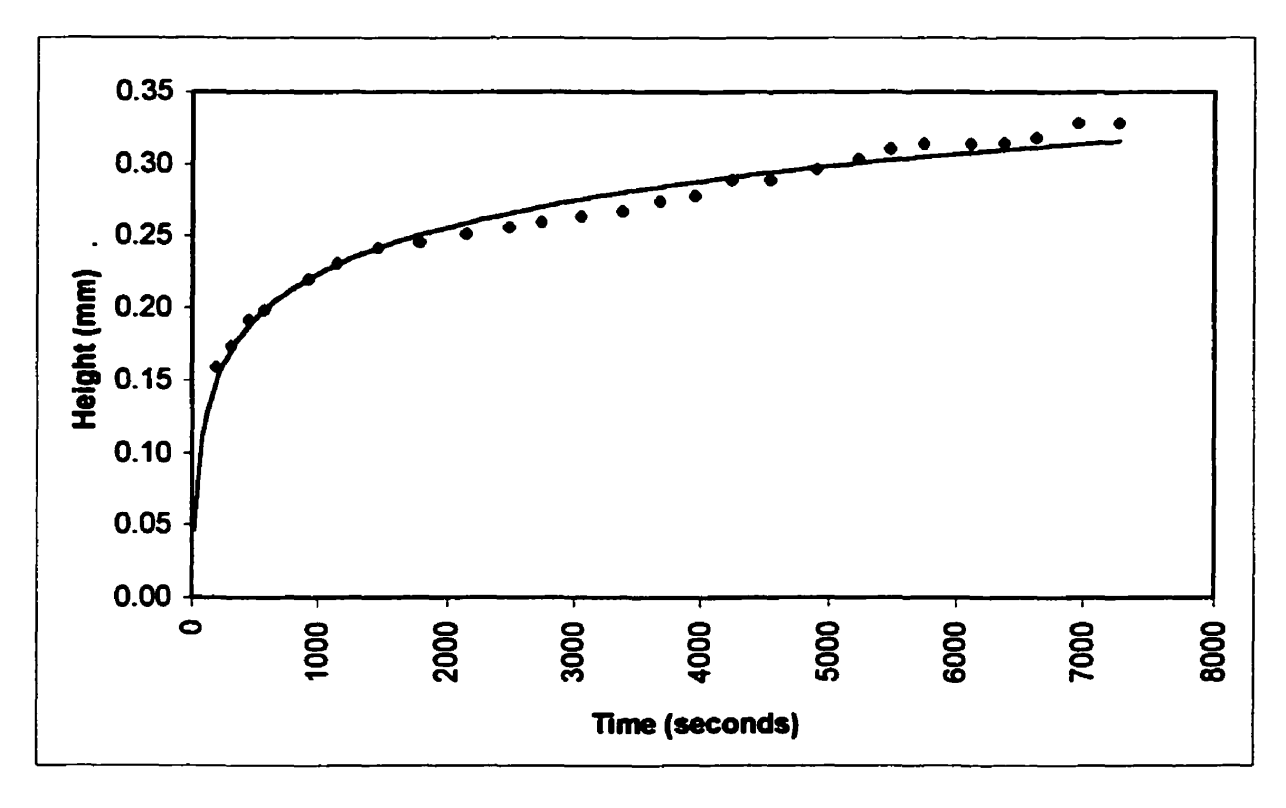


Figure 5.6 - Typical increase of the droplet height with time (Surface: borosilicate glass, Particle: sodium sulfate, $T_{base} = 25^{\circ}C$, $T_{vapor} = 57^{\circ}C$, $Q_{N2} = 417$ ml/min)

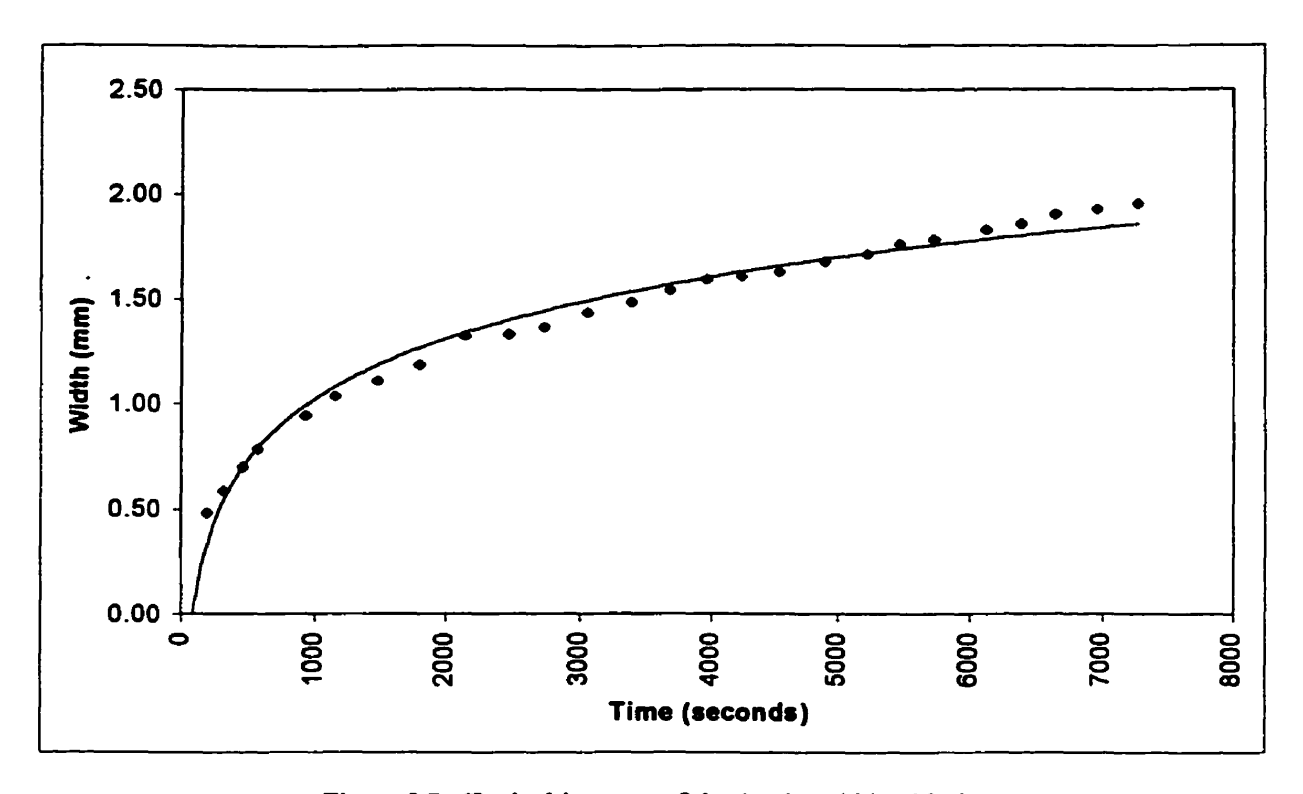


Figure 5.7 - Typical increase of the droplet width with time (Surface: borosilicate glass, Particle: sodium sulfate, $T_{base} = 25^{\circ}\text{C}$, $T_{vapor} = 57^{\circ}\text{C}$, $Q_{N2} = 417 \text{ ml/min}$)

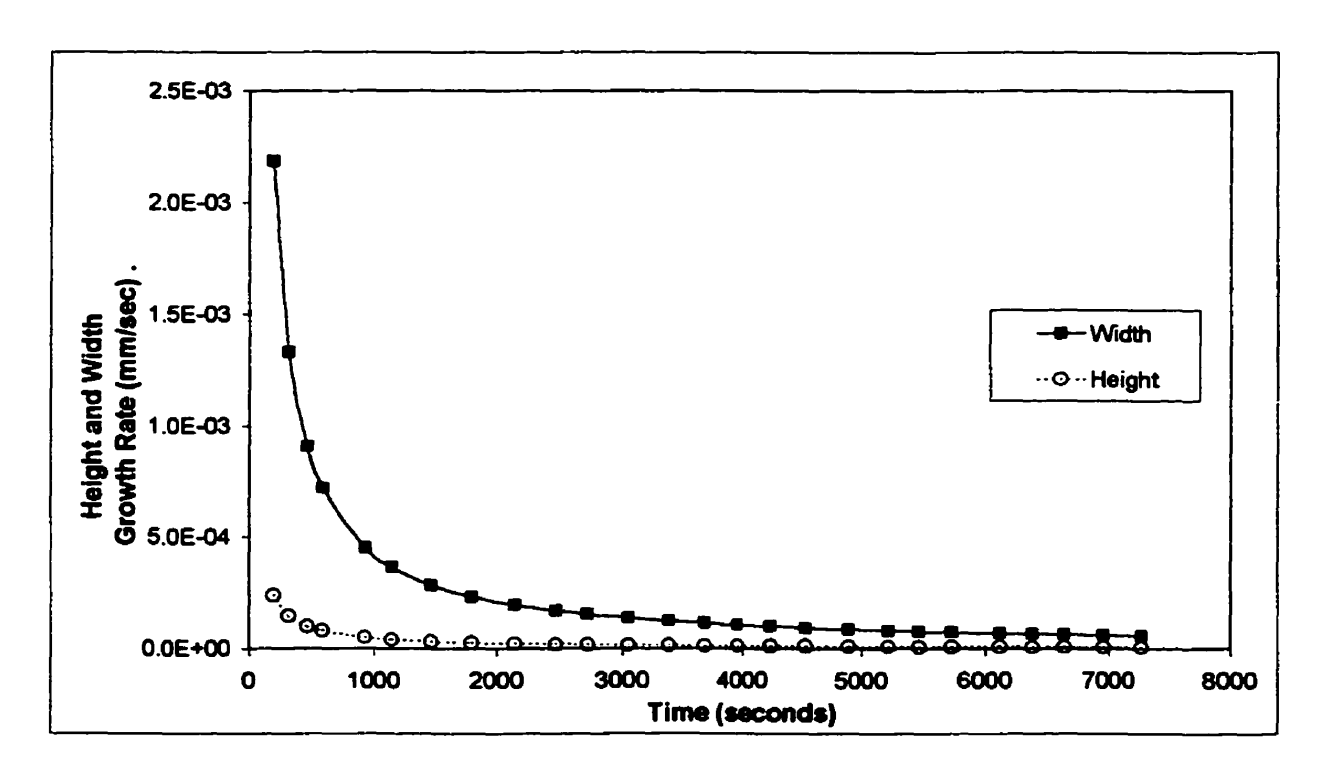


Figure 5.8 - Rate of change of the height and width (Surface: borosilicate glass, Particle: sodium sulfate, $T_{bese} = 25^{\circ}$ C, $T_{vepor} = 57^{\circ}$ C, $Q_{N2} = 417$ ml/min)

5.4 Droplet Volume

Typical increases in the volume of a droplet with time are shown in Figures 5.9 to 5.11. In general, the volume of the droplet continually increases as expected (Figure 5.9). There are, however, cases where the volume was found to reach a plateau at a certain value (Figures 5.10-5.11). These are conditions where the substrate temperature is elevated to a degree where the condensation of water is balanced by evaporation resulting in a constant value. This occurs when the substrate temperature is close to the vapor temperature. This can be seen in all experiments where the substrate temperature was approximately 42°C to 45°C and the vapor temperature was 55°C, regardless of the flow rate. In Figure 5.10 an oscillatory type of behavior is again observed which is probably the result of condensation and evaporation of water from the droplet.

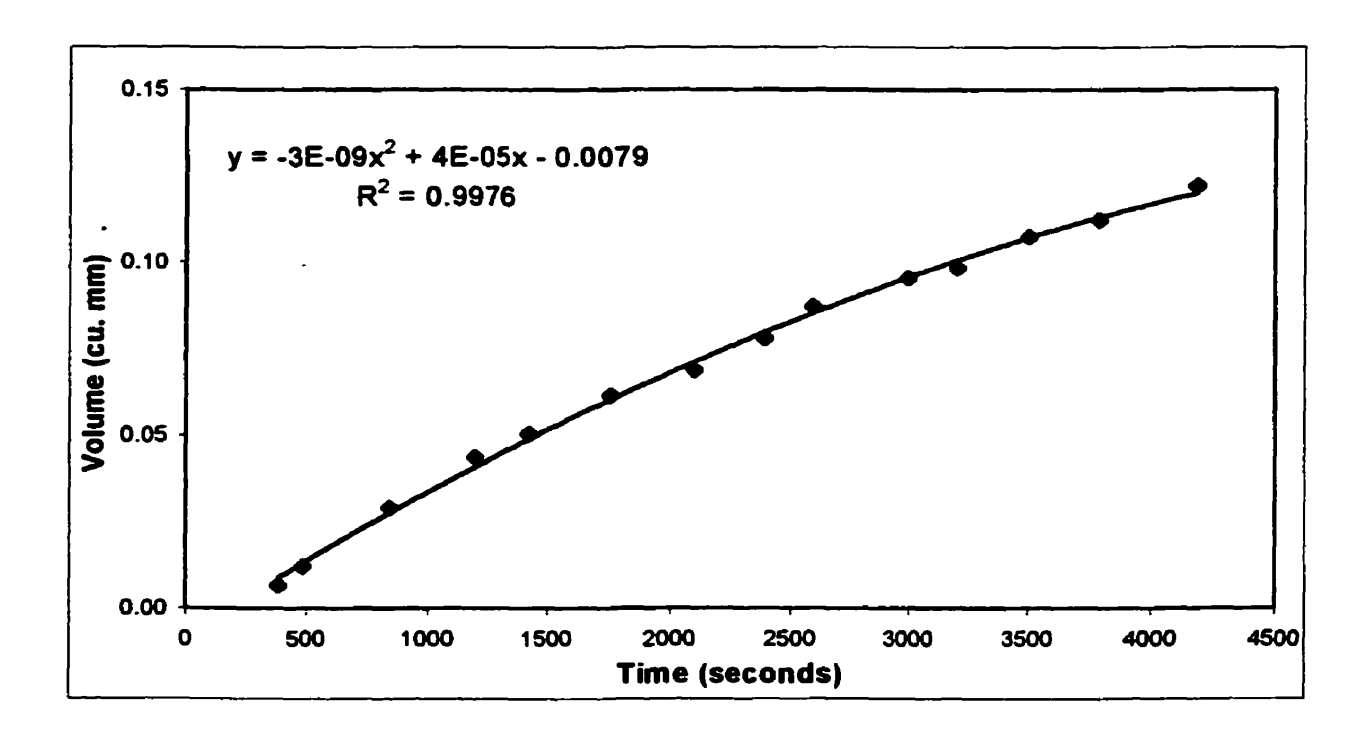


Figure 5.9 - Volume as a function of time (2^{nd} Order Polynomial Trend) (Surface: titanium nitride, Particle: sodium sulfate, $T_{base} = 23$ °C, $T_{vapor} = 48$ °C, $Q_{N2} = 417$ ml/min)

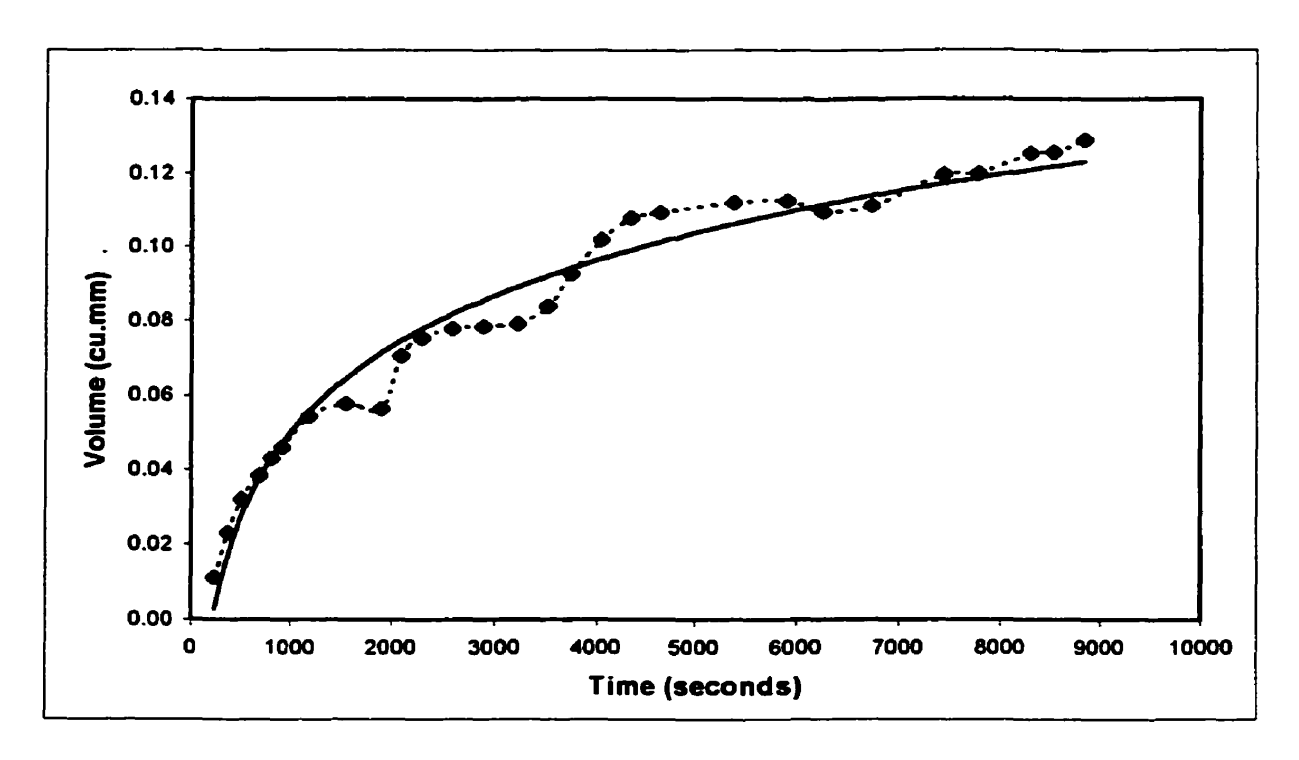


Figure 5.10 - Volume as a function of time - (plateau is being reached) (Surface: borosilicate glass, Particle: sodium sulfate, T_{base} = 42°C, T_{vapor} = 56°C, Q_{N2} =417 ml/min)

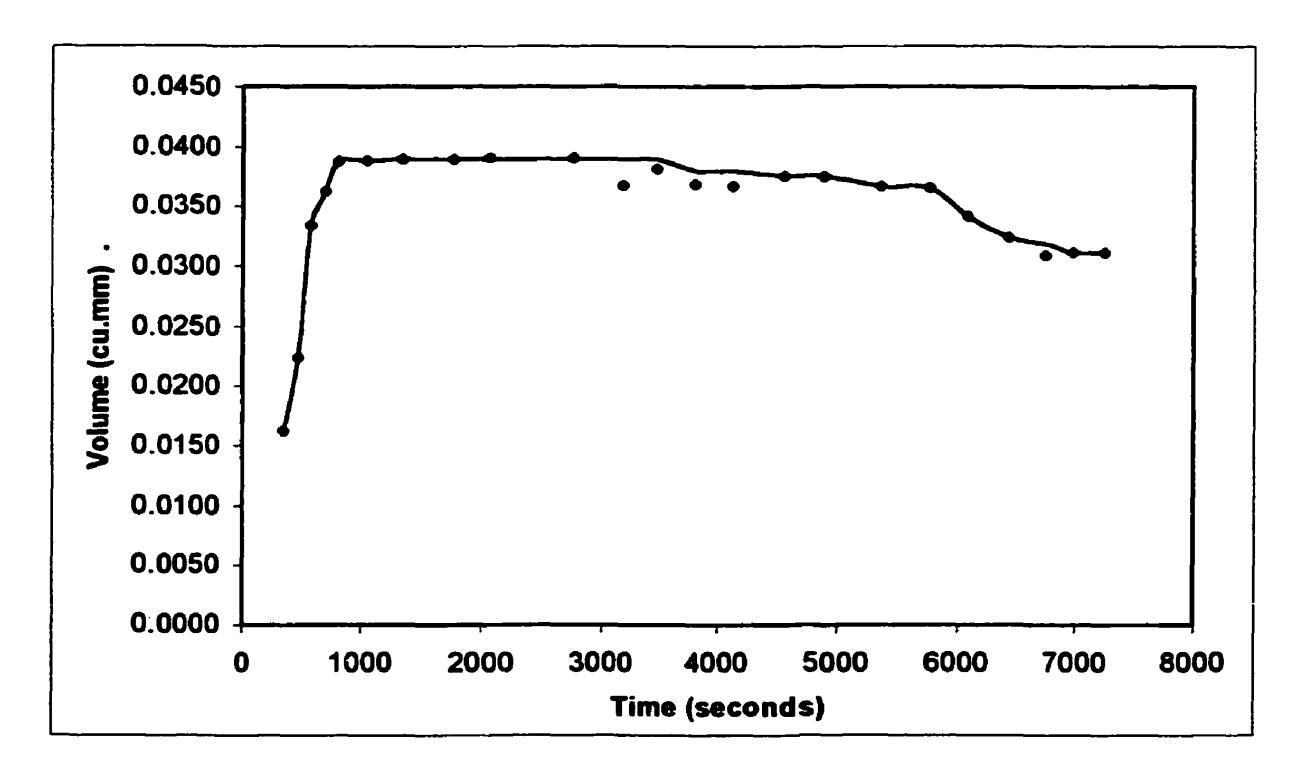


Figure 5.11 - Volume as a function of time - (plateau is reached) (Surface: borosilicate glass, Particle: sodium sulfate, $T_{base} = 43$ °C, $T_{vapor} = 56$ °C, $Q_{N2} = 842$ ml/min)

5.5 Initial Droplet Growth Rate Reproducibility

Three replicates of the initial rate measurements for sodium sulfate on borosilicate glass (two sets for the low flow rate and two for the high flow rate) were taken at different ranges of ΔT , $32 \pm 2^{\circ}C$ and $53 \pm 1^{\circ}C$. At the low flow rate and ΔT of $32^{\circ}C$ the rate varied from $4.4*10^{-4}$ to $4.87*10^{-4}$ mm³/sec (standard deviation of $2.37*10^{-5}$) while with a ΔT of $53^{\circ}C$ the rate was from $1.1*10^{-4}$ to $1.56*10^{-4}$ mm³/sec (with a standard deviation of $2.42*10^{-5}$). At the high flow rate the initial rate was seen to vary from $1.64*10^{-4}$ to $2.41*10^{-4}$ mm³/sec (standard deviation of $3.85*10^{-5}$) at a ΔT of $32^{\circ}C$ whereas it varied from $3.03*10^{-4}$ to $3.60*10^{-4}$ mm³/sec (standard deviation of $3.15*10^{-5}$) for ΔT of $53^{\circ}C$. This indicates that the rate measurements are reproducible when examined over small ΔT values. Figures 5.12 and 5.13 show the reproducibility for sodium sulfate particles on borosilicate glass. Droplets grown under identical environmental conditions may grow at slightly different rates since the surface properties at the position of each site where the nucleation and condensation occur may not be the same. The next section shows the effect of the temperature difference, ΔT , and flow rate on the growth rate of the droplets.

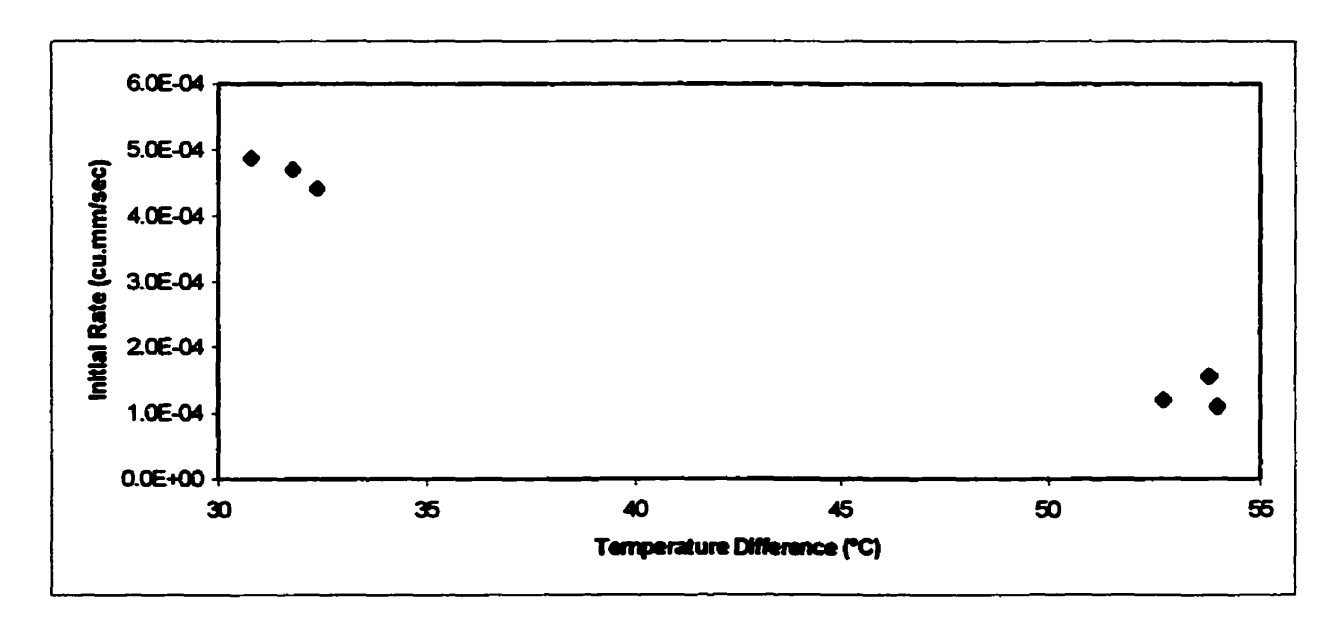


Figure 5.12 - Initial droplet growth rate reproducibility (Surface: borosilicate glass, Particle: sodium sulfate, Q_{N2}=417 ml/min)

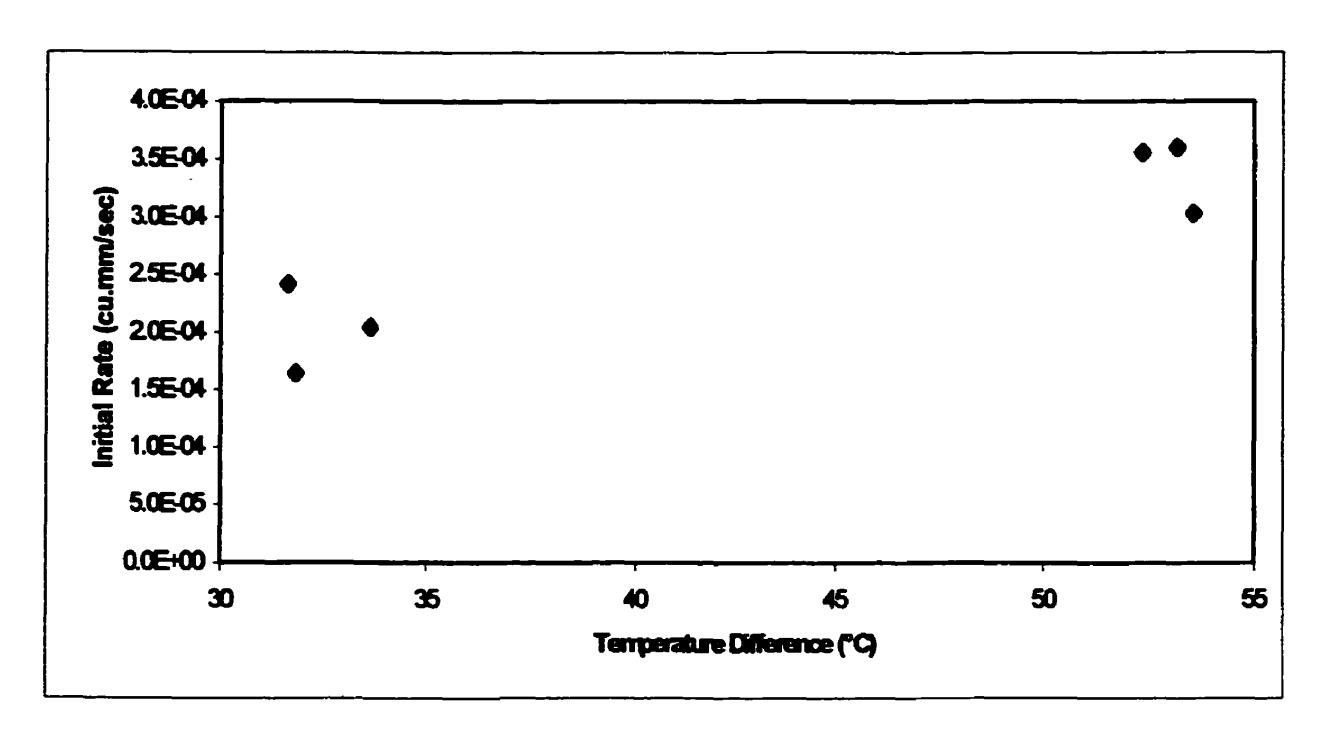


Figure 5.13 - Initial droplet growth rate reproducibility (Surface: borosilicate glass, Particle: sodium sulfate, Q_{N2}=842 ml/min)

5.6 Effect of ΔT on Initial Rate (dV/dt)

In the initial stages of the experiment just as the condensation of water vapor begins the saturated solution starts spreading and forming the droplet; thus the initial rates were obtained under conditions where the properties of the system were best defined. The initial growth rate curves (on borosilicate glass) which were obtained as a function of the temperature difference, ΔT, (defined as T_{vapor} - T_{substrate}) are shown in Figures 5.14 and 5.15. In all cases at a ΔT of 30°C regardless of the salt being used or the flow rate there was always a sharp decrease in the growth rate followed by a gradual increase. One possible hypothesis for this is that a temperature difference of about 30°C is a separation point between preferential nucleation on a contaminant particle and the nucleation or condensation over the entire surface. The sharp decrease in the rate as ΔT increases beyond a 30°C difference can be explained by a reduction in the amount of available water vapor present near the surface. For example when the nucleation/condensation occurs on a particle, all the water vapor present near the surface is available for nucleation on that particle; however, when the nucleation takes place over

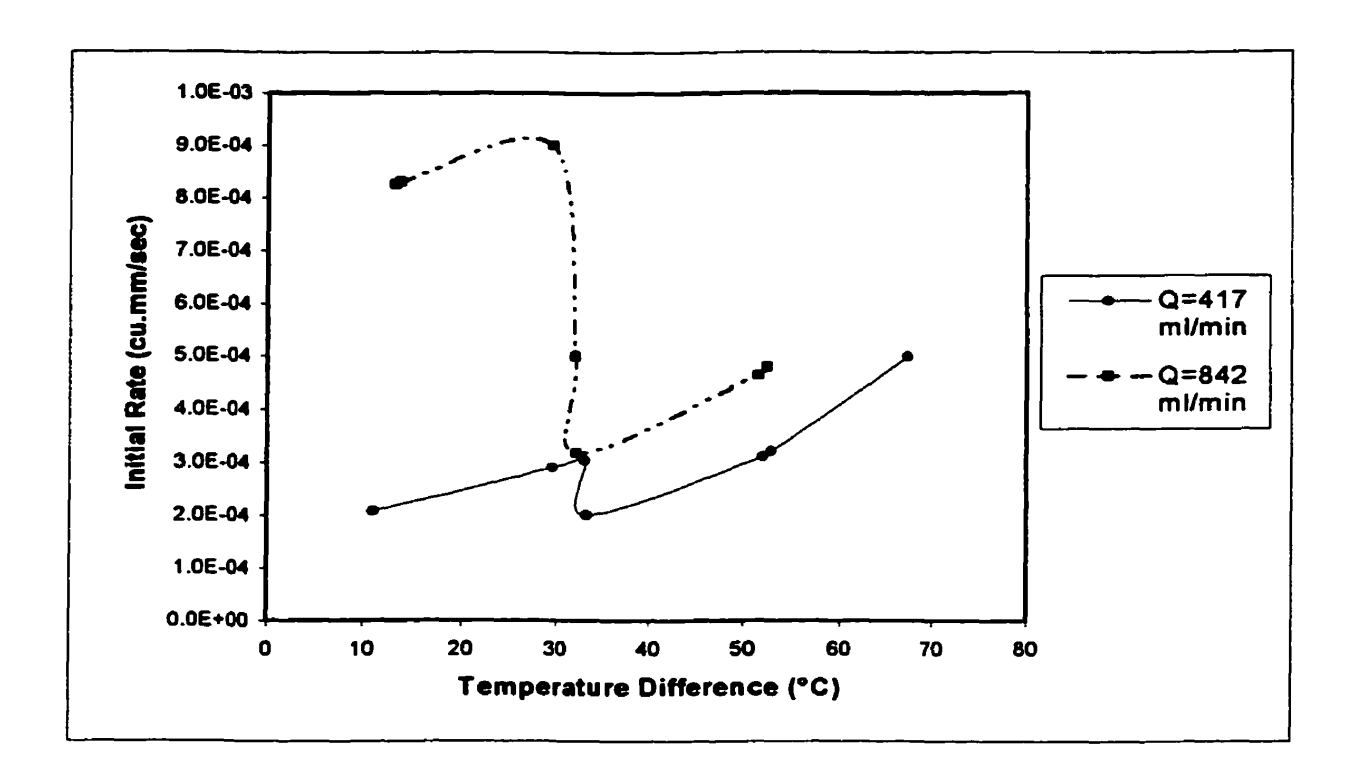


Figure 5.14 - Effect of the temperature difference (ΔT) on the rate of nucleation (Surface: borosilicate glass, Particle: sodium chloride)

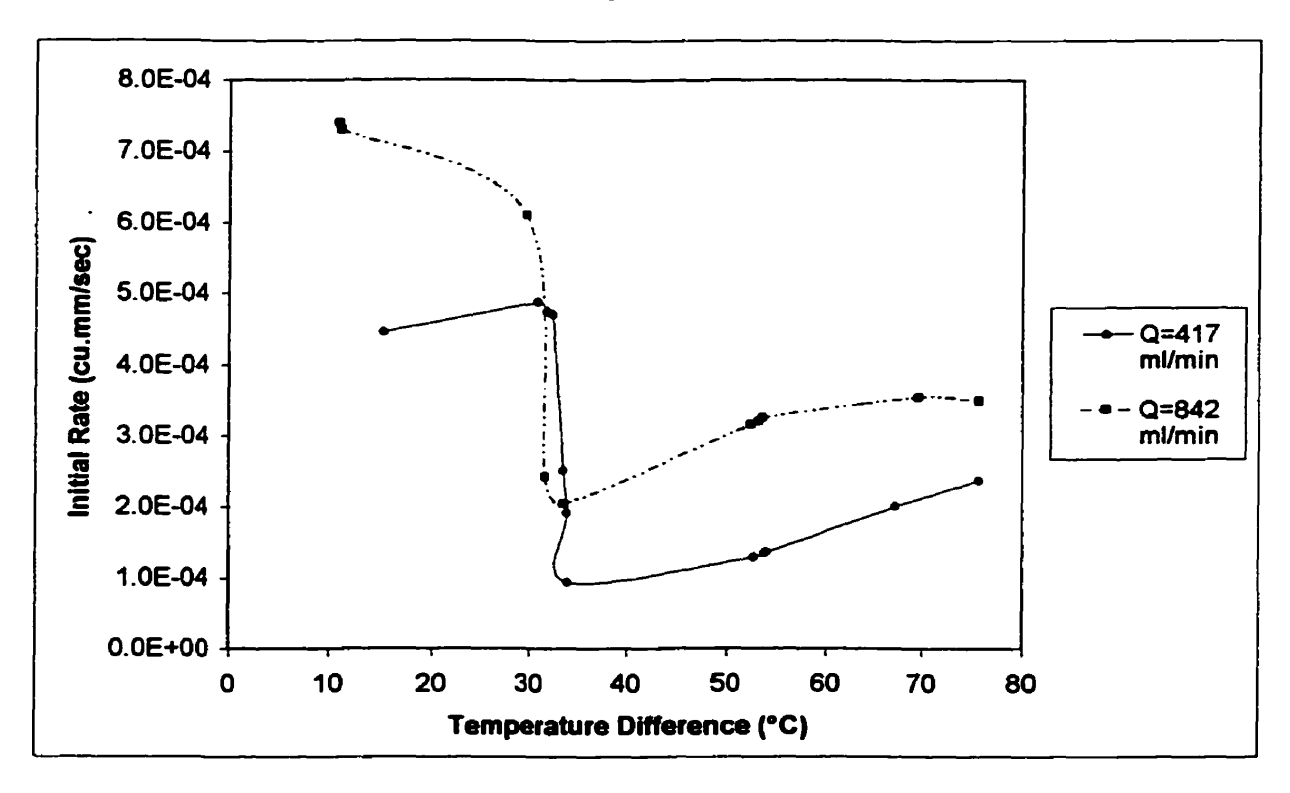


Figure 5.15 - Effect of the temperature difference (ΔT) on the rate of nucleation (Surface: borosilicate glass, Particle: sodium sulfate)

the entire surface there is a decrease in the amount of available water vapor near the surface because the water is condensing over the entire surface resulting in a reduction of the growth rate on the particle.

Another observation (for both salt solutions) is that at the higher flow rate the observed growth rate at the lowest ΔT of about 10° C are significantly higher when compared to the lower flow rate. Overall, the initial rates at the higher flow rate are greater than those produced at the lower flow which can be explained by the increase in water vapor availability. As can be seen in the Figure 5.16, with both cases when water is condensed on the droplet, there may be a boundary layer which has a reduced water vapor content especially in the initial stages of condensation when the rates are high. One of the potential limiting factors to the growth of the droplet is the diffusion of water vapor through this boundary layer. An explanation for the difference in the growth rates is that with the higher flow rate there is a reduction in the boundary layer thickness which allows for faster diffusion. Although this explanation needs to be better substantiated by calculating mass transfer coefficients, at least it qualitatively explains the observed rates.

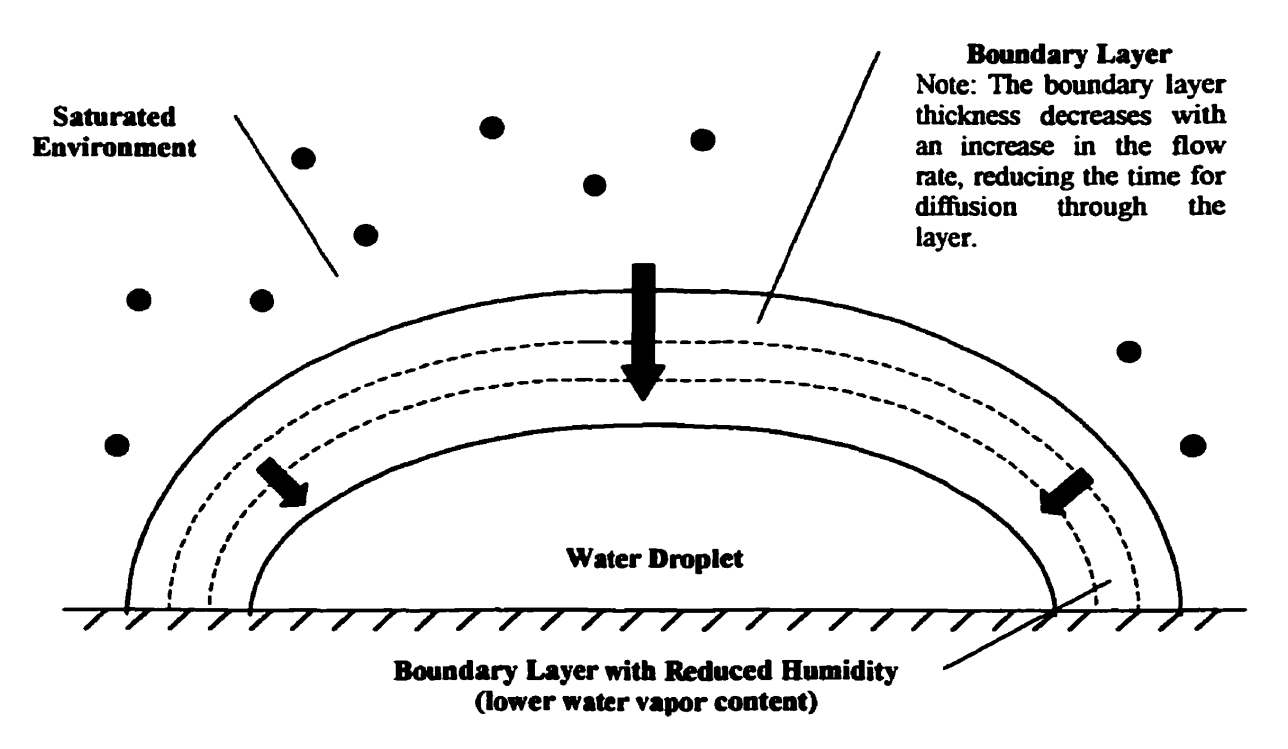


Figure 5.16 - Formation of Boundary Layer having Reduced Humidity

The initial droplet growth rates for sodium chloride and sodium sulfate on silicon, silicon dioxide, photoresist, and titanium nitride surfaces are shown by Figures 5.17 to 5.20. The initial rates for sodium chloride on silicon are always slightly lower than that for silicon dioxide. In addition the rates follow the same trend, either increasing in value with temperature difference or decreasing as was the case for a flow rate of 417 ml/min. Since the temperature difference is the driving force for nucleation and condensation, an increase in the temperature difference would also result in an increase in the rate. This is exhibited by a majority of the obtained growth rate curves. The only exception was for sodium chloride on silicon and silicon dioxide at a flow rate of 417 ml/min. For the sodium sulfate solution it was seen that the initial rate on the silicon dioxide surface regardless of flow rate was slightly lower than the rate produced on silicon. Generally it was observed that the sodium sulfate solutions produced rates which were very similar on all the tested surfaces regardless of the flow rate, while with the sodium chloride solution the rates are seen to be spread over a larger range of rate values.

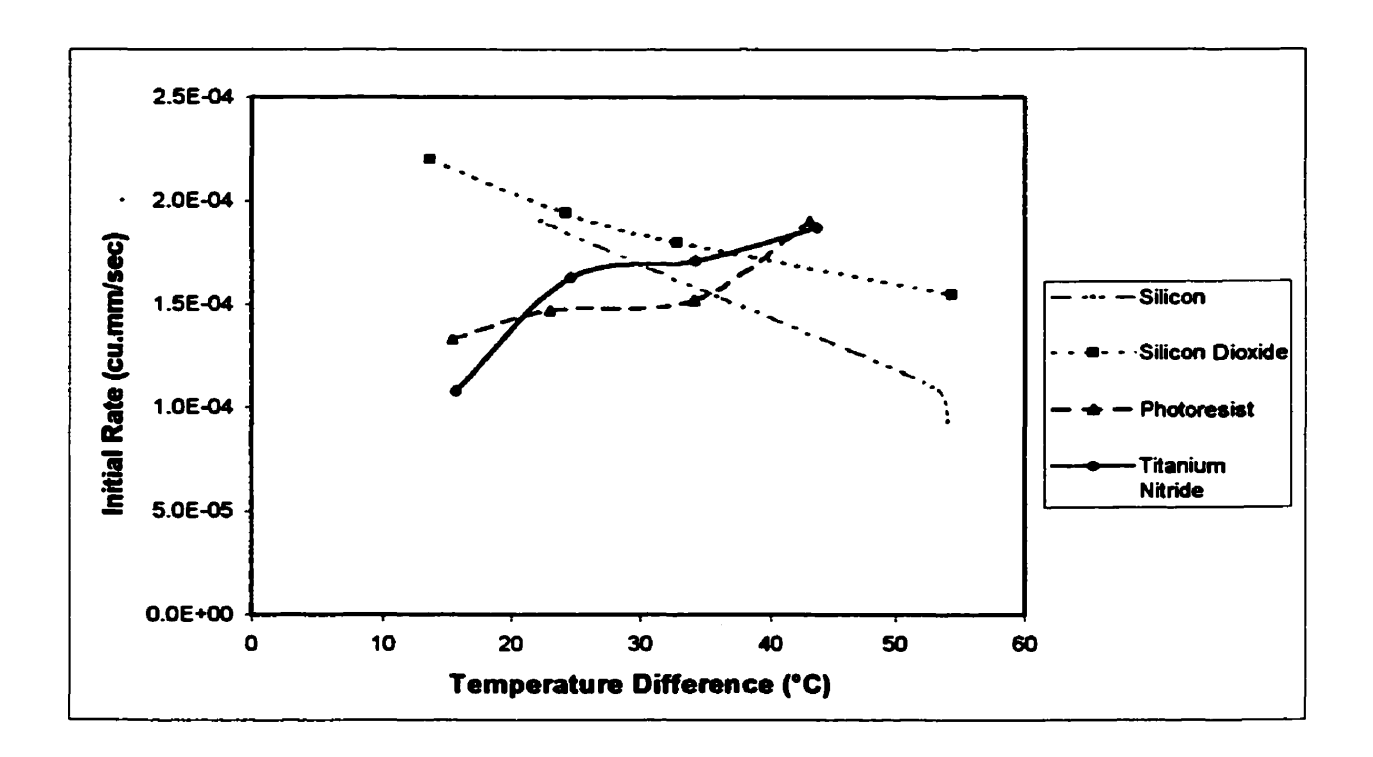


Figure 5.17 - Effect of the temperature difference (ΔT) on the rate of nucleation (Various Surfaces, Particle: sodium chloride, Q_{N2} =417 ml/min)

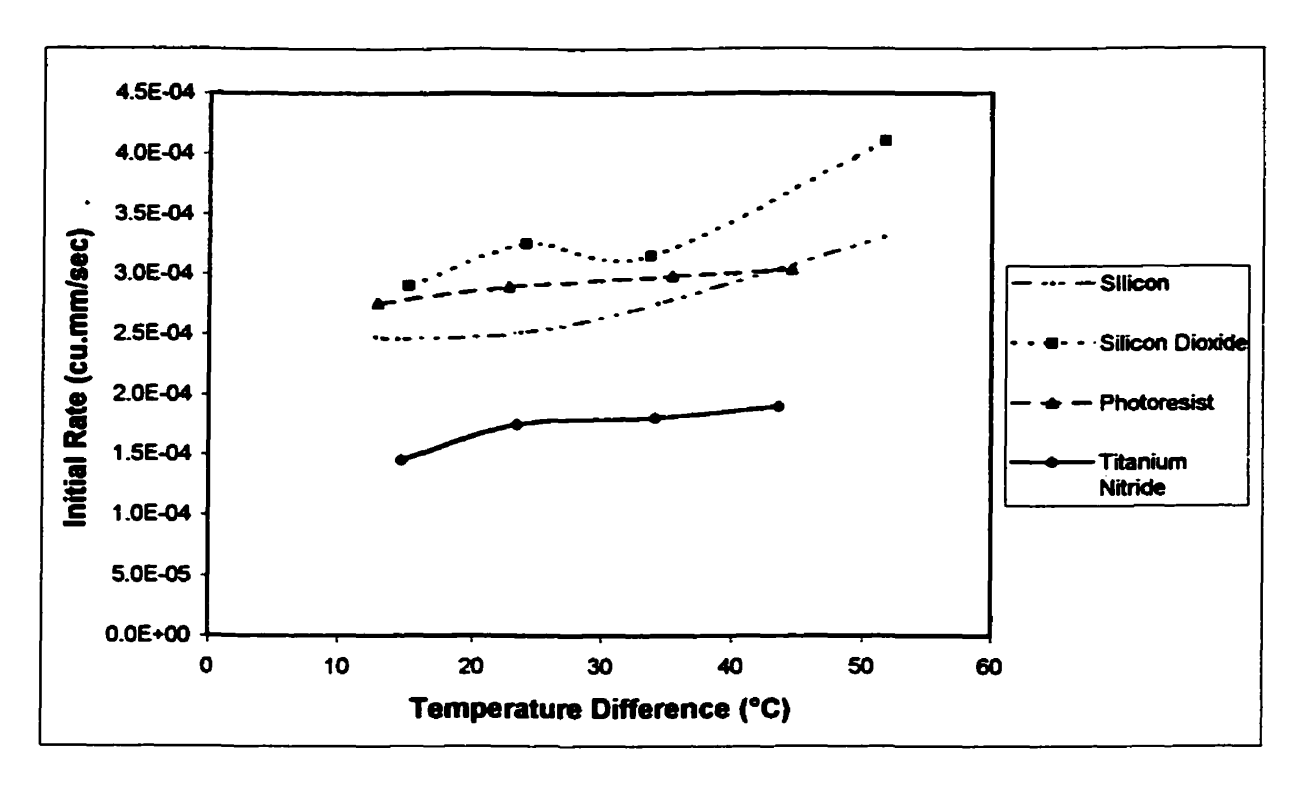


Figure 5.18 - Effect of the temperature difference (ΔT) on the rate of nucleation (Various Surfaces, Particle: sodium chloride, Q_{N2} =842 ml/min)

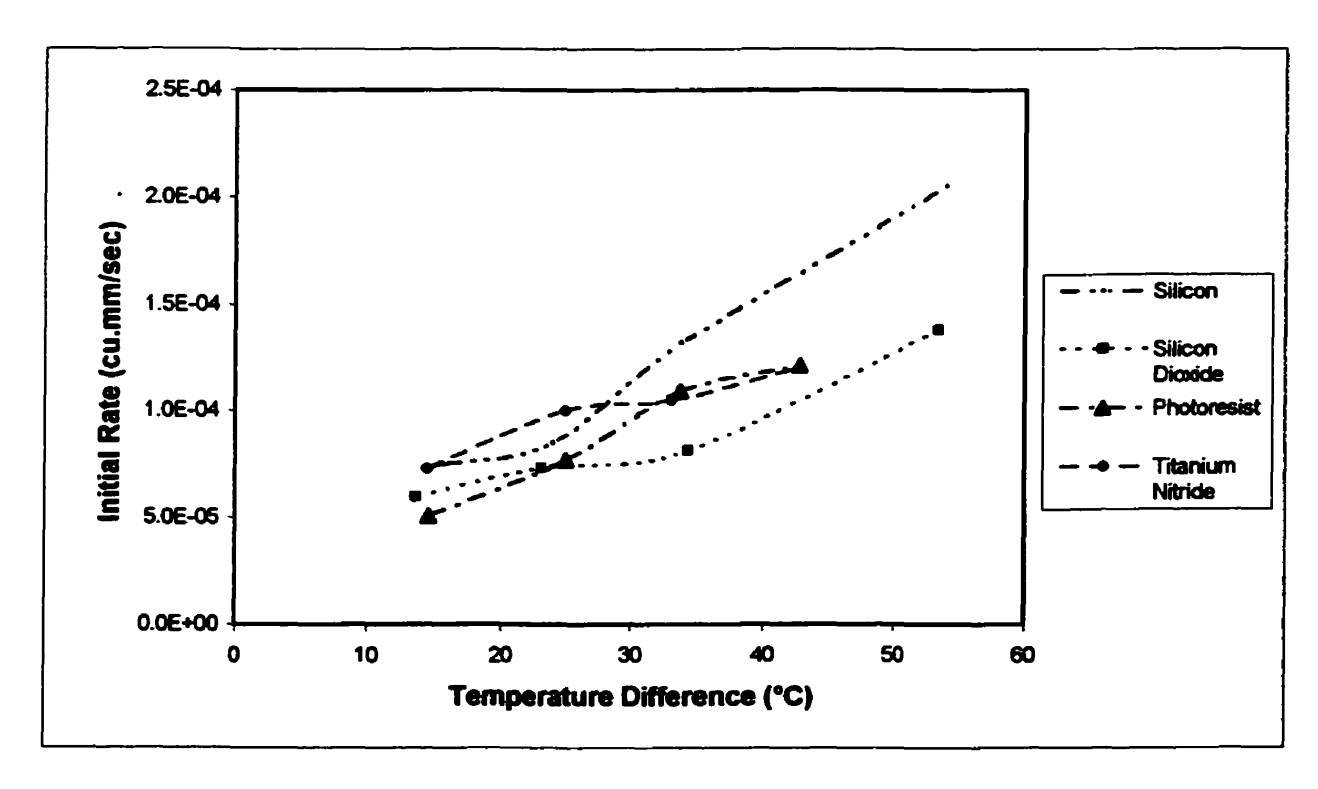


Figure 5.19 - Effect of the temperature difference (ΔT) on the rate of nucleation (Various Surfaces, Particle: sodium sulfate, Q_{NZ} =417 ml/min)

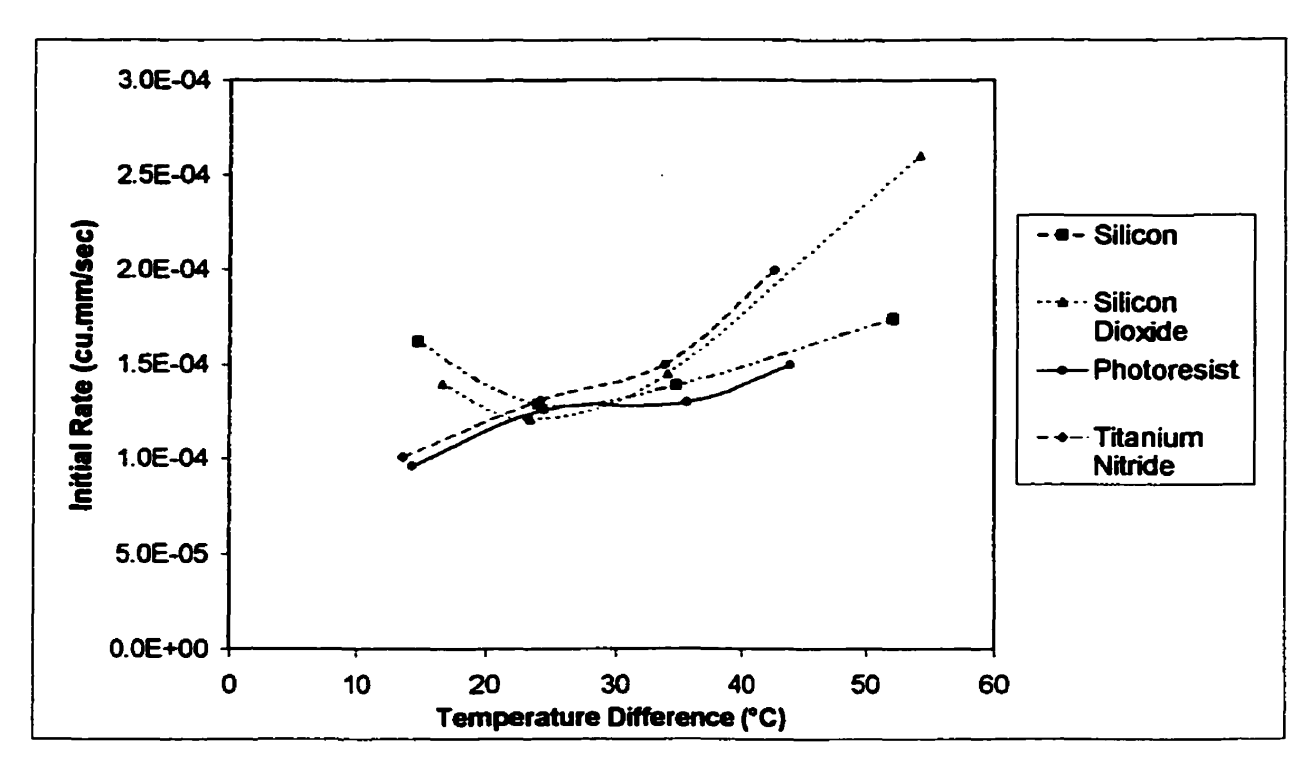


Figure 5.20 - Effect of the temperature difference (ΔT) on the rate of nucleation (Various Surfaces, Particle: sodium sulfate, Q_{NZ} =842 ml/min)

5.7 Contact Angle as a Function of Time

In order to determine the effect of wettability on the growth rate of the droplet, the contact angle of the growing droplet was determined as a function of time during the growth experiments. For the water soluble particles of sodium chloride and sodium sulfate on a borosilicate glass, silicon, and silicon dioxide surface as time progressed the angle decreased as can be seen in Figures 5.21 to 5.23. The high initial contact angle that was observed may have been a result of the solid particle core which supports the condensed water phase and creates an artificially high contact angle.

This type of decreasing trend was anticipated because initially as the salt particle (either sodium chloride or sodium sulfate) dissolves in the condensed medium the concentration of the salt in the droplet is near saturation leading to a higher contact angle. As the experiment progresses more water condenses on the particle resulting in the solution becoming more dilute. As was shown in the previous chapter the contact angle

decreases with concentration for both sodium chloride and sodium sulfate (Figures 4.16 to 4.27).

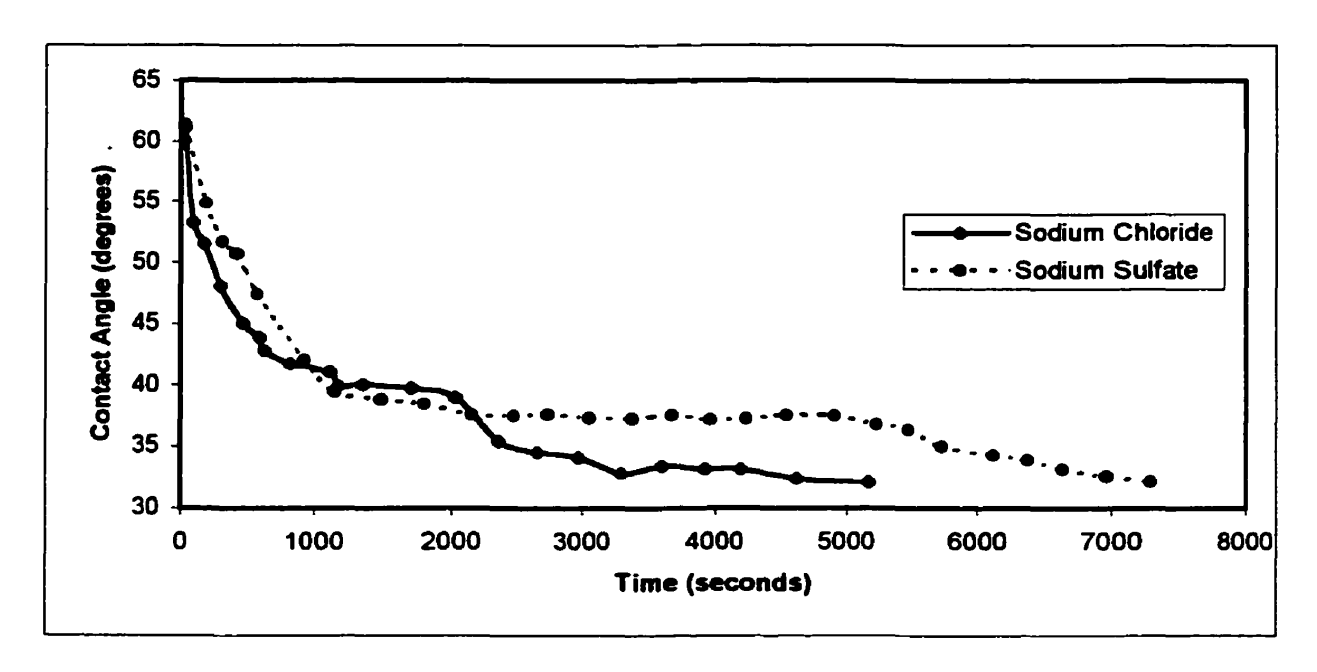


Figure 5.21 - Contact Angle as a function of time (Surface: borosilicate glass, T_{base}=20°C)

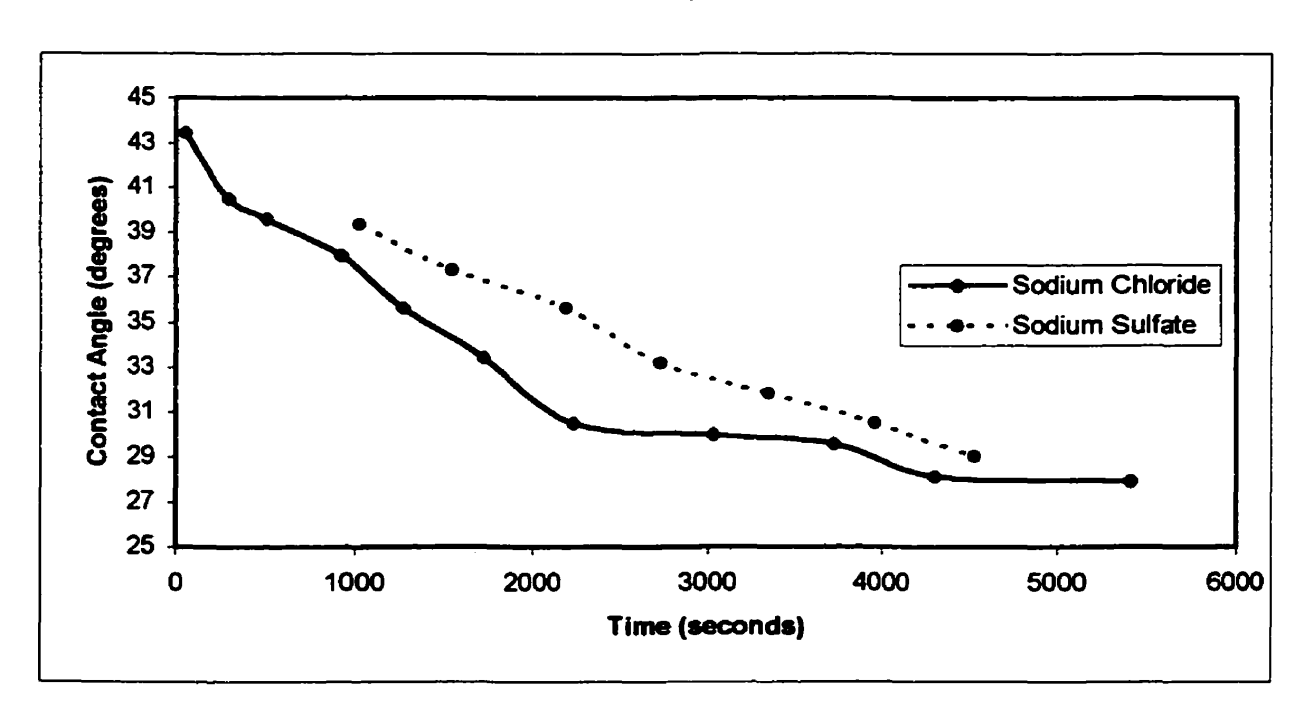


Figure 5.22 - Contact Angle as a function of time (Surface: silicon , T_{base} =20°C)

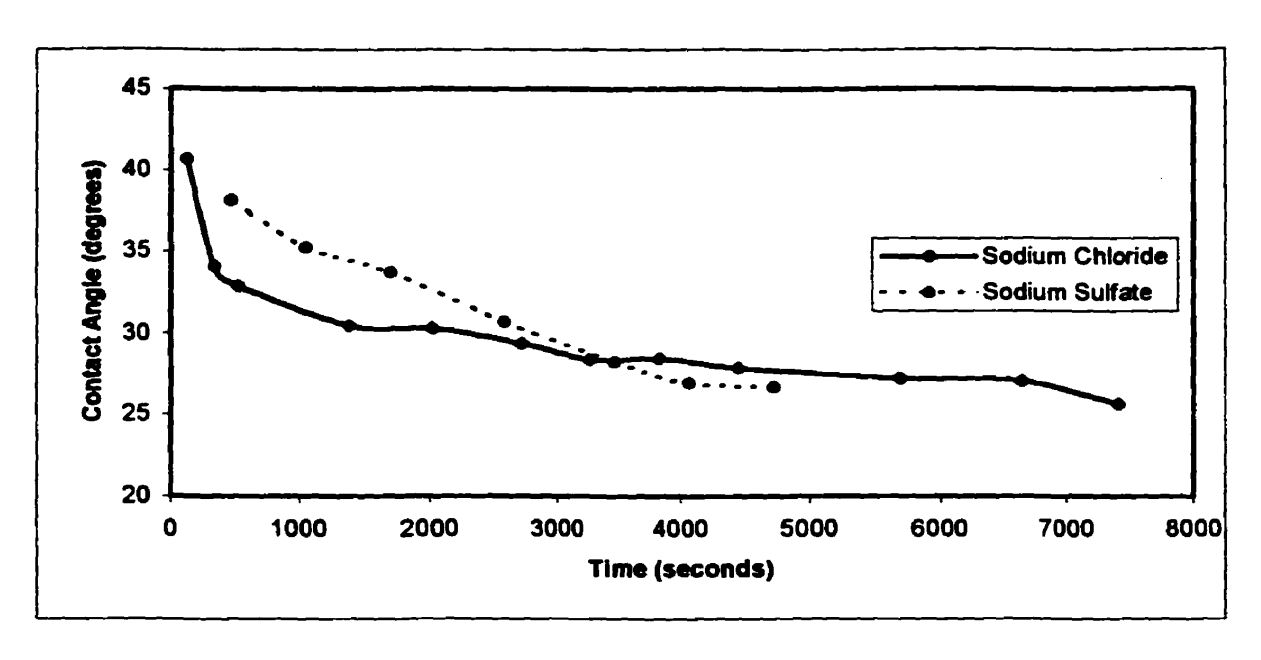


Figure 5.23 - Contact Angle as a function of time (Surface: silicon dioxide, T_{base}=20°C)

The nucleation experiments with soluble particles have shown that in the initial stages of growth, the water droplet which has condensed on the salt particle has a high contact angle ($\geq 40^{\circ}$). As the experiment progresses the contact angle changes because of the changing dissolved salt concentration which affects the surface tension resulting in different contact angles. For sodium sulfate the contact angles range from 37 to 40 degrees which corresponds to salt concentrations in the range of 0.005g/l to 1 g/l, whereas for the sodium chloride solutions the contact angles were from 31 to 50 degrees. Inspecting the contact angle versus sodium chloride concentration curve the salt concentration was seen to vary between 0.005g/l to 10 g/l. If the entire range was considered the solutions could still be considered dilute compared to the saturated solution.

5.7.2 Effect of Concentration on the Growth Rate

Since the change in the droplet volume is known as a function of time, the instantaneous rate of growth can be calculated from the regression curve as described in Section 3.10. This allows the determination of the effect of the wettability on the growth

rate of the droplet. Figures 5.24 and 5.25 show the calculated rate (dV/dt) for sodium sulfate on silicon dioxide as a function of the condensed water droplet contact angle for varying temperature differences and flow rates. The trends which are discussed are applicable to all tested surfaces and aqueous salt solutions and similar results were obtained with all the other surfaces (silicon, photoresist, and titanium nitride).

In all the experiments as the contact angle increased, the droplet rate of growth also increased; this trend is observable for all tested surfaces. Furthermore, at any one particular contact angle as the temperature difference increased so did the rate. Thus a temperature difference of 14°C shows the lowest rate and a temperature difference of 54°C shows the highest. This trend with the contact angle and the temperature difference is observed at both gas flow rates.

Another factor that effects the growth rate is the driving force for the condensation, which is the difference in the actual vapor pressure of water in the bulk gas and the equilibrium vapor pressure at the surface of the droplet (Figure 5.26). During the initial stages of the condensation, the vapor pressure of pure water is greater than that of the aqueous salt solution at the same temperature; thus the pressure difference, $\Delta P = P_{\text{vapor}} - P_{\text{solution}}$, is found to increase as both the salt concentration and the substrate temperature increases. This can be seen in Figures 5.27 and 5.28 for both sodium chloride and sodium sulfate, respectively.

As an experiment progresses, the substrate temperature remains constant, and the salt concentration slowly decreases as a function of time. Therefore, at the start of an experiment and after the particle is completely dissolved, the ΔP value is at its largest value, which produces a large driving force allowing for a higher rate of condensation to occur. As the experiment progresses the salt concentration slowly decreases as more water is added to the droplet through condensation, decreasing the ΔP value. This in turn reduces the driving force and slows the rate of condensation.

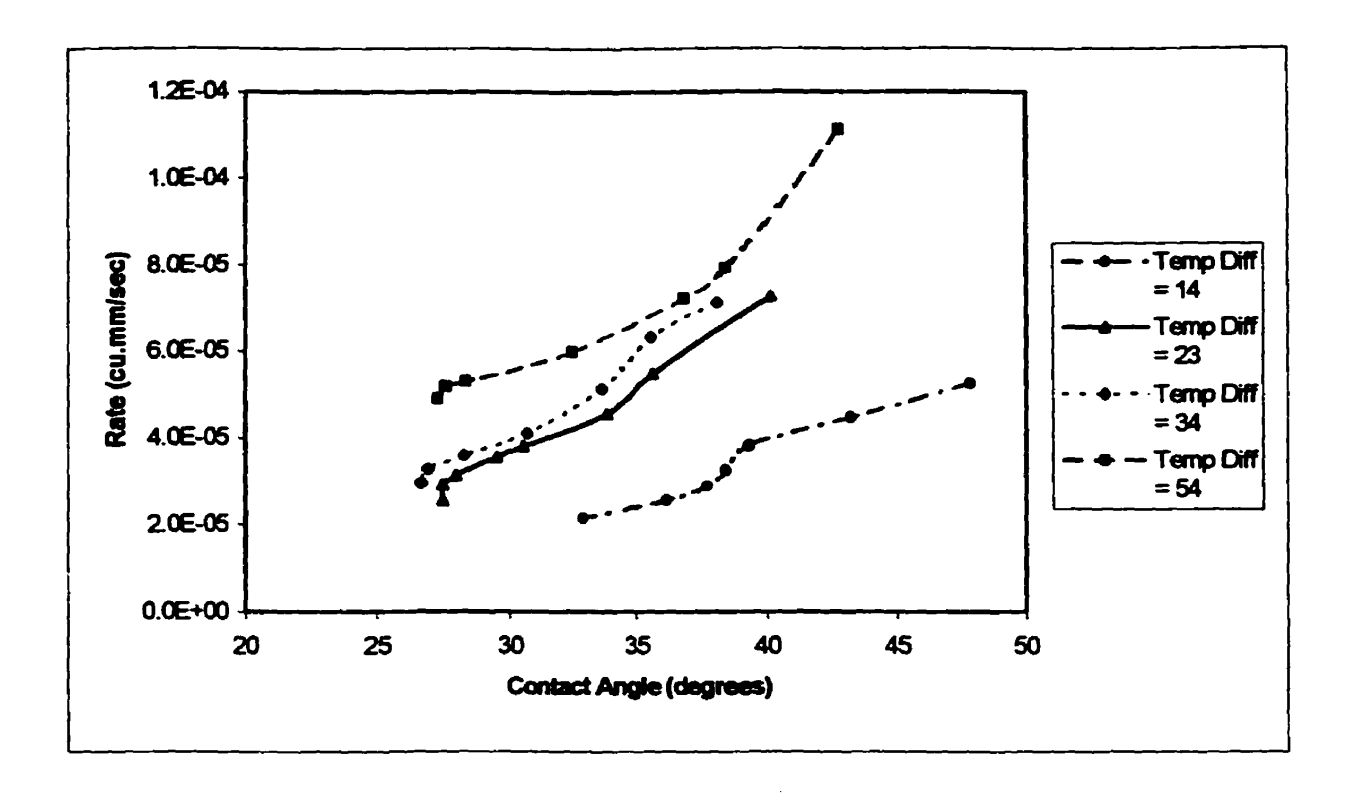


Figure 5.24 - Rate as a function of Contact Angle (Surface: silicon dioxide, Particle: sodium sulfate, Q_{N2} =417 ml/min)

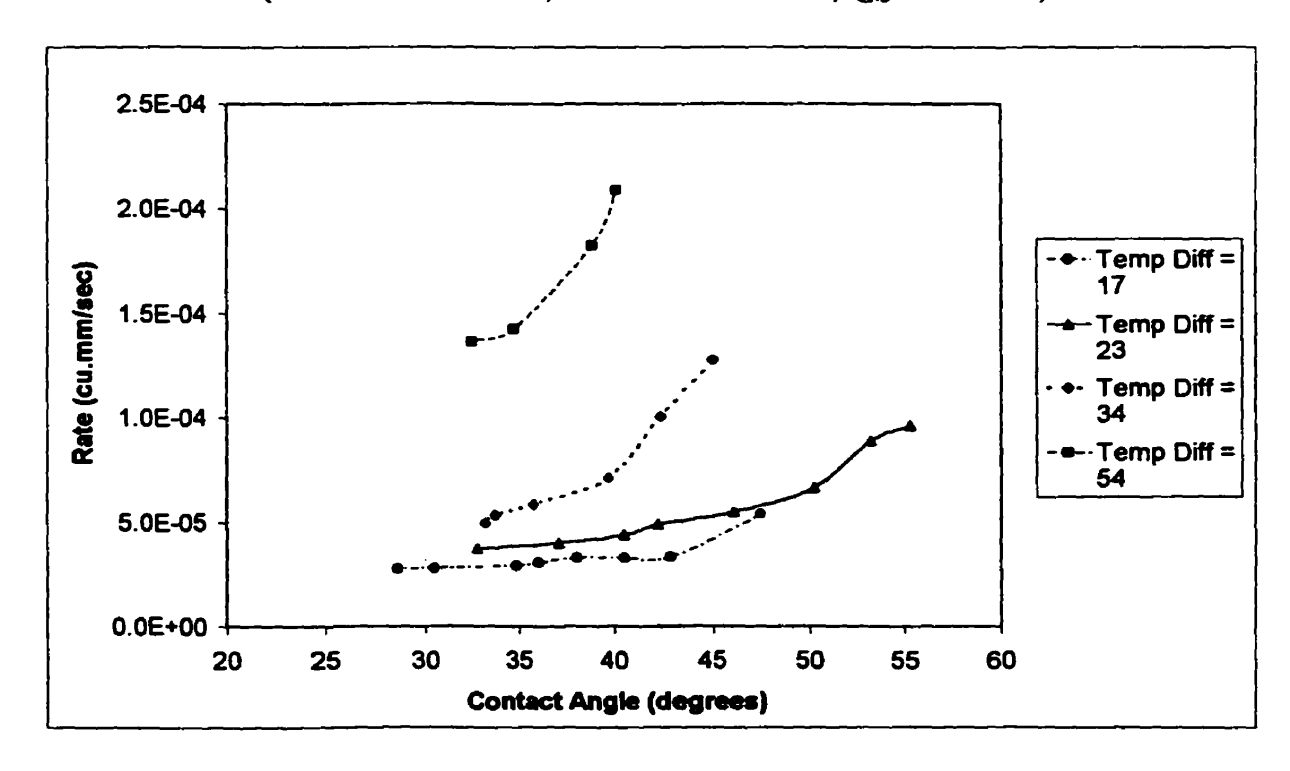


Figure 5.25 - Rate as a function of Contact Angle (Surface: silicon dioxide, Particle: sodium sulfate, Q_{N2} =842 ml/min)

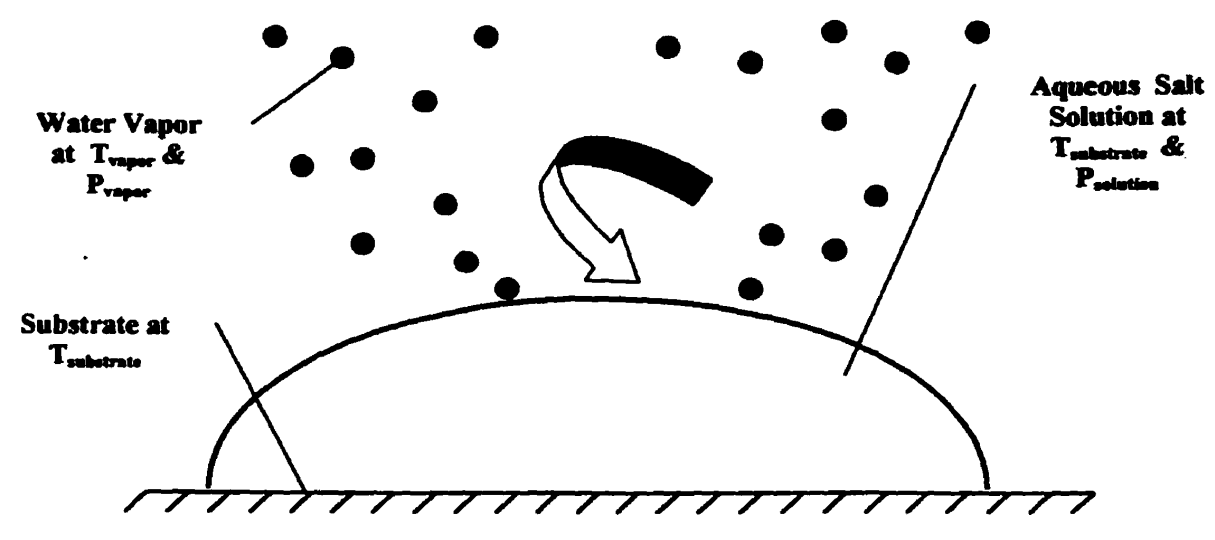


Figure 5.26 - Diagram of a Droplet in a Saturated Environment

This hypothesis is supported by the decreasing trends observed in all experiments. Also this explanation verifies the rate trends shown as a function of contact angle. Since the contact angles are an indirect measure of the concentration, the changing ΔP indicates how the decrease in solution concentration effectively lowers both the contact angle and the droplet growth rate.

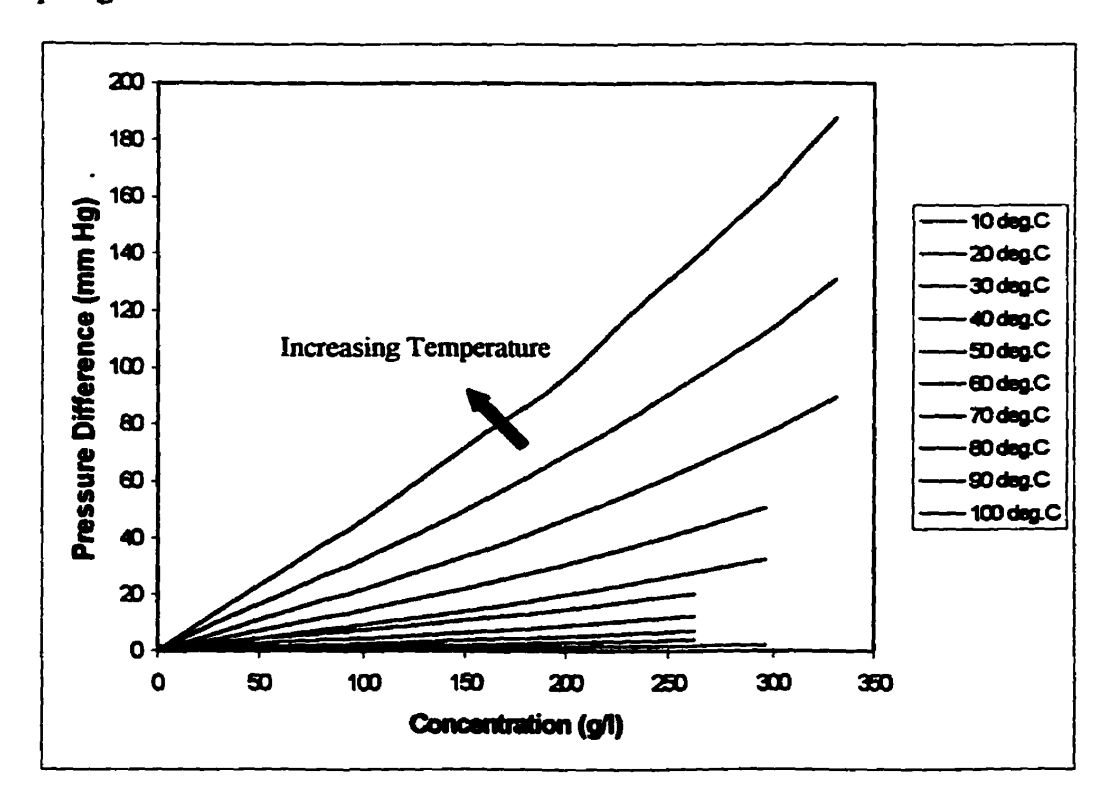


Figure 5.27 - Variation of Pressure Difference with Sodium Chloride Concentration

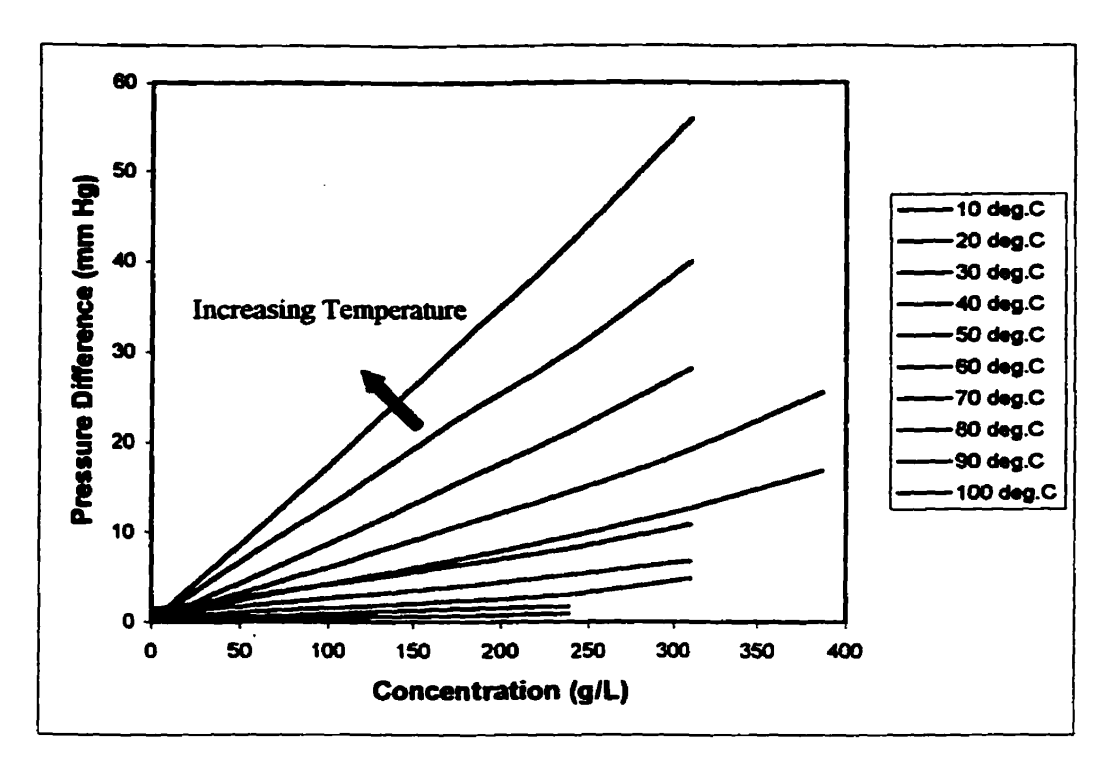


Figure 5.28 - Variation of Pressure Difference with Sodium Sulfate Concentration

5.7.3 Droplet Height, Width, and Growth Rate Trends

When the rate as calculated from the volume equation (equation 25 and 28) is examined, the results for all semiconductor surfaces appear to overlap, and lie within a relatively small region of rate values. This is the result of the equation used to calculate the volume which has a canceling effect when the height and width are changing in opposite directions (one increases as the other decreases). For instance on a fairly hydrophilic surface, such as silicon, (as determined by the contact angle of water) it was seen that the droplet spreads producing large width values but relatively small heights. With a relatively hydrophobic surface, such as titanium nitride, the droplet does not spread to a large extent on the surface resulting in relatively small width measurements; however the height of the droplet increases resulting in roughly the same volume as that found on a hydrophylic surface.

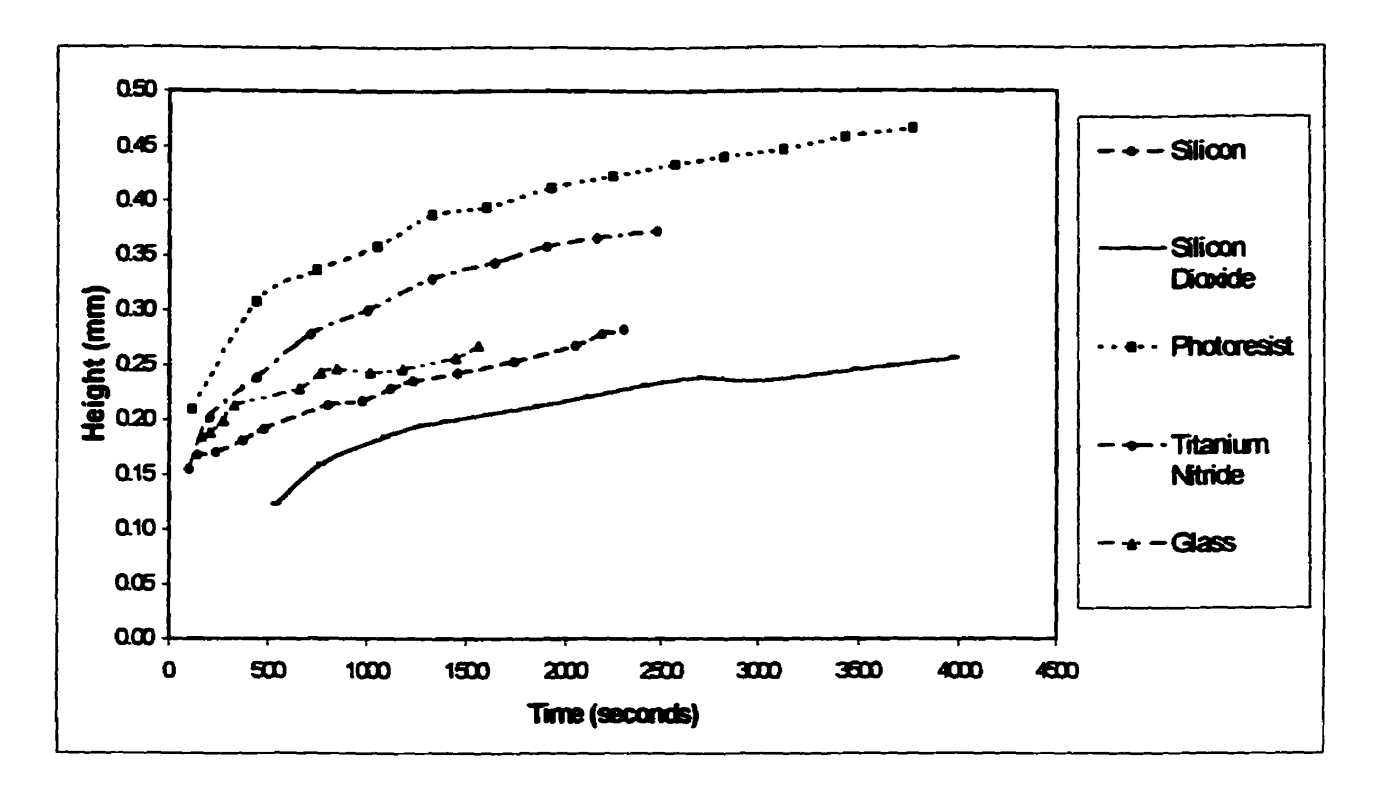


Figure 5.29 - Effect of Wettability on the Droplet Height (Particle: sodium chloride, Temperature Difference = 30°C, Q_{N2}=842 ml/min)

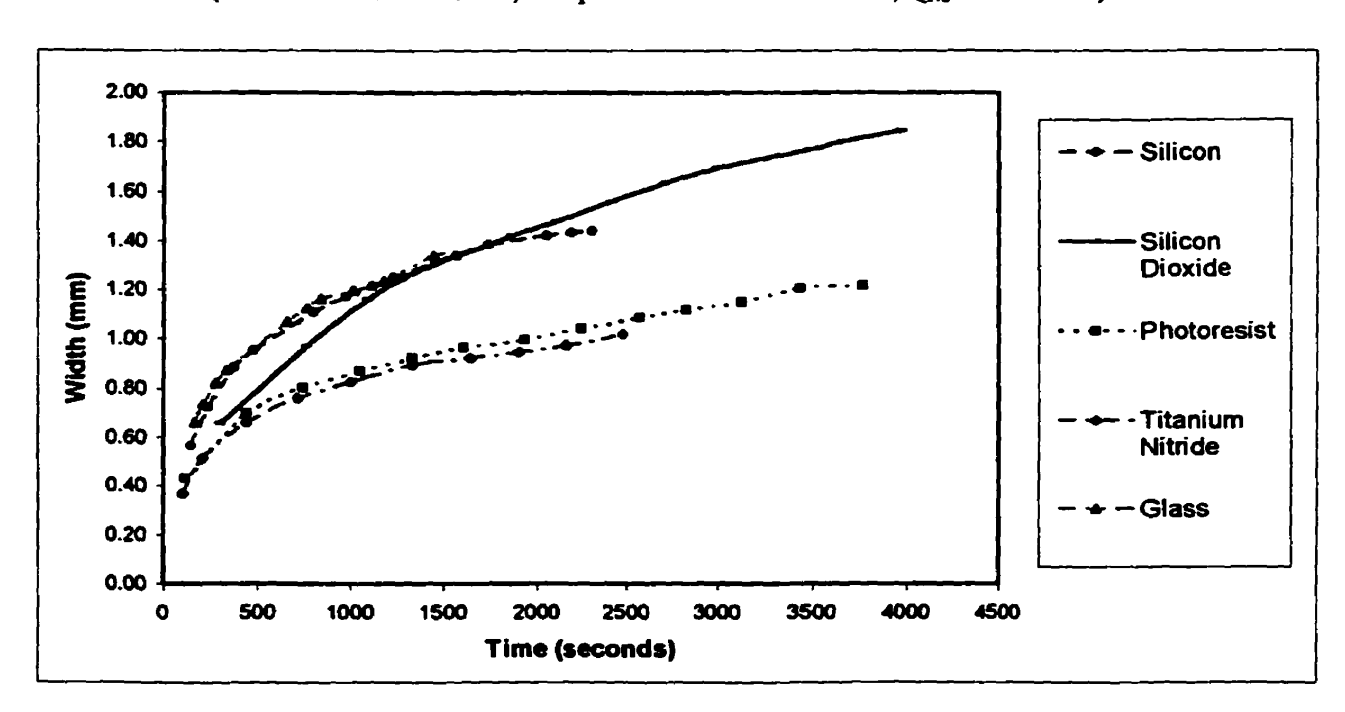


Figure 5.30 - Effect of Wettability on the Droplet Width (Particle: sodium chloride, Temperature Difference = 30°C, Q_{N2}=842 ml/min)

The effect of wettability on the increase in the height and width is shown in Figures 5.29 and 5.30. The surface of silicon, silicon dioxide and borosilicate glass all have roughly the same wettability (as seen in Figures 5.29 and 5.30) and are hydrophilic surfaces when compared to that of the other two surface, the titanium nitride and photoresist, which are more hydrophobic in nature as shown by the contact angle measurements (Table 4.3).

Based on the above arguments, rates based on width measurements indicate that silicon and silicon dioxide surfaces produce higher rates than those of the titanium nitride and photoresist, whereas considering droplet height the silicon and silicon dioxide have rates which are lower than the titanium nitride and photoresist surfaces. The trends produced by the height and width rates are shown in Figures 5.31 and 5.32.

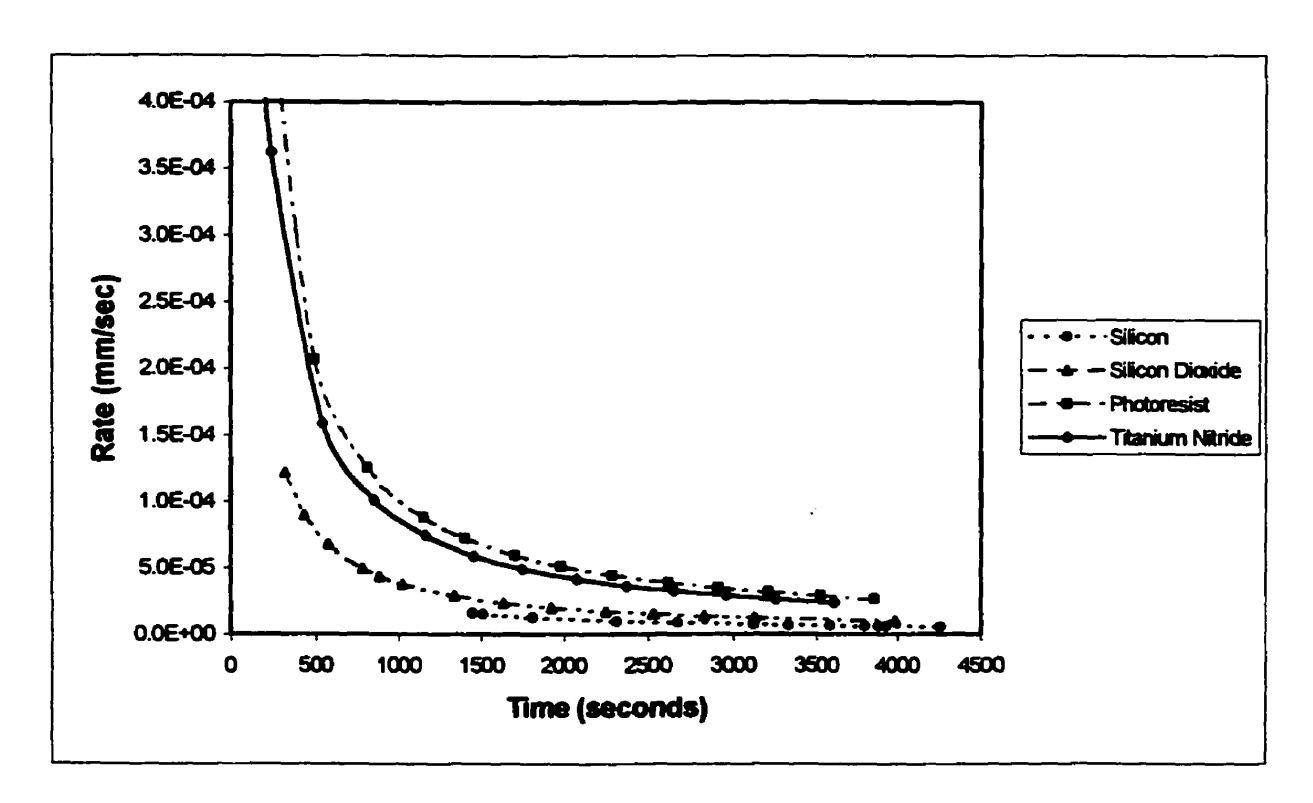


Figure 5.31 - Rate (height) versus time for various surfaces (Particle: sodium chloride, Temperature Difference = 30° C, Q_{N2} =842 ml/min)

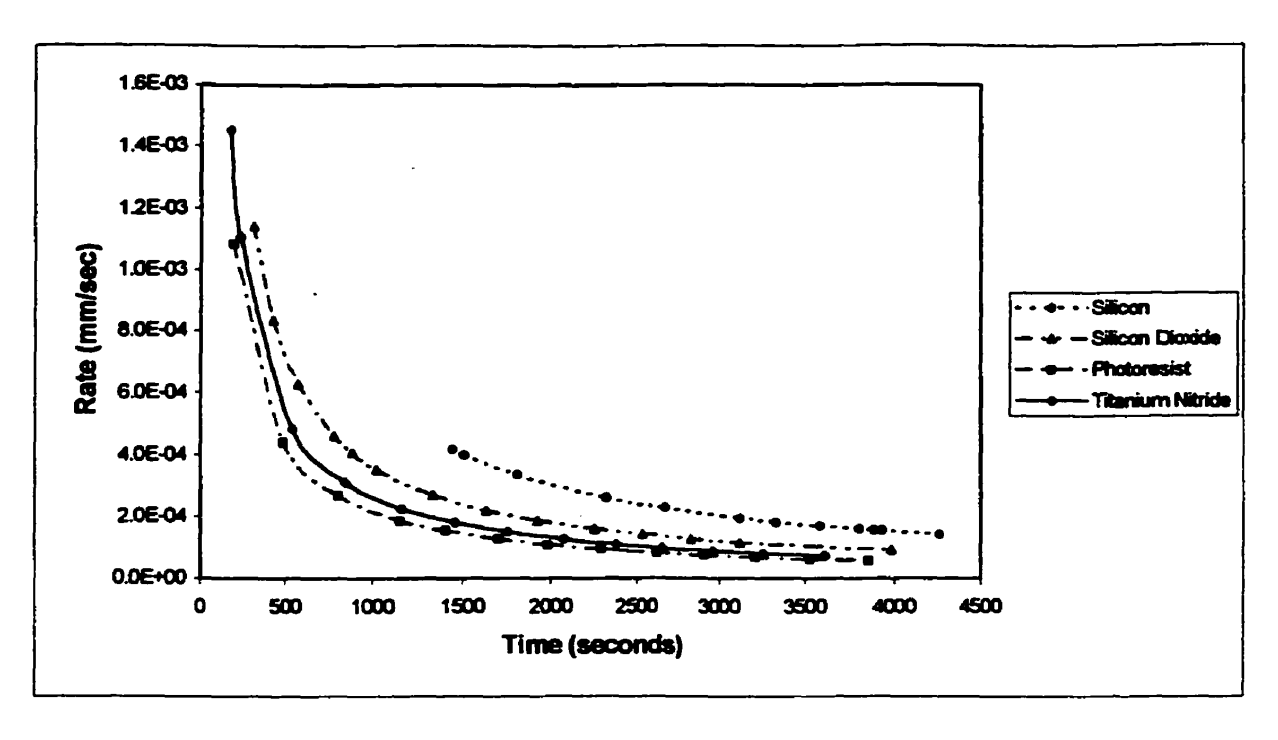


Figure 5.32 - Rate (width) versus time for various surfaces (Particle: sodium chloride, Temperature Difference = 30° C, Q_{N2} =842 ml/min)

5.8 Contamination Distribution & Composition

In this section the results of the particle detection experiments on wafer samples obtained from Nortel Networks are discussed. The surface of these wafers were examined with a scanning electron microscope (SEM) and the resulting contaminant distributions and composition profiles can be seen in Figures 5.33 to 5.54. A general contaminant distribution can be described by imagining a surface of roughly 25mm by 45 mm. Along its scribed edges contaminant particles are deposited anywhere from a minimum of 3mm to a maximum of between 7 and 9mm in from the edge. This type of distribution was seen to occur for all the wafer surfaces which were scribed. Along the edges which were not scribed and towards the center of the surface a small, if not negligible, amount of particles were present. This can be seen in Figures 5.35, 5.40, 5.46, and 5.55.

As shown by Figure 5.33 adjacent to the scribed edges on the wafer there was a small area where the contaminants could be seen. When the center (not shown here) of the sample was examined it was seen to be relatively void of any impurities. On this particular sample (Figure 5.33-5.34) the particles varied in size between 0.1 µm and 10 µm

and as seen by the spot analysis (Chapter 3, section 3.11) the impurities were composed of silicon (Figure 5.35). This supports the hypothesis that these impurities were added to the surface during the scribing and subsequent breaking of the substrate where the particles would consist of the substrate material or the layered material.

As shown by Figure 5.40 and the enlargement in Figure 5.41 there are a large number of contaminant particles present on the surface due to the use of laser lithography (used for producing the identification markers) which caused a small eruption of liquid silicon to spill over onto the surface. The enlargement shows the particles range in size from 0.1 µm to approximately 5 µm in length. When these particles where examined by x-ray analysis the majority of them were composed of silicon (Figure 5.42) which verifies that they are a result of producing the identification markers as was anticipated.

The composition of these particles was determined by performing a spot analysis (Chapter 3, section 3.11). Overall, a large portion of the contaminants which were examined had a composition of either silicon or silicon dioxide. This was expected because when the wafers were scribed and broken sub-micron particles from the substrate and any subsequent layers could redeposit on the wafer. Also detected were numerous silicon dioxide particles which were seen to be present on the silicon, silicon dioxide, and titanium nitride wafers and where generally attributed to the scribing of the surface as well as any potential oxidation of silicon particles present on the surface. A silicon dioxide impurity can be seen in Figures 5.38 and 5.39.

Another common type of contaminant that was present on a majority of the examined surfaces, as shown by Figures 5.36 and 5.37 were salt deposits, such as potassium chloride, sodium chloride, and magnesium chloride. These salt deposits could be easily added to the wafers from human sources. On the titanium nitride and photoresist surfaces seen by Figures 5.43 to 5.50, it was shown that a majority of the contaminants were salt deposits composed mainly of sodium chloride and potassium chloride.

Classical nucleation theory suggests that preferential nucleation of a condensing fluid may not only occur on soluble or insoluble nuclei but also on dislocations, such as a substrates edge. The figures shown in 5.51, 5.53 and 5.54 show various types of surface imperfections that occur along the edge of a wafer and that would provide adequate sites for preferential nucleation and condensation to occur. These are possibly additional sites for nucleation due to the discontinuous surface that results at the edge of the wafers.

5.9 Nucleation on Particulate Impurities

Nucleation and condensation on solid surfaces is a complicated process because solid surfaces are usually neither really geometrically smooth nor completely chemically homogeneous. As a result droplets form at the positions of the active sites. For the purpose of simplification nucleation occurring on absolutely smooth and homogeneous surfaces will be considered.

5.9.1. Nucleation on Soluble Particles (Various Surfaces)

The particle size of the soluble particles was seen to have a smaller effect on the nucleation time then that seen with the insoluble particles. With particles that range in size from roughly 10µm to 100µm the time frame in which condensation begins is between two and five minutes for both flow rates. As the particle size decreases below 10µm and approaches 1µm the nucleation times are seen to decrease below two minutes and can be shorter for the higher flow rate. At the high flow rate the nucleation/condensation occurs quickly; however condensation is also seen to occur on the surface at a faster rate and at times can make the determination of whether contaminant particles are present on the surface very difficult.

For all surfaces it was observed that as the temperature difference (ΔT) increased the time frame over which the condensation occurred on the particulate impurity decreased. However, there was a threshold temperature above which condensation simultaneously occurred on the particle and the surface of the substrate.

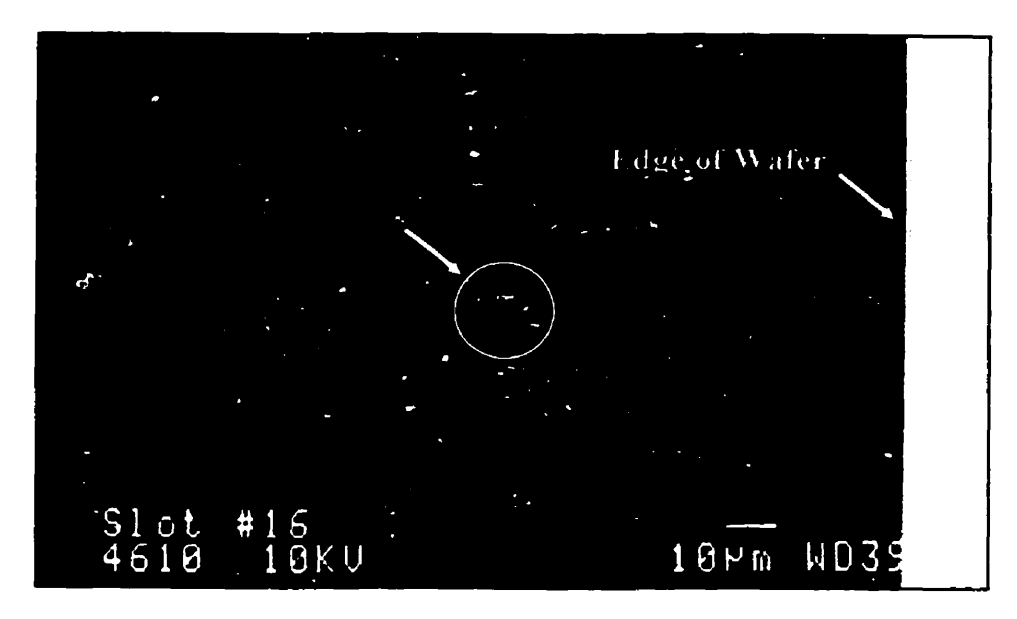


Figure 5.33 - Silicon Dioxide wafer with impurities

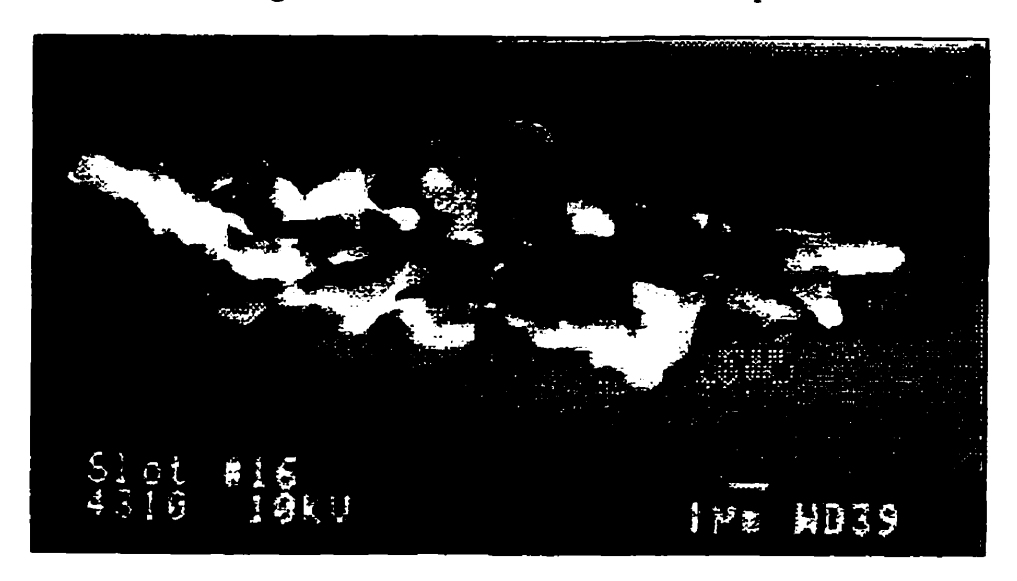


Figure 5.34 - Enlargement of an impurity

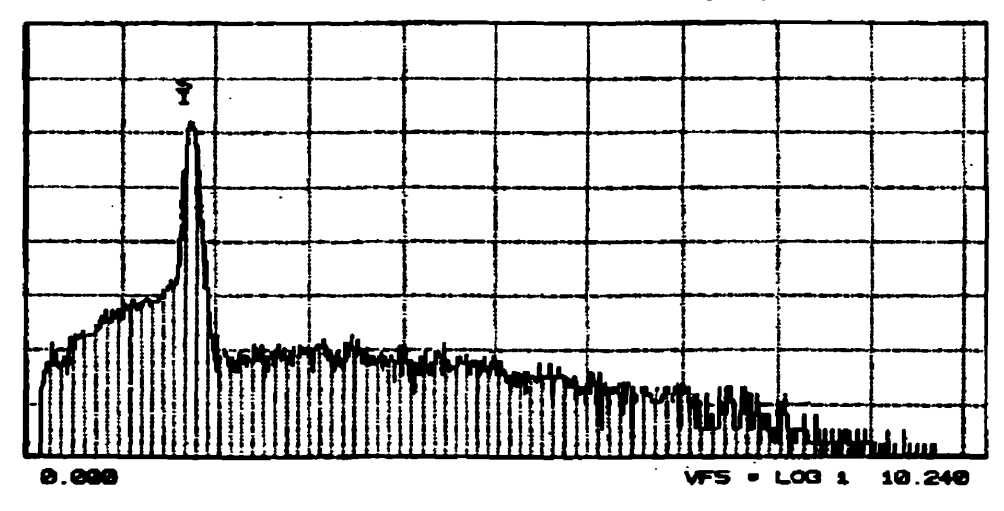


Figure 5.35 - Spot Analysis of Silicon Particle

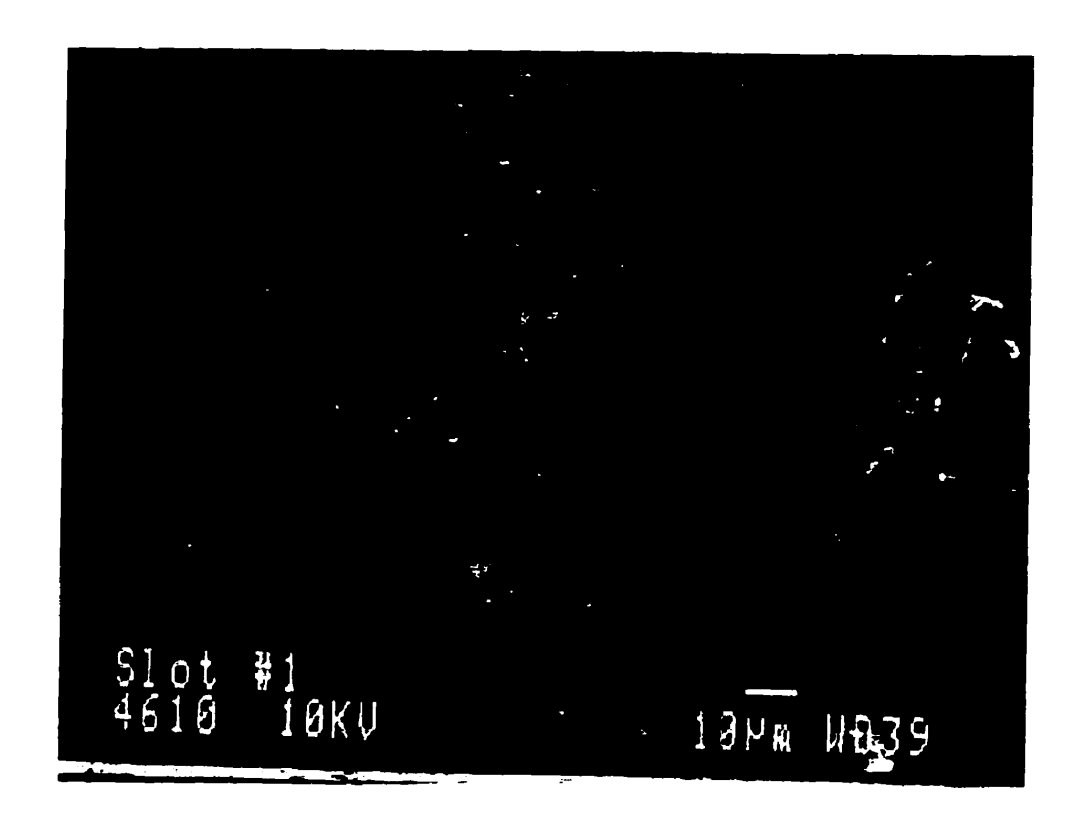


Figure 5.36 - Silicon wafer with a salt deposit

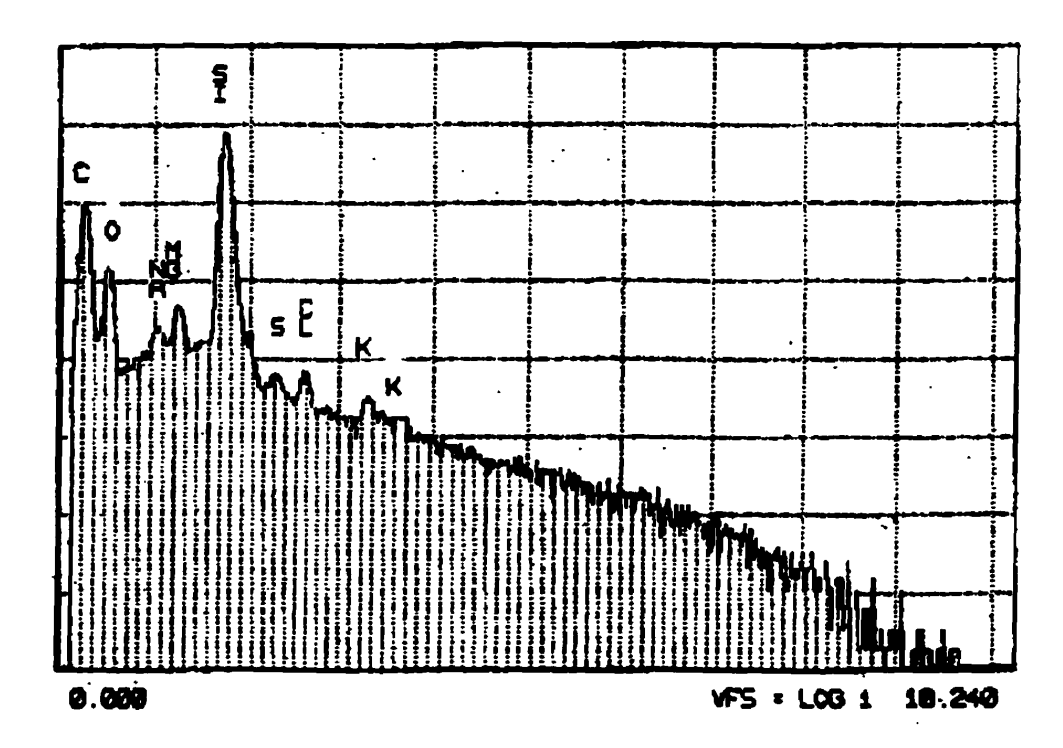


Figure 5.37 - Spot Analysis of salt deposit

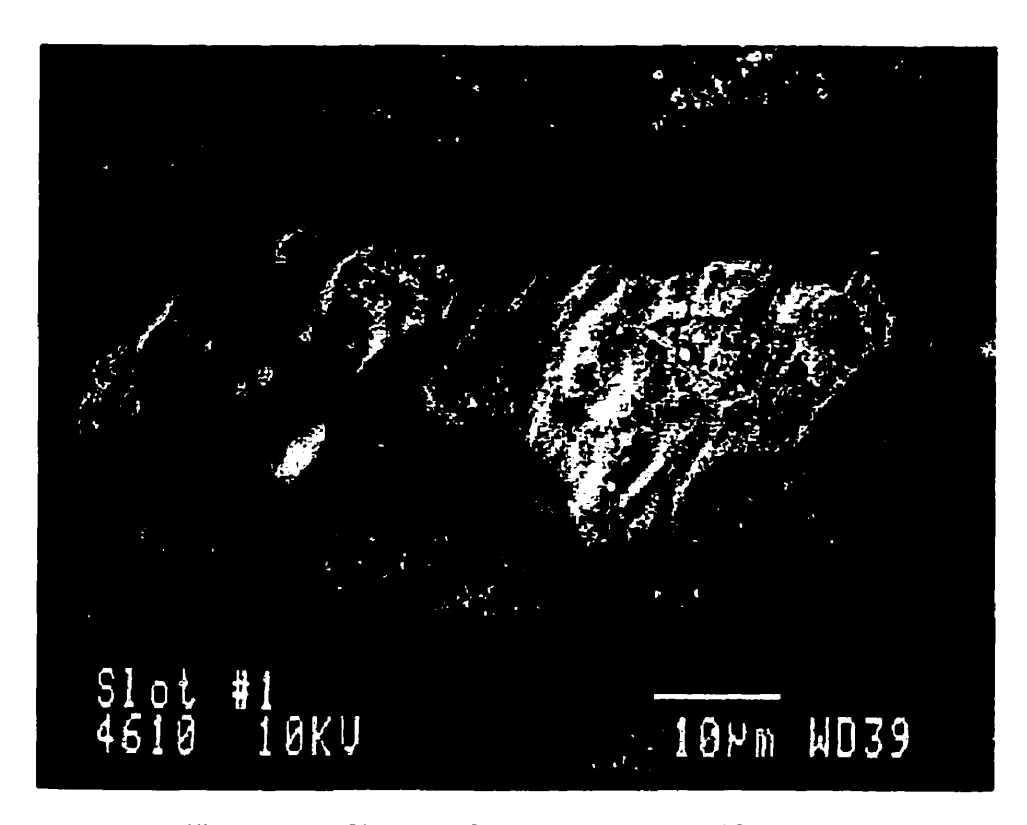


Figure 5.38 - Silicon wafer with a silicon dioxide impurity

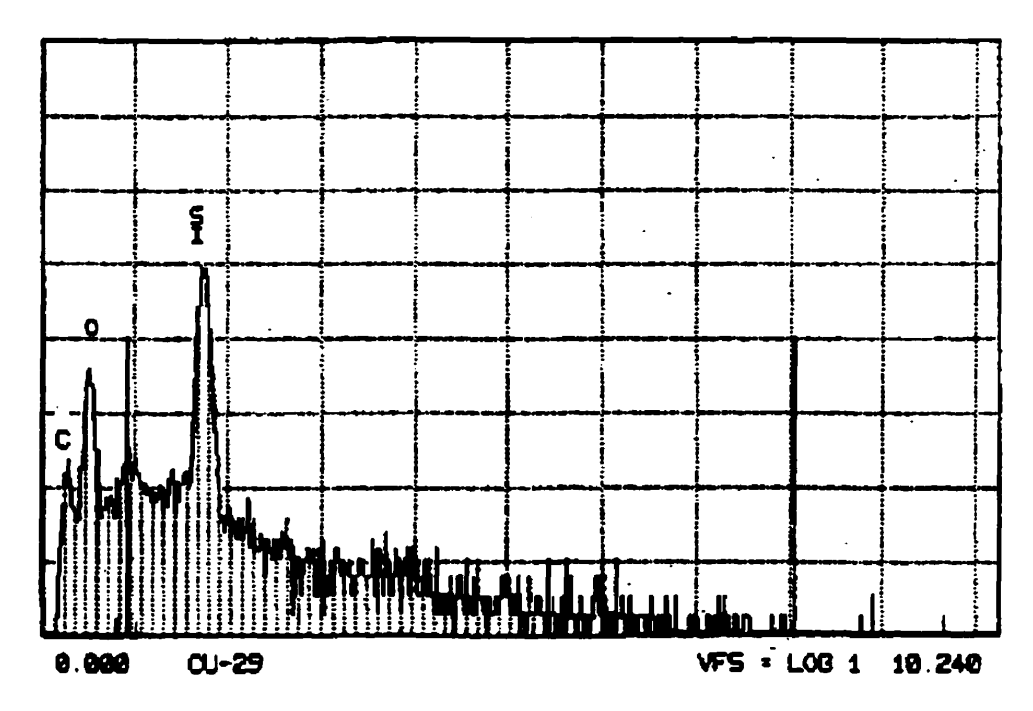


Figure 5.39 - Spot Analysis of a silicon dioxide impurity

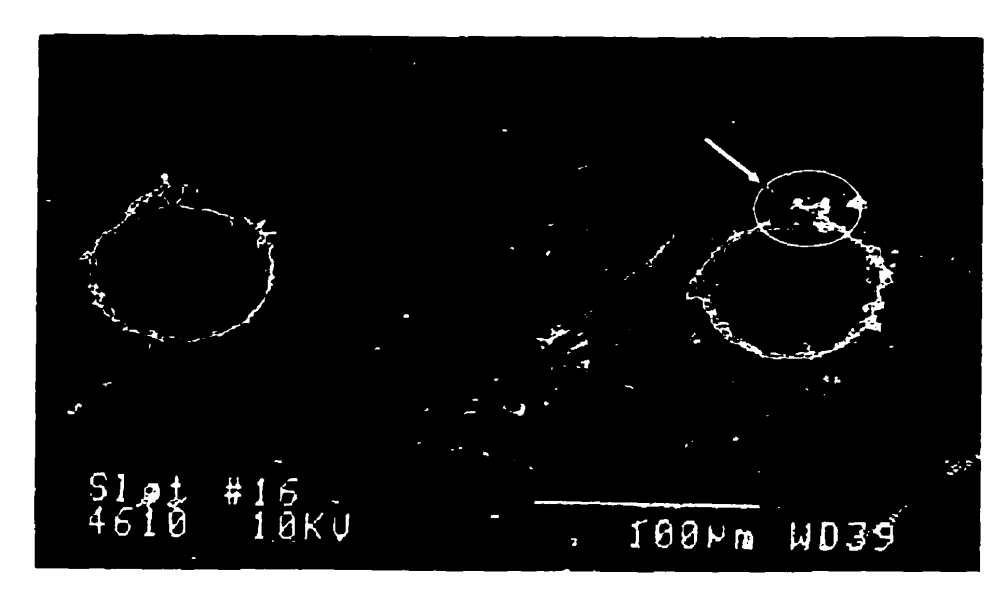


Figure 5.40 - Marks produced by Laser Lithography



Figure 5.41 - Enlargement of marks produced by Laser Lithography

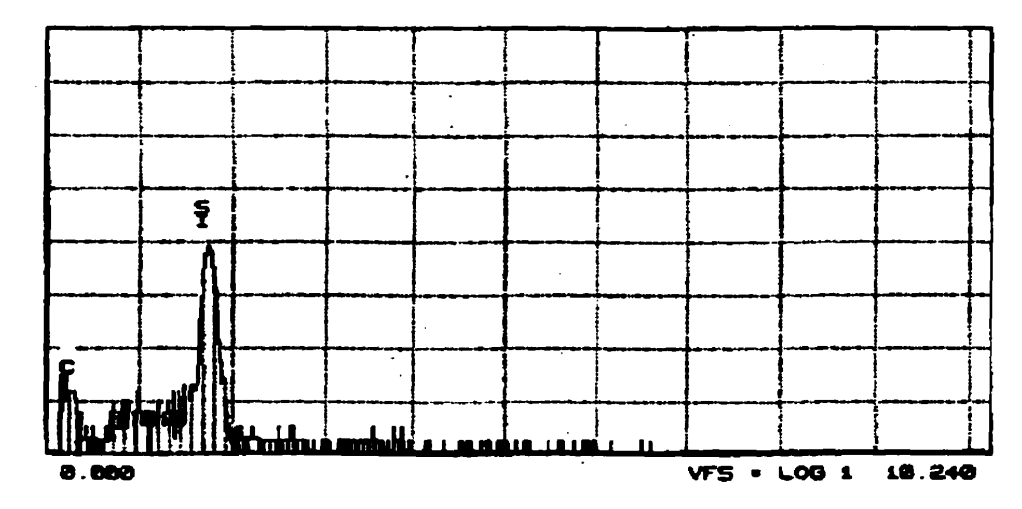


Figure 5.42 - Spot Analysis of Silicon Particle

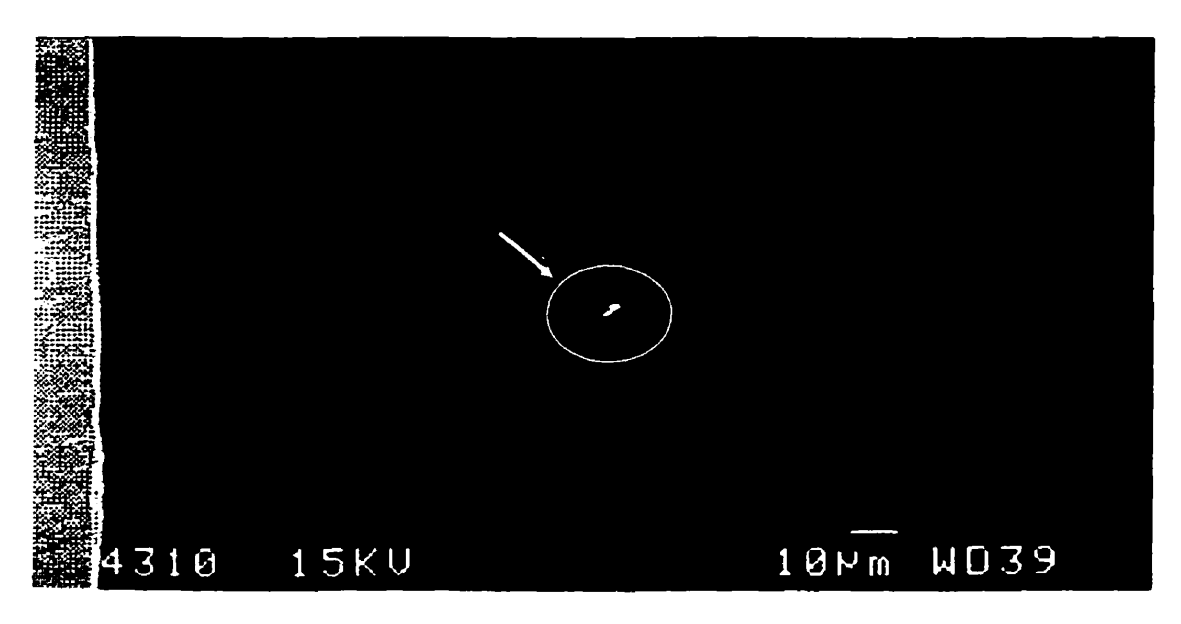


Figure 5.43 - Salt deposit on Titanium Nitride Surface

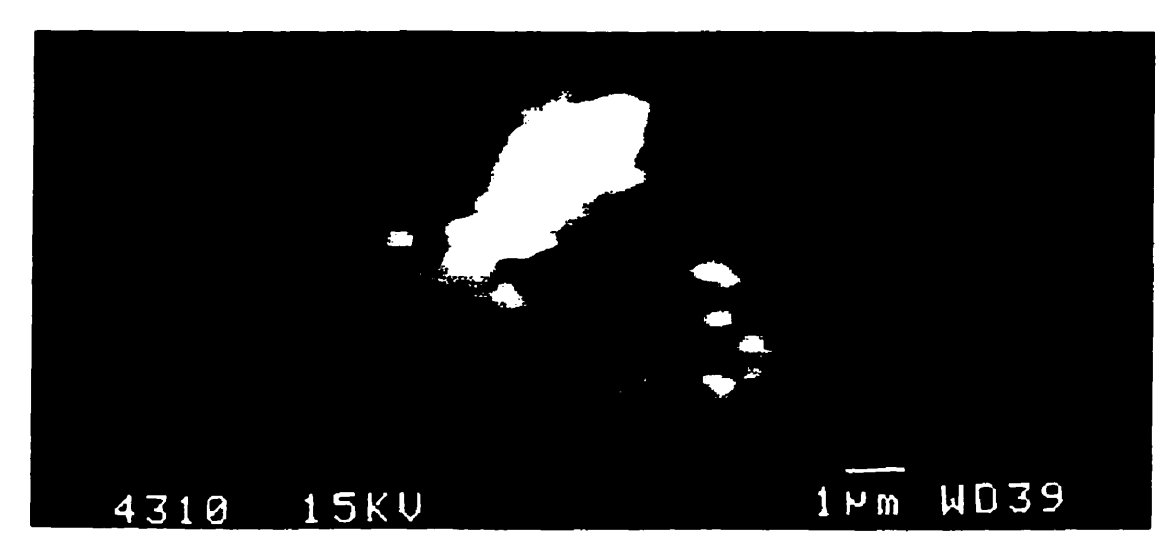


Figure 5.44 - Enlargement of Impurity

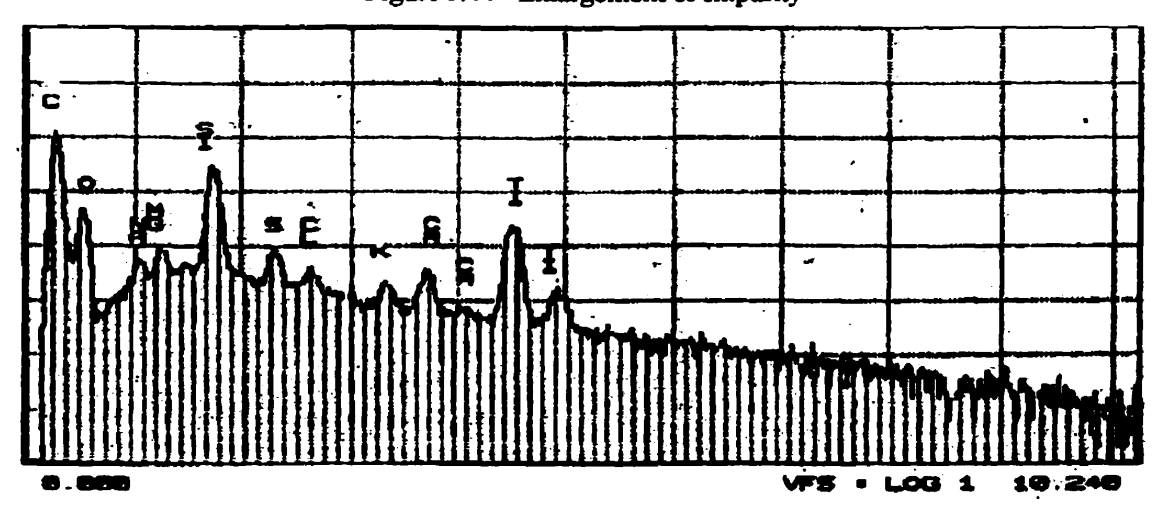


Figure 5.45 - Spot analysis of salt deposit

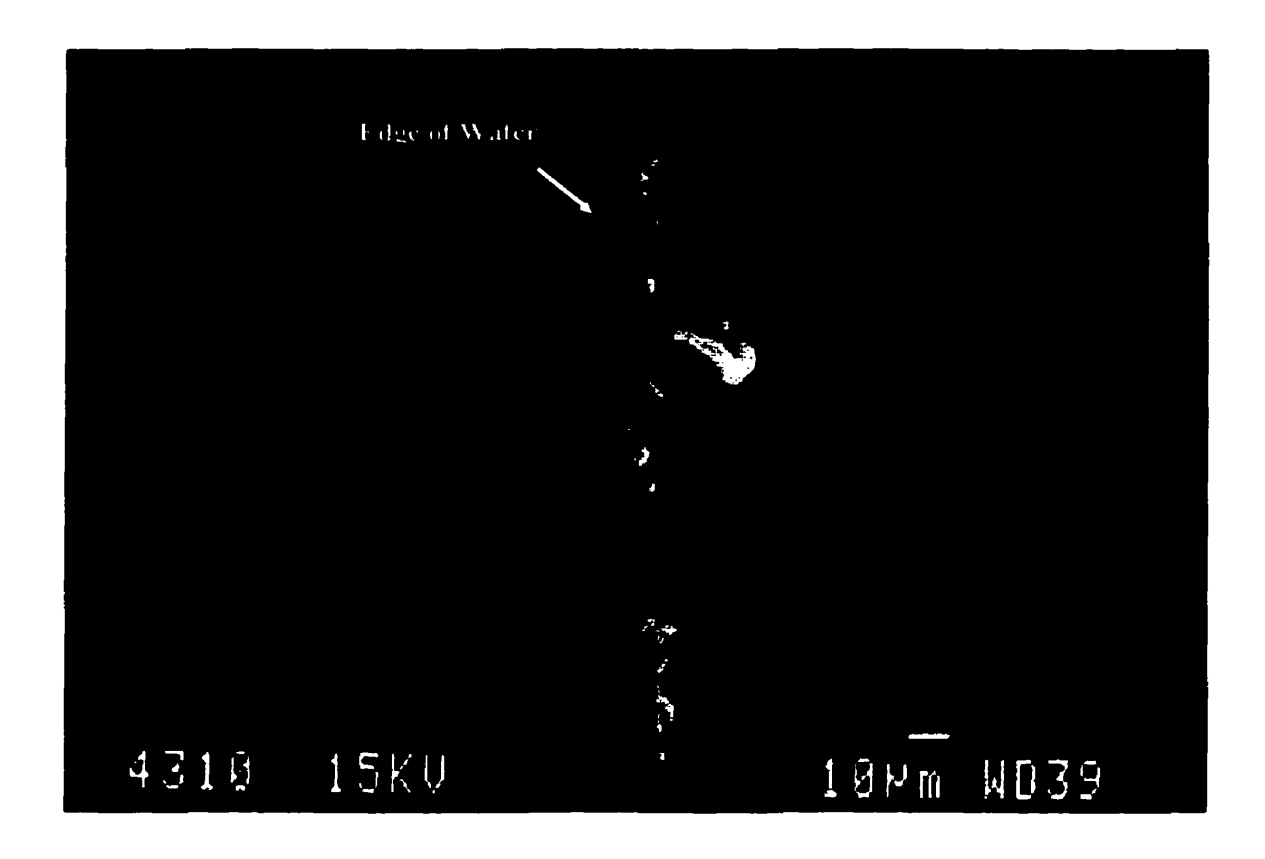


Figure 5.46 - Edge of Titanium Nitride Surface

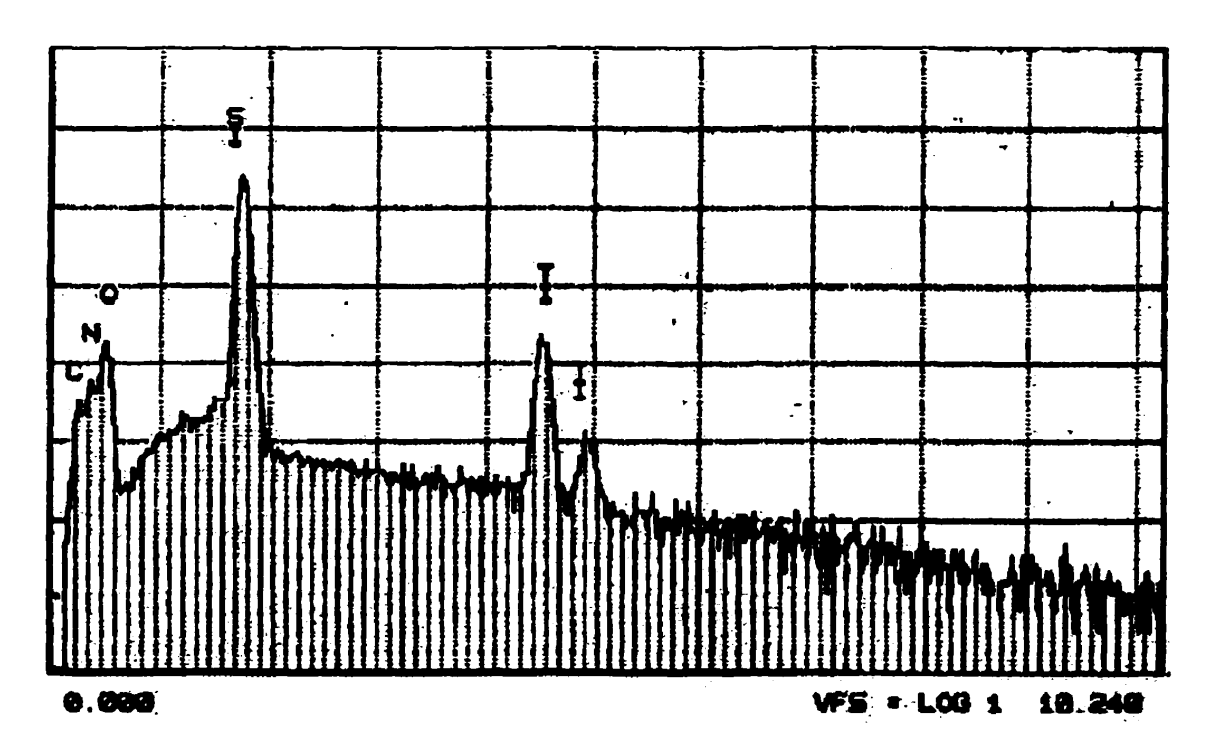


Figure 5.47 - Spot Analysis of Titanium Nitride Surface

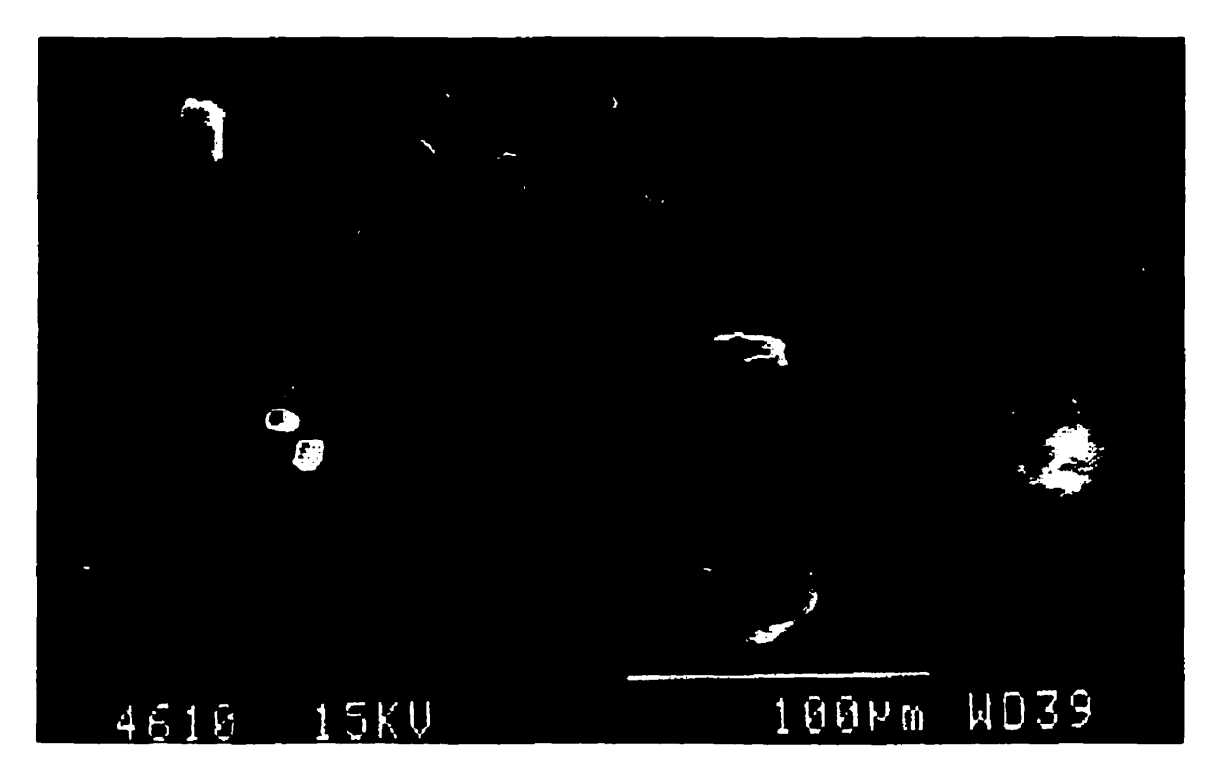


Figure 5.48 - Salt deposit on a Photoresist Surface

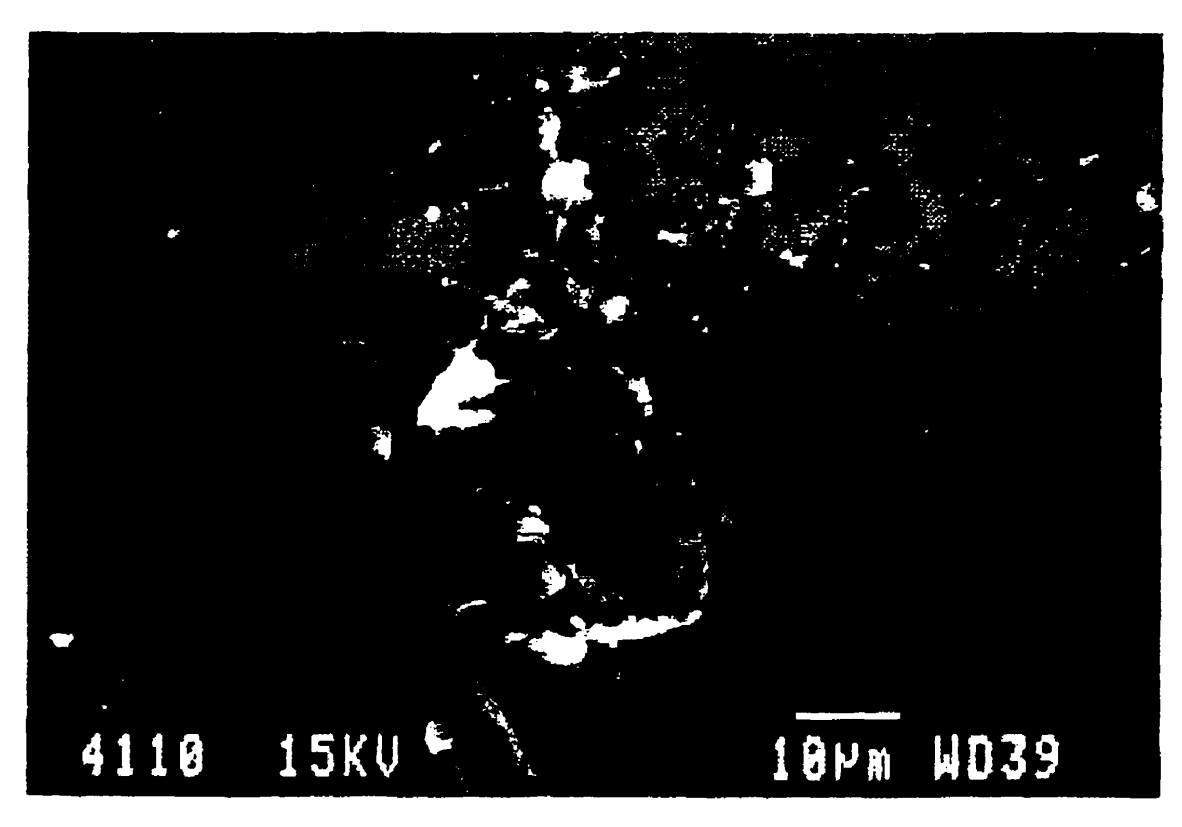


Figure 5.49 - Salt deposit on a Photoresist Surface

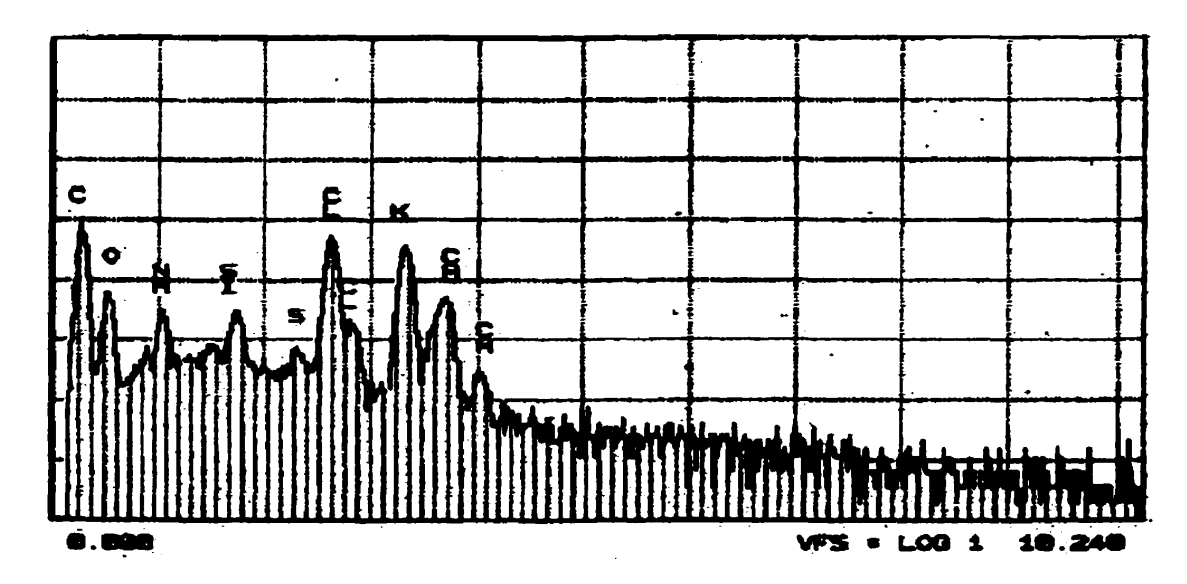


Figure 5.50 - Spot Analysis of salt deposit

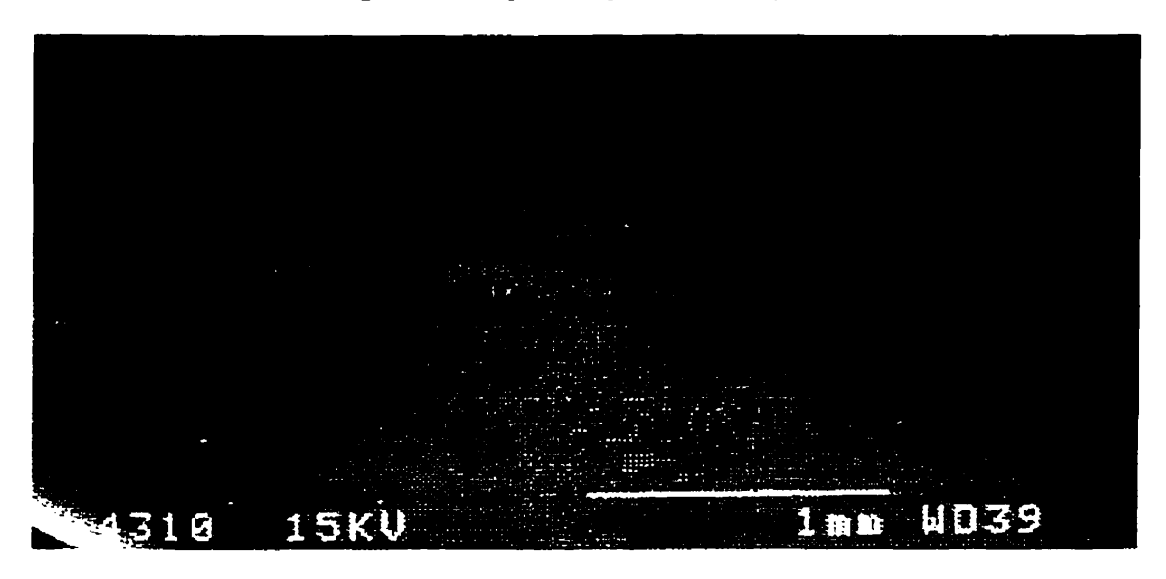


Figure 5.51 - Edge of Photoresist Layer

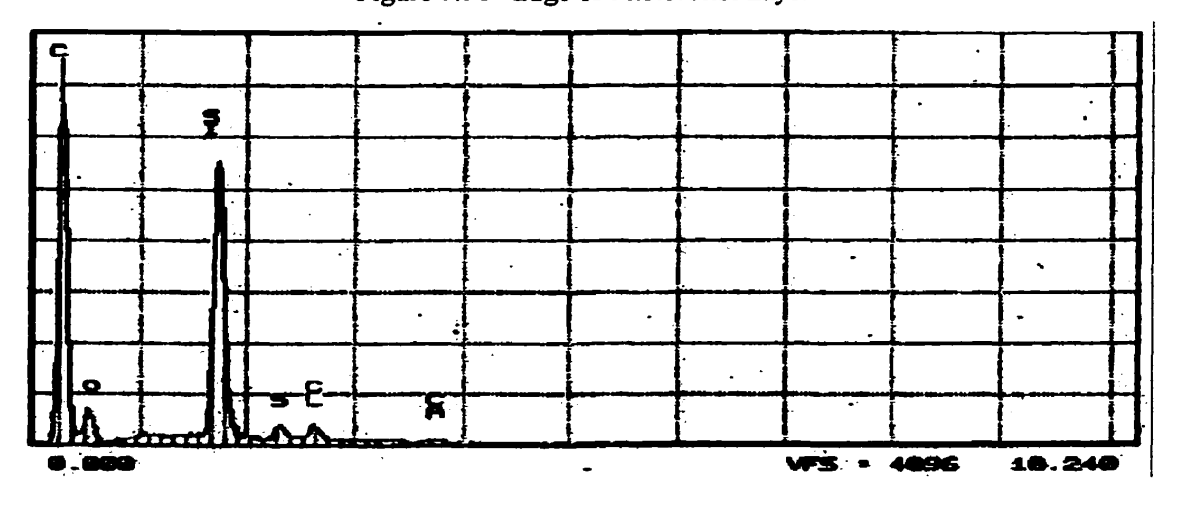


Figure 5.52 - Spot Analysis of Photoresist Layer



Figure 5.53 - Edge of Wafer

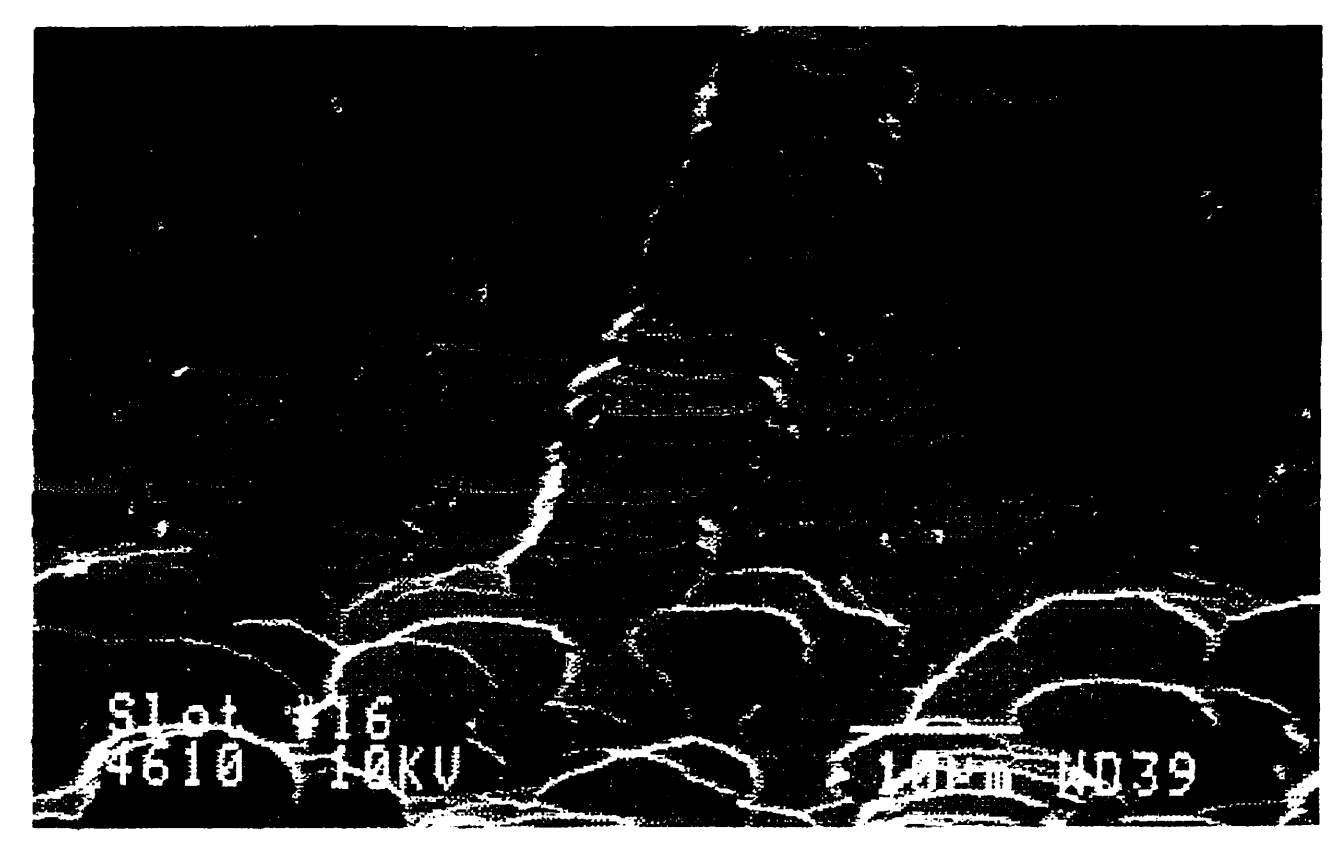


Figure 5.54 - Edge of Wafer

5.9.2 Nucleation on Insoluble Particles (Borosilicate Glass Surface)

Several particle types have been used to simulate a solid water insoluble particulate contaminant on a borosilicate glass surface; however none have been successful nucleation sites on which a droplet forms. The types of particles which have been examined are barium sulfate, silicon, silicon dioxide, and silver chloride. Barium sulfate and silicon dioxide are hygroscopic in nature so they absorbed a finite amount of water vapor from the atmosphere; however it was not enough to form a preferential nucleation site.

One possible hypothesis for this effect is that the free energy of the particle in question is greater than the free energy of the glass surface. Therefore the energy barrier which the water vapor must over come in the nucleation on one of these particles is much greater than that for nucleation on the borosilicate glass surface. Thus, the water vapor will condense on the glass surface rather than on the particle. Another more likely potential explanation is that the contaminant particle size was too large and therefore didn't act as a preferential nucleation site for the condensing water vapor.

5.9.3 Nucleation on Insoluble Particles (Silicon, Silicon Dioxide, Photoresist, and Titanium Nitride Surfaces)

When the tested semiconductor surfaces were placed in the environmental chamber and under the specified preferential nucleation experimental conditions, small water droplets formed along the scribed edges where potential 0.1 to 10µm contamination sites existed as seen by the scanning electron microscope. These distributions were observed for several different wafers and under varying conditions. Furthermore, these potential contaminants were examined with the SEM to identify the contamination region and to verify the origin and composition of the particle.

Initially two types of insoluble particles were examined, silicon dust and silicon dioxide, these impurities were artificially added to the various surfaces. The general observation was that at the high nitrogen flow rate on the silicon and silicon dioxide

surfaces after two to three minutes nucleation began on the particle. However, after five to eight minutes, water began to condense on the surface; thus there was a small window in which preferential nucleation may occur in as shown in the sequenced images in Appendix C. As with the soluble particles, both a droplet with an equilibrium contact angle and a clear-ring (defined as the area on the surface from which the droplet adsorbs condensed water) were formed; however unlike the soluble particles the contact angle remained constant and unchanging. With the low flow rate of 417 ml/min their was no visible condensation on the surface though the time required for water vapor to condense on the particle to an extent that a droplet was produced was increased, taking more than 25 minutes in some instances.

On the photoresist and the titanium nitride surfaces, preferential nucleation did occur following the same trends as discussed above; however the time frame in which the nucleation and condensation occurred on the particle were lengthened increasing the time frame by an additional 10% to 20%. This was expected since the literature suggested that hydrophilic surfaces (such as silicon and silicon dioxide) should decrease the thermodynamic barrier of nucleation and allow the preferential nucleation to occur at a faster rate, whereas the opposite is true for the hydrophobic surfaces (Fowkes, 1964).

One unforeseen difficulty was that the particle size had an effect as to whether or not nucleation would occur on the impurity. Thus in order for preferential nucleation to occur the particle size of the silicon dust and the silicon dioxide had to remain below a specific size which was approximated to be less than 0.1mm (100µm). This circumstance is in the favor of the semiconductor industry since many of the contaminant particles which are present in the process are sub - 1.0 micron in size.

The silicon dust used caused several problems with measuring the growth rate of the condensing water vapor. Since the silicon dust is extremely fine it was difficult to artificially add only a single particle to any given area, as a result several particles resided in one region and acted as multiple seeds for nucleation. Therefore, it was impossible to have only one droplet to observe and as they grew in size they would come into contact

with one another and spread over the surface. The silicon dioxide also resulted in difficulties determining the growth rate since this particle type had a tendency to conglomerate and as a result the same difficulties as discussed above were present for this particle type.

As mentioned above, the contact angle of the droplet for the insoluble particles remained fairly constant. This was anticipated since there were no variations in the solution concentration as was seen with the soluble particles. Thus, the droplet growth rate was not a function of solution concentration and was dependent on the temperature difference and the flow rate.

5.10 Recommended Conditions for Detection of Particles

Even though the droplet growth rates on a majority of the tested surfaces have indicated that the growth rate increased with increasing temperature difference, there was a point beyond which preferential nucleation would no longer occur on the soluble and insoluble particulate impurities. Past this threshold temperature, condensation would begin almost immediately over the entire surface and as a result the impurities would be obscured by the condensed water. To that end there was the need to balance the droplets growth rate against the need to have preferential nucleation and condensation.

The overall conditions which allowed preferential nucleation to occur at the two flow rates are as follows:

Table 5.1 - Experimental Conditions for Preferential Nucleation

Conditions	Flow rate	Flow rate	
·	Q = 417.44 ml/min	Q = 842.47 ml/min	
T _{substrate}	22 - 24°C	22 - 24°C	
T _{vapor}	35 - 55 °C (max.)	35 - 45 °C (max.)	
Duration	2-30 minutes after which	2 - 10 minutes after which	
(surface: silicon and	condensation begins to	condensation begins to	
silicon dioxide)	interfere with determining	interfere with determining	
	the contamination sites.	the contamination sites.	
	(depending on particle size)	(depending on particle size)	
Duration	Overall duration increases	Overall duration increases	
(surface: photoresist and	by approximately 10- 20%.	by approximately 10-20%.	
titanium nitride)			

Chapter 6

Conclusions and Recommendations

6.1 Conclusions

In this research project the nucleation and condensation of water droplets was used to determine the presence of contaminant particulate impurities on several important surfaces used in the microelectronics industry. Also the relationship between the wettability of the surfaces and the droplet growth was studied. The experimental results showed that preferential nucleation does occur and was a technique for determining the presence of both water soluble and insoluble contaminants. A threshold temperature was also established beyond which nucleation would no longer occur. This was found to vary with flow rate. The temperature range in which preferential nucleation was observed decreased with an increasing the nitrogen flow rate, decreasing by approximately 10°C when the flow rate was roughly doubled from 417 ml/min to 842 ml/min. It was also found that the droplet growth rate increased with increasing temperature difference (defined as the difference between the gas phase and the surface of the substrate), increasing surface hydrophobicity, and nitrogen flow rate. The droplet growth rate was affected by the type of solute (sodium chloride or sodium sulfate), solution concentration, and the type of surface (hydrophilic or hydrophobic). Unlike the water soluble particulate impurities, the insoluble impurities the particle size did have an effect as to whether or not preferential nucleation and condensation would occur. If the particle was greater than 100µm it was seen that preferential nucleation would occur over an extended duration (greater than 25 minutes) or not occur at all depending on the flowrate.

Equilibrium contact angle measurements were performed on borosilicate glass, silicon, and silicon dioxide surfaces, and the observed trend was that at relatively low concentrations, from 0 to 10 g/l of the salt solution there was a significant increase in the measured angle. At the higher concentrations (>10 g/l) the values remained constant in value.

A scanning electron microscope (S.E.M) analysis of the surface indicated the types of contaminant particles present on the surface of the wafers, the composition of the impurities, the size range, and their distribution on the surface. A majority of the particles ranged in size from approximately 0.1 to 10µm and were mainly composed of either the substrate material (silicon or silicon dioxide), the layer material (photoresist or titanium nitride) or were a combination of salts.

6.2 Recommendations

For future work on this topic it may be beneficial to use other types of condensing vapor media, such as organic solvents which may allow for a large temperature range in which preferential nucleation occurs and possibly more controllable conditions. The proposed technique was applicable to particles greater than 10µm. Future work should concentrate on smaller particles by using a more powerful optical lens. Also, a wider range of both soluble and insoluble particles can be investigated. Finally, the use of a larger number of industrial important surfaces and the study of how wettability properties change as a function of time would also be beneficial.

From this study it may be possible to further develop techniques capable of effectively removing contaminants once they are deposited on the surface. Furthermore, this data may provide indicators that lead to the sourcing and overall elimination of these contaminants through control of their generating mechanisms and thereby improve the reliability and yielding parameters of the product.

Chapter 7

References

7.1 Literature Cited

- 1. Abraham, Homogeneous Nucleation Theory, Academic Press, New York, (1974)
- 2. Beck, M.A. George, D.A. Bohling, B.J. Shemanski, J.T. McGuire, Advanced Semiconductor Manufacturing Conference, pp. 100, (1994)
- 3. Blewer, Advanced Semiconductor Manufacturing Conference, pp.83, (1994)
- 4. Cahn, J.E. Hillard, *Ibid.*, 28, pp.258, (1958)
- 5. *Ibid.*, 31, pp.688, (1959)
- 6. Cheung, D.L. Jensen, G.L. Mooney, Advanced Semiconductor Manufacturing Conference, pp.107, (1994)
- 7. Dunning, Chemistry of the Solid State, Academic Press New York, (1955)
- 8. Fletcher, J. Chem. Phys., 29, pp.572, 31, pp.1139, (1992)
- 9. Fowkes, F. M., Contact Angle, Wettability, and Adhesion, Advances in Chemistry Series, (1964)
- Garnier, G., Dept. of Chemical Engineering, McGill University, PAPRICAN,
 Personal Communication, (1998)
- 11. Garnier, G., Wright, J., Godbout, L., Yu, L., Colliods & Surfaces A: Physicochemical & Engineering Aspects, 145, pp.153-165, (1998)

12. Geankoplis, C.J. Transport Processes and Unit Operations, Prentice Hall, New Jersey, (1993)

- 13. Hinsberg, S. MacDonald, N.Clerk, and C. Synder, J. Photopolymer Sci. Technology, 6 (4), pp. 535, (1993)
- 14. Ho, J.R. Maa, J. Colloid & Interface Sci., 85 (2), pp.413, (1982)
- 15. Hwu, J.S. Sheu, and J.R. Maa, J. Colloid & Interface Sci., 121 (2), pp.303, (1988)
- 16. International Critical Tables (1977)
- 17. Kasi and M. Luch, J. Vac. Sci. Technology, 10 (4), pp.795, (1992)
- 18. Katz, H. Wiedersich, J. Colloid & Interface Sci., 61 (4), pp.351, (1977)
- 19. Masliyah, J.H., Electokinetic Transport Phenomena, Aostra Technical Publication, Series 12, Edmonton, pp. 363, (1994)
- 20. Muller, L.A. Psota-Keltg, H.W. Kratter, and J.D. Sinclair, Solid State Technology. 37 (9), pp.61, (1994)
- 21. Perry, Chemical Engineers' Handbook, McGraw-Hill, New York, (1963)
- 22. Quilantang, A.Sharif, Advanced Semiconductor Manufacturing Conference, pp.112, (1994)
- 23. Rappa, Advanced Semiconductor Manufacturing Conference, pp.87, (1994)

24. H.Shinagawa, K. Sotowa, Y. Kawamura, and K. Okuyama, J. Chem. Eng. Japan, 25 (2), pp.139, (1992)

- 25. H.Shinagawa, Y. Kawamura, and K. Okuyama, J. Chem. Eng. Japan, 25 (2), pp.448, (1992)
- 26. Tamaoki, K. Nishiki, A. Shimazuki, Y. Sasaki, S. Yanagi, Advanced Semiconductor Manufacturing Conference, pp.322, (1995)
- 27. Turnbull, J. Chem. Phys., 18, pp.198, (1950)
- 28. Zettlemoyer, Nucleation, Marcel Dekker, New York, (1969)

Appendix A -

Image Analysis Techniques

A.1 Manual Contact Angle Measurements

Once the procedures described in Chapter 3, section 3.9 have been used to produce and record an image of the required quality the image can be transferred to the computer. This method is simpler and uses TCI Pro and Visilog Image Analysis software. The analysis begins with using the software called TCI Pro to capture the required images, first use the toolbar and click on the **Grab** function. This allows the user to scroll through the video tape in order to find the appropriate time index. Once the appropriate time index was located, click on the **Freeze** function from the toolbar, this allows the user to capture and save the image. At this stage it was necessary to save the image by going to the File menu and scrolling down to the **Save As** function and saving the file in the appropriate file folder, the file will be saved with a .TIFF extension.

Once this is completed it is now possible to analyze the image. Once the image is opened in Visilog, go to the toolbar menu and scroll down to **Measurement**. This will give several options such as line measurements (for height and width of the droplet), angle measurement (contact angle), and calibration (from pixels to mm).

At this point it was possible to refine the image, for example it can be smoothed, sharpened, and the threshold taken in order to clearly indicate the profile and the apex of the droplet, as seen in Figure A.1. All processing of the image can be done by clicking on the **Processing** icon in the lower right hand corner of the screen. This will give several options such as filters, morphology, threshold, etc.

With the static contact angle measurement both the right and left contact angles were measured by separately magnifying each apex by an additional 4X. Once the image has been processed, as was described above, independent measurements were performed on each apex of the droplet. The contact angle was measured by going to the measurement toolbar and clicking on the angle icon (\angle). This will allow the user to manually trace the drop profile and determine the contact angle to within approximately \pm 1.0 degree. An overall average of the left and the right contact angles was calculated and the reported values represent the equilibrium contact angle for that particular solution

concentration or condensate-substrate combination under the stated experimental conditions.

This method allows the user to examine the images one at a time in order to determine the contact angle and growth rate and has no difficulties making measurements for droplets which are in a state of flux. This technique doesn't have any constraints on the contact angle which are quite common with macro aided contact angle measurements, and so can be accurately measured.

In addition a confidence interval was calculated for each series of angle measurements in order to find the particular length of the interval consisting of upper and lower limits that bound the parameter with a 95% probability. Generally it was observed that the 95% confidence interval fell within a range of \pm 1.5 degrees for the borosilicate glass surfaces and \pm 1.0 degrees for the remaining surfaces of the calculated average contact angle for the solution droplet on the substrate.

A.2 Threshold Function

This section will give a brief introduction and an understanding of one of the functions commonly used in Visilog. The threshold function requires very clear images in order for it to be used and with minimal user input but must be set-up properly in order to generate useful results.

The scan technique is based on the pixel values which are a numerical representation of the darkness of the pixels in the gray scale image. A pixel value of 0 represents white and 255 is black. The integer values in between represent a range of grays. This technique interprets large sharp changes in these values to represent the edges of the droplet image. The detection procedure analyses the array of pixel values from top to bottom (i.e. vertical scan lines) and from left to right (i.e. horizontal scan lines). The detection procedure looks for two points along each scan line, one for the droplet and one for its reflection. These are the points at which there is the greatest jump in pixel values from light to dark and the point where the pixels have the greatest fall from a dark pixel

Appendix A 106

to a light pixel and this was determined to be a point along the profile of the droplet. These coordinates are then stored in the results array as one of the points on the droplet profile and allows a threshold to be produced as seen below;

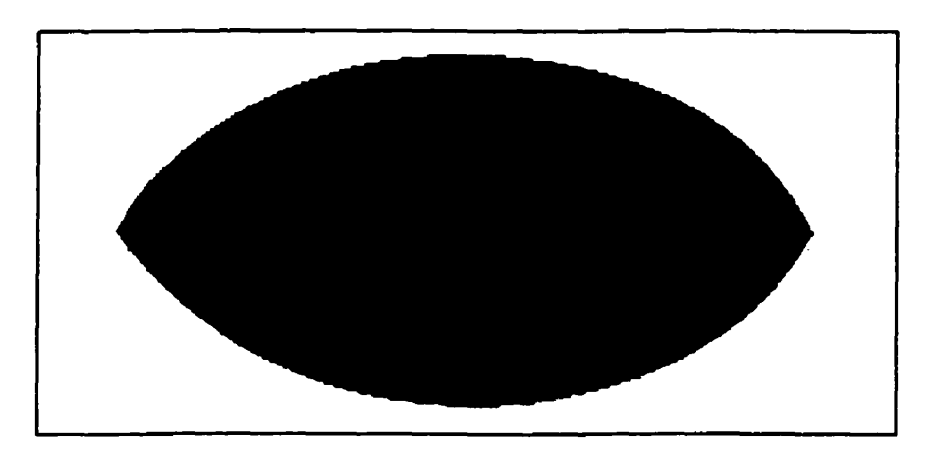


Figure A.1 - Threshold of a Droplet

A.3 Height and Width Measurements

For the measurement of the height and width of the droplet the same general procedure (as for the contact angles) was used; however the image was magnified by 2X to 3X. Again, the threshold of the image was taken. The line measurements are made by going to the measurement menu and clicking on the line icon (<). This will allow the user to manually measure the linear distance between two specified points in either pixels or millimeters by using a predetermined set of calibrations.

Appendix B -

Determination of Droplet Volume for Batch Type Nucleation

To determine whether a batch or continuous flow of the vapor mixture (nitrogen and water vapor) should be used, several theoretical calculations were performed to ascertain the droplet volume produced for a batch system. It was hypothesized that if the chamber was entirely filled with a saturated vapor and all the water vapor in that system was condensed onto one particular point, would the droplet be of a sufficient size to see. If an excessive amount of water vapor is possible in the chamber a large droplet volume would be expected. By knowing the relative humidity (inside the chamber) varied between 95 and 100% and the volume of the environmental chamber it was possible to ascertain the amount of water vapor present as a function of the gas phase temperature. The following series of sample calculations show the procedure used for determining the droplet volume.

The percentage relative humidity (HR) is the amount of saturation of an air-water vapor mixture and it was possible to experimentally determine the relative humidity inside the environmental chamber using a humidity probe and sensor.

$$HR = 100 \frac{p_a}{p_{as}}$$

Assuming for the sample calculation that HR = 100%

$$100 = 100 \frac{p_a}{p_{as}}$$

therefore

$$P_a = P_{as}$$
 [kPa]

Knowing the value of both P_a and P_{as} it was possible to calculate the humidity. The humidity H of an air-water vapor mixture is defined as the kg of water vapor contained in 1 kg of dry air. The humidity so defined depends only on the partial pressure P_a of water vapor in the air and on the total pressure P (assumed in this case to be 101.325 kPa). Using the molecular weight of water and air, the humidity can be defined as follows;

$$H = \frac{18.02}{28.97} \cdot \frac{p_a}{P - p_a}$$
 [kg H₂O/kg dry air]

Saturated air is air in which the water vapor is in equilibrium with liquid water at the given conditions of pressure and temperature. In this mixture the partial pressure of the water vapor in the air-water mixture is equal to the vapor pressure P_{ss} of pure water at the given temperature (the values of P_{ss} can be obtained from the steam tables). Hence, the saturation humidity Hs is determined by;

$$H_s = \frac{18.02}{28.97} \cdot \frac{p_{as}}{P - p_{as}}$$
 [kg H₂O/kg dry air]

The humid volume of air water mixture (V_H) is the total volume in m³ of 1 kg of dry air plus the vapor it contains at a pressure of 101.325 kPa and the given gas temperature. Using the ideal gas law the humid volume can be calculated from;

$$V_H = \frac{22.41}{273}T(K)\left[\frac{1}{28.97} + \frac{1}{18.02}H\right]$$

$$V_H = \frac{22.41}{273} \cdot 308 \left[\frac{1}{28.97} + \frac{1}{18.02} * 0. \right] = 0.92297 \quad [m^3 / dry air]$$

The interior dimensions of the environmental chamber to be 34.9mm X 50.7mm X 47.5mm, therefore the interior volume of the chamber can be determined to be,

$$V_{chamber} = 84047.925 \text{ mm}^3 \approx 8.4048 \cdot 10^{-5} \text{ m}^3$$

Knowing the volume of the environmental chamber and the humid volume (V_H) it is possible to ascertain the mass of dry air.

$$M_{dryair} = \frac{V_{chamber}}{V_H}$$

$$M_{dryair} = \frac{8.4048 \cdot 10^{-5}}{0.92297} = 9.10624 \cdot 10^{-5}$$
 [kg dry air]

By calculating the amount of dry air in the environmental chamber and the humidity it is possible to find the amount of water vapor present within it.

$$M_{water} = M_{drvair} \cdot H$$

$$M_{water} = 9.10624 \cdot 10^{-5} \cdot 0.03655 = 3.3283 \cdot 10^{-6}$$
 [kg H₂O]

Assuming that all the available water vapor is condensed onto the surface in one particular area and using the density of water the volume of that droplet can be easily determined

$$\rho_{water} = 997.08 \text{ [kg/m}^3\text{]}$$

Since that

$$V_{droplet} = \frac{M_{water}}{\rho}$$

$$V_{droplet} = \frac{3.3283 \cdot 10^{-6}}{997.08} = 3.33804 \cdot 10^{-9} \, m^3 \approx 0.00338804 cm^3 (ml)$$

It can be said that the produced droplet is small in size. Using the volume equation for a spherical segment of one base;

$$V = \frac{1}{6}\pi h \left(3r^2 + h^2\right)$$

and assuming a droplet width (w) of 0.12 cm or a radius (r) of 0.06 cm and solving for the droplet height (h), one gets a value of 0.28344 cm.

If all the available water vapor present in the chamber was used for condensation on one contaminant particle, the size of the droplet produced would be as indicated above, however, if there were multiple contaminants on one surface and taking into account possible condensation on the interior walls of the chamber itself, there would be an insufficient amount of vapor to condense on these particles. Thus it is required to have a continuous flow of water vapor. A

summary of the results for the varying gas phase temperature and its effect on the droplet volume can be seen in Figure B.1 and Table B.1.

Figure B.1 shows the relative humidity range from 90 to 100% where there is only a slight change in the volume of the droplet which decreases with decreasing relative humidity. This change in droplet volume is seen to increase as the gas phase temperature increases.

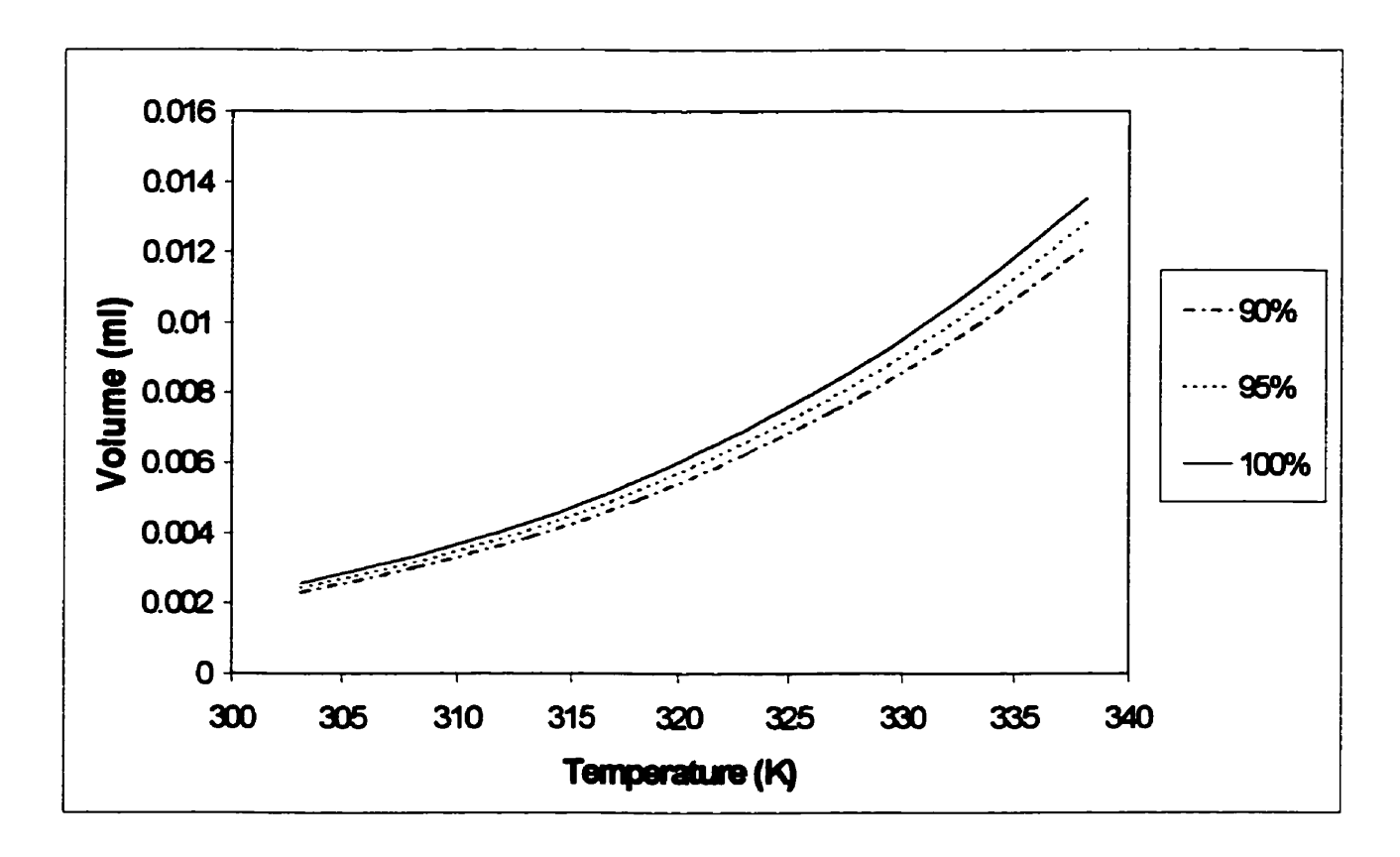


Figure B.1 - Droplet Volume as a Function of Gas Phase Temperature and Percent Relative Humidity (Theoretical Calculation)

Table B.1 - Calculated Results

Relative	Gas Phase	Humidity	Humid Volume	Mass dry air	Mass water vapor		
Humidity	Temperature	(kg water / kg dry air)	(cu.m / kg dry air)	(kg)	(kg)		
(%)	(° C)			*10-5	*10 ⁻⁶		
95	30	0.0258	0.8935	9.4063	2.4234		
	35	0.0346	0.9207	9.1286	3.1604		
	40	0.0462	0.9522	8.8266	4.0795		
	45	0.0614	0.9895	8.4943	5.2167		
	50	0.814	1.0344	8.1252	6.6112		
	55	0.1077	1.0899	7.7118	8.3076		
	60	0.1429	1.1599	7.2462	10.3541		
	65	0.1906	1.2509	6.7192	12.8072		
100	30	0.0272	0.8955	9.3857	2.5510		
	35	0.0365	0.9234	9.1018	3.3267		
	40	0.0488	0.9560	8.7920	4.2941		
	45	0.0650	0.9946	8.4501	5.4912		
	50	0.0862	1.0416	8.0691	6.9591		
	55	0.1144	1.0999	7.6414	8.7447		
	60	0.1523	1.1741	7.1584	10.8990		
	65	0.2039	1.2714	6.6107	13.4801		

Appendix C -

Images of Preferential Nucleation On Silicon Particles

This appendix gives a brief overview of how the images look when preferential nucleation and condensation occurs on an insoluble particle. It shows what was basically being looked for during the experimental runs. For this particular run the impurity which was being examined was silicon and the surface was a silicon production wafer. The experimental conditions are as follows; the nitrogen flowrate was set at 842 ml/min, the substrate temperature was 22° C, and the gas phase temperature was 39° C producing a temperature difference of 17° C. All the images were magnified by approximately 160X.

Initially the silicon particle was measured to be 0.02166mm x 0.01805mm x 0.02105mm (LxHxW). As seen from the images below within 6 minutes a water droplet formed around the insoluble particle and was easily identifiable.

01-23-99 TUE 10:55:30

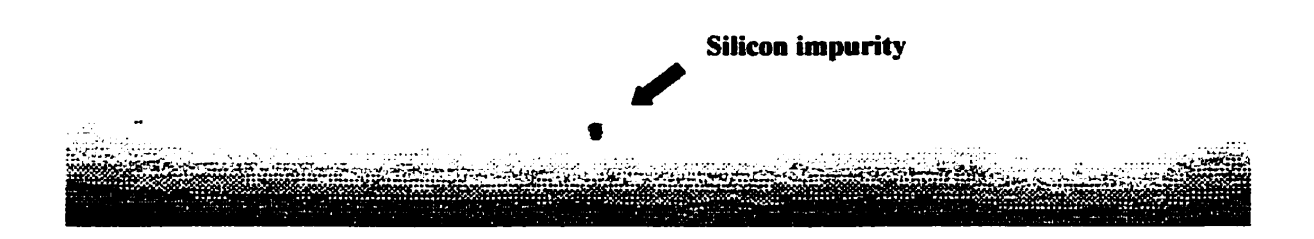


Figure C.1 - Image #1 (time index:10:55:30 AM)

01-23-99 TUE 11:01:33



Figure C.2 - Image #2 (time index:11:01:38 AM)

01-23-99 TUE 11:02:00

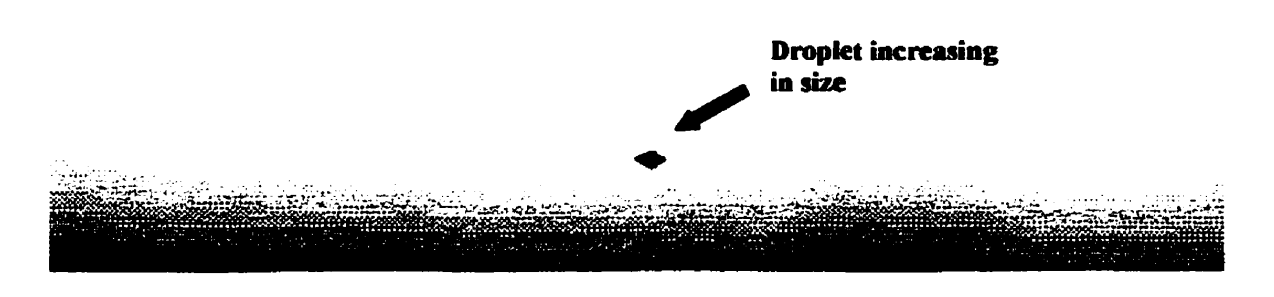


Figure C.3 - Image #3 (time index:11:02:00 AM)

01-23-99 TUE 11:02:53

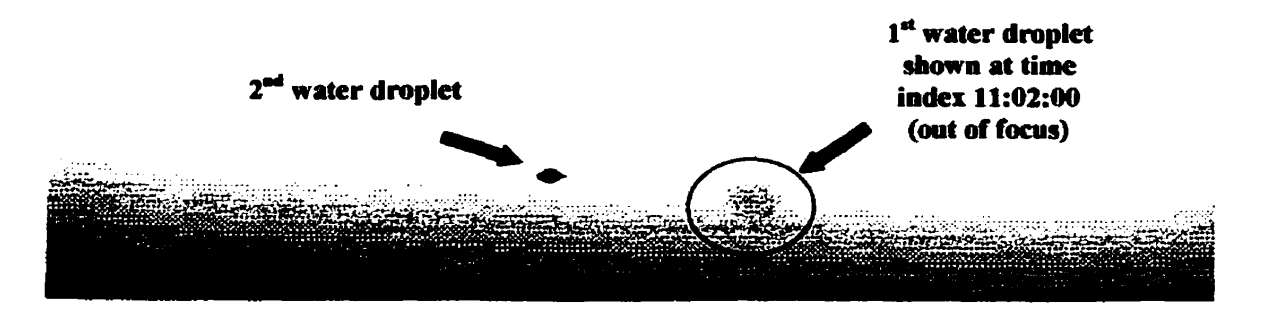


Figure C.4 - Image #4 (time index:11:02:58 AM)





Figure C.5 - Image #5 (time index:11:03:20 AM)

01-23-99 TUE 11:10:33

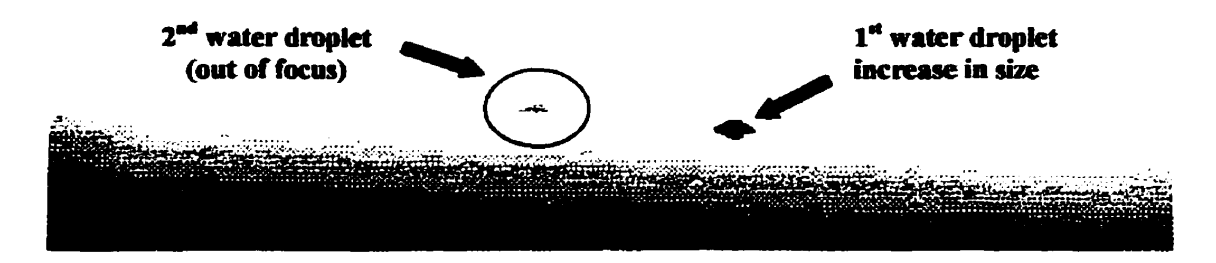


Figure C.6 - Image #6 (time index: 11:10:33 AM)

01-28-99 TUE 11:10:55

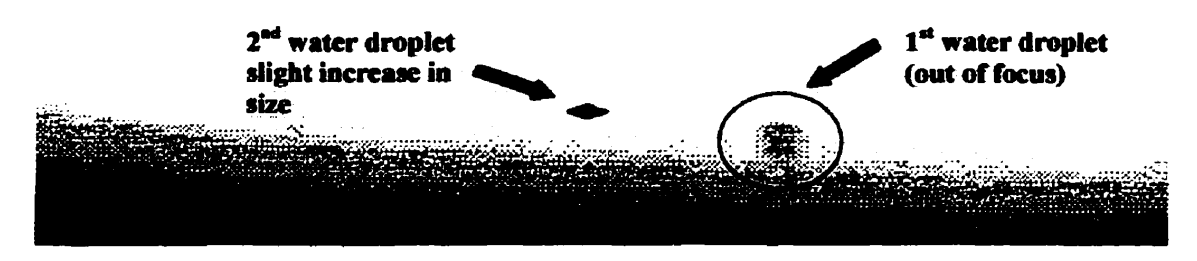


Figure C.7 - Image #7 (time index: 11:10:55 AM)

01-23-99 TUE 11:11:11

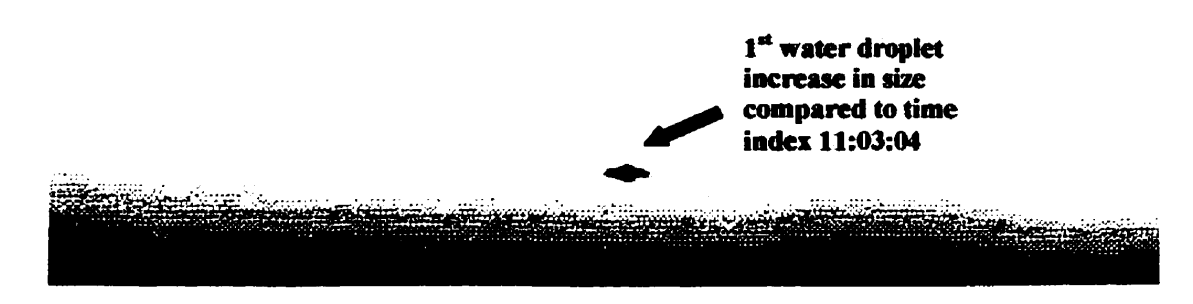


Figure C.8 - Image #8 (time index: 11:11:11 AM)



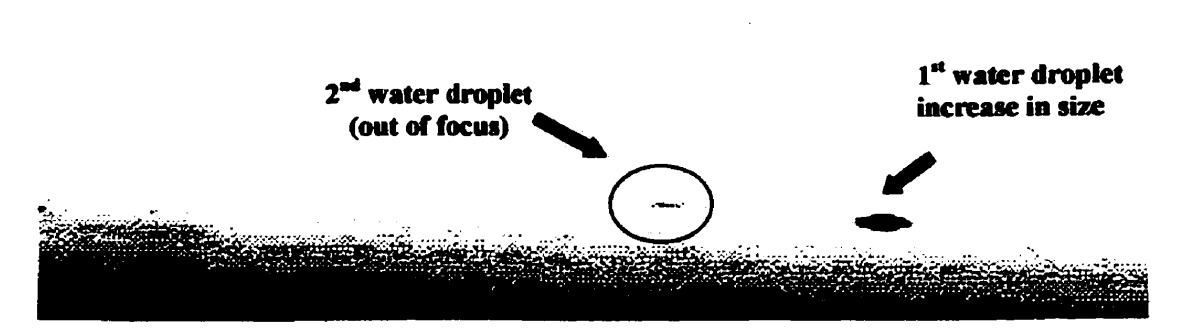


Figure C.9 - Image #9 (time index 11:24:27 AM)